Università degli Studi di Trieste

Dipartimento di Fisica
Corso di Laurea Magistrale in Fisica

Theory and Numerical Simulation of Heat Transport in Disordered Systems

Teoria e Simulazione Numerica del Trasporto Termico in Sistemi Disordinati

Laureando:
Alfredo Fiorentino

Relatore:
Prof. Stefano Baroni

Anno Accademico 2019–2020

Abstract

Negli isolanti solidi, cristallini o amorfi, il trasporto termico è determinato principalmente dalla dinamica delle vibrazioni reticolari. Recentemente è stata sviluppata una teoria unificata del trasporto termico, chiamata Quasi-Harmonic Green-Kubo (QHGK) approximation, che si applica ad entrambi i tipi di isolanti solidi, purchè siano abbastanza al di sotto della temperatura di fusione. Per i cristalli, tale teoria si riduce alla linearized Boltzmann Transport Equation (BTE), sia nel caso classico che quantistico. Inoltre QHGK fornisce una trattazione puramente quantistica per gli amorfi, che finora erano stati trattati classicamente utilizzando la Molecular Dynamics assieme alla teoria della risposta lineare di Green-Kubo. Uno dei fondamenti di questa QHGK approximation è che gli effetti di interazione anarmonica, responsabili per il valore finito della conducibilità, possano essere trattati introducendo una vita media nell'espressione armonica delle funzioni di correlazione dei modi normali, anche note come i propagatori dei fononi. All'ordine più basso dell'interazione anarmonica, questa approssimazione risulta in un propagatore con uno spettro di forma Lorentziana, dovuto al fatto che stiamo trascurando gli effetti di memoria sul propagatore per tempi brevi. Questo causa la violazione di diverse sum rules.

Lo scopo di questa tesi è esaminare l'effetto della forma di riga del propagatore dei fononi sul valore della conducibilità termica del sistema vetroso. Il risultato principale è stato trovare un miglior propagatore dei fononi, basato sul Mori memory function formalism, ed implementarlo nel calcolo del coefficiente di trasporto termico. Si è mostrato che la rilevanza o meno degli effetti di memoria è fortemente legata alla Density of States (DOS) vibrazionale. In particolare, all'aspetto di "coerenza" del sistema: ovvero quanti modi oscillano quasi alla stessa frequenza. Infine, l'effetto di memoria è stato brevemente discusso anche per i cristalli.

Durante il lavoro di tesi si è affrontato anche un altro problema relativo al trasporto termico negli amorfi: la dipendenza dalla taglia finita. Gli amorfi richiedono simulazioni con taglie molto grandi, che sono computazionalmente molto costose, per avere una DOS fisicamente affidabile, specialmente a basse frequenze. Il non avere abbastanza basse frequenze porta a sottostimare fortemente la conducibilità termica a basse temperature ($T \lesssim 50K$). Per migliorare i risultati a basse temperature, senza però rendere le simulazioni troppo computazionalmente pesanti, è stato sviluppato un nuovo metodo numerico.

Abstract

In solid insulators, be they crystalline or amorphous, heat transport is determined by the dynamics of lattice vibrations. Recently, a unified theory of heat transport, called the Quasi-Harmonic Green-Kubo (QHGK) approximation, has been developed, which applies to both kinds of solid insulators, well below the melting point. For crystals, this theory reduces to the linearized Boltzmann Transport Equation, both in the quantum or classical regimes. Moreover, it gives a fully quantum description of heat transport in amorphous systems, which, until now, could be treated only in the classical regime using Molecular Dynamics and the Green-Kubo linear response Theory. The central tenet of the QHGK approximation is that the interaction effects, responsible for the finite value of the heat conductivity, can be properly accounted for by introducing anharmonic lifetimes in the harmonic expression of the normal-mode correlation functions, AKA phonon propagators. To lowest order in the anharmonic interactions, this approximation results in a phonon propagator that has a Lorentzian lineshape in the frequency domain, resulting from the neglect of memory effects in the short-time behavior of the normal-mode correlation function and the consequent violation of a number of sum rules.

The purpose of this thesis is to examine the effects of the phonon-propagator line shape on the value of the heat transport coefficients of glassy systems. The main results are an improved form of the phonon propagator, based on Mori memory function formalism and the consequent effects on the heat conductivity. It has been shown that the relevance, or not, of the memory strongly depends on the vibrational Density of States (DOS). In particular, the memory effect is related to the "coherence" of the systems i.e. how many modes oscillate with almost the same frequency. Finally, the effect of memory has been briefly discussed also for crystals.

While studying the heat transport in glasses, another problem has been treated: the finite-size dependence. Amorphous systems require very large samples to have a reliable DOS, especially in the low frequency range. Such lack of low-frequencies leads to greatly underestimate the heat conductivity at low temperatures ($T \lesssim 50K$). In order to improve the results at low temperature while avoiding the immense computational cost of simulating large amorphous systems, a novel numerical method has been developed.

Contents

Chapter 1

Introduction

Heat conduction is a phenomenon we all experience since childhood: whenever an object is not in thermal equilibrium there is a flux of heat from the warmer side to the cooler one. However not all materials are equal under this aspect, for example a metallic fork near a fire transmits heat faster than a wooden spoon. But what does determine this heat conductivity?

The question is surely not just speculative. Designing a good thermal insulator can greatly increase the energetic efficiency of a cooling system or thermal machine, protect a delicate system from overheating and last but not least it can help you save some money from the gas bill. Moreover, materials are not simply divided into good heat conductors and bad ones, the conductivity can depend on the direction of the heat flux and the consequent ability to better re-direct and distribute the heat flux can also help to save energy. To design and produce such materials a general and effective method to calculate the heat-conductivity is required.

This thesis will focus on computing heat conductivity in solid insulators, especially disordered ones like glasses. In solid insulators, both crystalline or amorphous, the heat conduction is dominated by the dynamics of lattice vibrations. Far from melting, atomic displacements from equilibrium are much smaller than interatomic distances and they can thus be treated in the (quasi-)harmonic approximation. As long as the system is a crystal, this observation enables a kinetic description of heat transport mediated by phonons that can be treated in the Peierls-Boltzmann Transport Equation (BTE) [15, 7]. Instead, in disordered systems the phonon mean free path is so small that the heat carriers picture of phonons does not hold anymore, and molecular dynamics (MD) is needed, in either its equilibrium or not equilibrium (EMD) flavors [7, 2]. MD is generally applicable to any solids, but it is subject to statistical errors, it needs long simulations and finally it can not account for quantum effects [3]. While BTE can easily treats them, but as said before it does not work for amorphous systems. There is need for a general theory able to treat both classical and quantum systems, either crys-

talline or amorphous. Moreover, since the transport coefficient is a linear response then it should be possible to obtain it from the equilibrium state.

The most general theory, up to now, to evaluate transport coefficients as the heat conductivity is the Green-Kubo's linear response theory (*Kubo 1957* [11]). Such theory connects the transport coefficient to the autocorrelation of the related flux. In our case, if κ is the heat conductivity, then:

$$\kappa \propto \int_0^\infty dt \ \langle J(t)J(0)\rangle, \tag{1.1}$$

where J is the energy flux evolved at time t through the hamiltonian of the system H and $\langle\rangle$ indicate the thermal average on the canonical ensemble. This formula has also the quantum version, where there is the operator flux $\hat{J}$. Since it is defined through the fluxes, the theory is far more general than a classical approach or BTE, where it is necessary to identify a "carrier". As long as we can define a density a of a conserved quantity A, and its time derivative through the Hamilton equations or the Heisenberg one, then we can define a current j_a using the continuity equation:

$$\partial_t a + \nabla \cdot j_a = 0 \tag{1.2}$$

Until recent years, GK theory was mainly used in a classical framework, together with Molecular Dynamics (MD). Indeed, MD numerically simulates the trajectories of the particles and as long as you can write the fluxes as a function of them, the GK classical formula can be computed. On the other hand, quantum GK requires the evolution of the operator and its autocorrelation and then the average of such autocorrelation. It goes without saying, in a MD simulation we are not treating the operator.

Isaeva et al.(2019) [9] used GK theory to create an unified theory to calculate the heat conductivity in solid insulators, either amorphous or insulators, in the quasi-harmonic approximation. Their method, called Quasi-Harmonic Green-Kubo (QHGK), leads to an explicit formula for heat conductivity which can account for the quantum effects like BTE, and indeed it is equivalent to BTE in crystals, but it is also valid for amorphous systems. To apply quantum Green-Kubo is necessary to find the Green's function/propagator of the flux. Since in a solid insulator electrons do not contribute to transport, the only way to transmit heat for is through lattice vibrations. Indeed, in Ref. [9] the evolution of the operator $\langle\hat{J}(t)\hat{J}(0)\rangle$ has been explicitly written through an approximation of the propagator of phonons $\langle\hat{a}^\dagger(t)\hat{a}(0)\rangle$. Such QHGK method has been later implemented in a program called kALDO.

The goal of this thesis is going beyond the QHGK method. In particular, I focused on how the lineshape of the propagator's spectrum affects the transport coefficient and how the memory effects could modify such lineshape. Moreover,

while studying the heat transport in amorphous systems another problem has been treated: the finite-size dependence.

The latter one is a common problem when treating amorphous systems, like glasses. To reproduce a reliable material, with its continuous density of states, it is needed a large system, since the number of modes is proportional to the number of atoms. However, without periodicity simulating an infinite, or at least very large, size is computationally heavy. This problem has been discussed, and partially resolved, in Ch. 4.

The former problem is instead more subtle, in [9] a typical propagator with exponential decay has been used $\sim e^{(i\omega_n - \gamma_n)t}$, where the linewidth γ_n introduces a decay with a characteristics time of order $\frac{1}{\gamma_n}$. Such propagator usually well describes the long time behaviour and the γ_n can be straightforwardly computed from the well-known Fermi Golden Rule (FGR). Unfortunately, as shown in Ch. 4 such propagator it is not correct for short times. Indeed, it can be shown that it does not respect the sum rules, which are connected with the zero-time derivatives. Since GK formula integrate the autocorrelation from time difference 0 to ∞, overlooking the propagator's short-time behaviour could affect the final result. To compute a correct propagator the memory effects must be taken in account. Instead, the exponential decay obtained with FGR describes a constant, instantaneous, effect of the anharmonicities:

$$\partial_t \langle \hat{a}_n^\dagger(t)\hat{a}_n(0)\rangle = (i\omega_n - \gamma_n)\langle \hat{a}_n^\dagger(t)\hat{a}_n(0)\rangle \tag{1.3}$$

This equation describe a system where the variation in the correlation depends only on its own instantaneous value and the effect of the anharmonicities is constant. But that is not true, the evolution depends also on the previous history of the correlation. Like a fish in the water which feels the currents created by its own previous movements. This discussion will be treated in Ch. 5, where using Mori memory function formalism an improved propagator of the phonons, with both a correct short and long time behaviour, will be calculated.

To summarize, the structure of this thesis is the following one. Firstly, GK linear response theory will be revised in Ch. 2. Then, in Ch. 3 there will be a discussion about the QHGK method [9], its derivation and its results. After that, a critical analysis of such method will be done in Ch. 4. Its range of validity will be discussed together with the possible effects that size and a wrong propagator could have on the calculation of the heat conductivity. In this chapter a novel method to calculate the conductivity of a large amorphous system will be presented, which involves the use of replicas of the amorphous supercell and a fit of certain quantities over small samples of the material. Finally, in Ch. 5-6 the focus will be on how improve the phonon propagator using Mori memory function formalism. In particular, in Ch. 5 the theory will be explained and re-derived,

while in Ch. 6 it will applied and implemented for our glassy system. It will follows a comparison of the results between the original QHGK method and the one with the memory-propagator. The method will be called QHGK-Memory or just QHGK-M.

Chapter 2

Green-Kubo linear response theory

Steady fluxes are generally out-of-equilibrium phenomena. Indeed, when we think of a stationary system in thermodynamic equilibrium, invariant under time-reversal symmetry, it can not sustain a flux. Fluxes are generated by perturbation of some kind. For instance, if we connect subsystems which are not in thermal equilibrium, there is an energy flux from the hotter side to the cooler one. In a isotropic material the intensity of such a flux would be $-\kappa\nabla T$, where κ is the coefficient of proportionality between the flux and the gradient of temperature. κ is the so-called transport coefficient or in this particular case the heat conductivity.

However, as it always happens the property of the linear response to the perturbation must be a function only of the unperturbed system. Indeed, Green-Kubo (GK) linear response theory [11] connects the autocorrelations of fluxes at thermal equilibrium to the transport coefficient, which is the stationary response function. Such theory is usually defined in the framework of Local Thermodynamical Equilibrium (LTE), so before re-deriving GK's theory let us make a little digression.

2.1 Fluxes and Local Thermodynamical Equilibrium

Fluxes in thermodynamics are a delicate subject, since they are usually an out-of-equilibrium phenomena. As explained in the next paragraph at thermodynamic equilibrium it is senseless to talk about gradient of temperature, density, charges et cetera ... However the discussion is well defined in the LTE framework.

Firstly, let us indicate as S the entropy of our system and let us say that $E, V, N \dots$ are its extensive arguments, such that:

$$S = S(E, V, N \dots). \tag{2.1}$$

From these extensive variables we can define intensive ones as $\alpha = \frac{\partial S}{\partial A}$; e.g. $\frac{\partial S}{\partial E} = \frac{1}{T}$.

Let $S(\Omega_1, A_1)$ and $S(\Omega_2, A_2)$ be the entropies of two subsystem as functions of their respective extensive variable, as entropy is also an extensive quantities one has that $S(\Omega_1, A_1) + S(\Omega_2, A_2) = S(\Omega, A)$. Entropy at equilibrium is maximized, therefore it must be stationary with respect to the variation of A_1 as long $A_1 + A_2 = A$, therefore:

$$\begin{aligned} \frac{\partial S}{\partial A_1} &= \frac{\partial S(\Omega_1, A_1)}{\partial A_1} + \frac{\partial S(\Omega_2, A - A_1)}{\partial A_1} \\ &= \alpha_1 - \alpha_2 \\ &= 0. \end{aligned} \tag{2.2}$$

From the last equation we obtain that at thermal equilibrium all the intensive variable must be equal in every subsystem. In other words, $\nabla\alpha = 0$. But the flux follows the gradient. Indeed when $\nabla\alpha \neq 0$, A will flow from regions of higher α to those of lower α. This is why we must abandon in our description the global thermodynamic equilibrium. Postponing this discussion to later, it is well known that if A is a conserved quantity and $a(\mathbf{r}, t)$ its density, then its value in a subsystem evolves as:

$$\dot{A}(V, t) = \int_V \dot{a}(\mathbf{r}, t) = -\int_{\partial V} dV\ \mathbf{j}_a(\mathbf{r}, t) \cdot d\sigma \tag{2.3}$$

where j_a and a are connected by the *continuity equation*

$$\partial_t a + \nabla \cdot j_a = 0 \tag{2.4}$$

and V is the volume. In the limit of long-wavelength, low frequencies and assuming isotropy, the flux obeys the following equation:

$$\mathbf{J}_a = \lambda \nabla \alpha \tag{2.5}$$

where λ is a positive constant (the sign is related to the second principle of thermodynamics). When more than an intensive variable is involved, this formula can be generalized as follows:

$$\mathbf{J}^i = \sum_j L^{ij} \mathbf{F}_j \tag{2.6}$$

where F_j are the *thermodynamical forces*, i.e. the space average of the $\nabla\alpha_j$: $F_j = \frac{1}{\Omega}\int d\mathbf{r}\ \nabla\alpha_j$ and L^{ij} are transport coefficients, for which the Onsager's relations $L^{ij} = L^{ji}$ hold.

A thermodynamic system at equilibrium is characterized by the relation between entropy and its derivatives, but we have seen that this derivatives yields to the spatial constancy of intensive variables. On the other hand, in Eq. 2.5 we define current by the gradient of these intensive variables. In order to have well defined intensive variable we need to suppose local equilibrium. If the inhomogeneities due

to perturbations have long-wavelength, as assumed before, we can consider a zone where thermal equilibrium is hold and consequently there is a equation of state with the modified $\alpha + \alpha_{pert}$ constant intensive variable. Finally, We can define $\alpha(\mathbf{r})$.

2.2 Linear response theory and the Green-Kubo formula

Following *Kubo 1957* [11], let us limit our discussion to external disturbances that can be expressed definitely as an extra term in the hamiltonian, for instance an electric field. Later it will be discussed how to include a gradient of temperature in this framework.

Let us consider an isolated system which at equilibrium has a *natural motion* determined by H. Then, we suppose that an external force $F(t)$ is applied to the system, represented by the energy correction:

$$H' = -AF(t). \tag{2.7}$$

The motion of the system is perturbed by it and there will be a response. Assuming that the force is weak we can focus only on the linear response. The response will be seen by the change of certain quantity $\Delta B(t)$. Our problem now is to express $\Delta B(t)$ through only the natural motion of the system. In a statistical framework, we measure the average value, which is the observable weighted with the distribution function of the phase-space $f(q,p)$. Therefore, we must study the evolution of f, whose equation of motion is

$$\partial_t f = \{H, f\} \tag{2.8}$$

where q, p are the coordinate and momenta and the parenthesis are the Poisson brackets:

$$\{A, B\} = \sum \left(\frac{\partial A}{\partial q}\frac{\partial B}{\partial p} - \frac{\partial A}{\partial p}\frac{\partial B}{\partial q} \right) \tag{2.9}$$

We assume that at infinite past $t = -\infty$ the system it is at equilibrium with function f, such that $\{H, f\} = 0$. Then the perturbation is inserted adiabatically ($\lim_{t\to-\infty} F(t) = 0$). Therefore the distribution function f' evolves as:

$$\partial_t f' = \{H, f'\} + \{H'(t), f\}. \tag{2.10}$$

If we write perturbatively $f' = f + \Delta f(t)$ and we keep everything at first order we obtain:

$$\partial_t \Delta f = \{H, \Delta f\} - F(t)\{A, f\} \tag{2.11}$$

The formal solution of this equation, imposing the initial condition $\Delta f(-\infty) = 0$, is:

$$\Delta f(t) = -\int_{-\infty}^{t} dt' \; e^{i(t-t')L} F(t')\{A, f\} \tag{2.12}$$

where L is the Liouvillian operator defined as:

$$iLg = \{H, g\} \tag{2.13}$$

With a straightforward derivation it can be verified that indeed Eq. 2.12 reduces to Eq. 2.11. Now that Δf is obtained, the statistical average of ΔB is by definition:

$$\begin{aligned} \Delta B(t) &= \int d\Gamma \; \delta f B(q,p) \\ &= -\int d\Gamma \; \int_{-\infty}^{t} dt' \; e^{i(t-t')L} F(t')\{A, f\} B(q,p) \\ &= -\int d\Gamma \; \int_{-\infty}^{t} dt' \; \{A, f\} B(t-t') F(t') \end{aligned} \tag{2.14}$$

where $d\Gamma$ is volume element in the phase space and it has been used that $e^{i(t-t')L} B(q,p) = B(t-t', q, p)$, since the dynamical motion of $B(q,p)$ follows the equation:

$$\dot{B} = \{B, H\} \tag{2.15}$$

It is important to notice that with $B(t)$ it is intended the evolution through the natural hamiltonian H. The response function $\phi_{AB}(t)$ is defined as:

$$\Delta B(t) = \int_{-\infty}^{t} dt' \phi_{AB}(t-t') F(t'). \tag{2.16}$$

In other words, the difference from the equilibrium value $\Delta B(t)$ caused by A is given by the superposition of the effect of the perturbation at every previous moment, with weight $\phi_{AB}(t-t')$. Comparing the previous equations, we obtain that :

$$\phi_{AB}(t) = -\int d\Gamma \; \{A, f\} B(t) \tag{2.17}$$

Through the ϕ_{AB} we can also define the admittance χ_{AB}:

$$\chi_{AB}(\omega) = \int_{0}^{\infty} dt \; \phi_{AB}(t) e^{-i\omega t} \tag{2.18}$$

The stationary admittance $\chi(\omega = 0)$ is usually our transport coefficient, the response to a stationary perturbation switched on at $t = 0$.

For the quantum case, the discussion is similar. If $\hat{\rho}$ is the operator density matrix at equilibrium $t \to -\infty$ such that $[\hat{H}, \hat{\rho}] = 0$, where now the parenthesis indicate a commutator, then the dynamic equation for $\hat{\rho}'$ is:

$$\partial_t \hat{\rho}' = \frac{1}{i\hbar}[\hat{H} + \hat{H}', \hat{\rho}']. \tag{2.19}$$

Following the same procedure as before, we obtain:

$$\Delta\hat{\rho}(t) = -\frac{1}{i\hbar}\int_{-\infty}^{t} dt' \ \exp(-i(t-t')\hat{H}/\hbar)[\hat{A}, \hat{\rho}]\exp(i(t-t')\hat{H}/\hbar)F(t') \tag{2.20}$$

Then, mimicking the procedure for ΔB (for details see Ref. [11]) we obtain the following results:

$$\phi_{AB}(t) = \begin{cases} \int d\Gamma\{f, A\}B(t) & \text{(classical)} \\ \dfrac{1}{i\hbar}\mathrm{Tr}[\hat{\rho}, \hat{A}]\hat{B}(t) & \text{(quantal)} \end{cases}. \tag{2.21}$$

Using the property of the trace or a proper integration by part with right border condition, respectively for the quantal and classical case, these expression can be rewritten as:

$$\phi_{AB}(t) = \begin{cases} \int d\Gamma f\{A, B(t)\} & \text{(classical)} \\ \dfrac{1}{i\hbar}\mathrm{Tr}\hat{\rho}[\hat{A}, \hat{B}(t)] & \text{(quantal)} \end{cases}. \tag{2.22}$$

2.2.1 Response function in the canonical ensemble

The formulas for $\phi_{AB}(t)$ can be further simplified if we work in the canonical ensemble, where we know how to write explicitly $\hat{\rho}$. The discussion will be done only in the quantum case, since the classical one can be obtained promoting each observable to operator $A \to \hat{A}$, substituting $i\hbar\{,\} \to [,]$ and performing $\lim \hbar \to 0$.

In the canonical ensemble the density matrix operator is defined as:

$$\hat{\rho} = e^{-\beta(\hat{H}-\Phi)} \tag{2.23}$$

where $\beta = 1/k_b T$ as usual and

$$\exp(-\beta\Phi) = \mathrm{Tr}e^{-\beta\hat{H}}.$$

Then we remind this useful identity:

$$\begin{aligned}[\hat{A}, \exp(-\beta\hat{H})] &= \exp(-\beta\hat{H}) \int_0^\beta \exp(\lambda\hat{H})[\hat{H}, \hat{A}] \exp(-\lambda\hat{H}) d\lambda \\ &= \frac{\hbar}{i} \exp(-\beta\hat{H}) \int_0^\beta \exp(\lambda\hat{H}) \dot{\hat{A}} \exp(-\lambda\hat{H}) d\lambda \\ &= \frac{\hbar}{i} \exp(-\beta\hat{H}) \int_0^\beta \dot{\hat{A}}(-i\hbar\lambda) d\lambda \end{aligned} \tag{2.24}$$

where we defined:

$$\exp(\lambda\hat{H}) \dot{\hat{A}} \exp(-\lambda\hat{H}) = \dot{\hat{A}}(-i\hbar\lambda)$$

and used that $\dot{\hat{A}}(t) = \frac{1}{i\hbar}[\hat{A}(t), \hat{H}]$.

Introducing Eq. 2.24 in Eq. 2.21 we obtain:

$$\begin{aligned}\phi_{AB}(t) &= \frac{1}{i\hbar} \mathrm{Tr}[\hat{\rho}, \hat{A}] \hat{B}(t) \\ &= \int_0^\beta \langle \dot{\hat{A}}(-i\hbar\lambda) \hat{B}(t) d\lambda \rangle \end{aligned} \tag{2.25}$$

This is almost the desired formula, the only thing left is to show that $\dot{\hat{A}}$ is connected to flux and therefore the response function depends on the flux's autocorrelation.

2.2.2 Example: electric conductivity

Let us consider the electric conductivity. For an electric field $\mathbf{E}(t)$, the perturbation energy is:

$$\hat{H}'(t) = -\sum_i e_i \hat{\mathbf{r}}_i \cdot \mathbf{E}(t) \tag{2.26}$$

where e_i and r_i are respectively the charge and position of the $i-th$ particle. In other words, the electric field couples with the dipole $e\hat{\mathbf{r}}$. Let us neglect any discussion about periodic systems where the operator position $\hat{\mathbf{r}}$ is not well-defined, in any case its time derivative is in any case a current. Now, let us calculate the response of current in μ direction when a pulse of electric field is applied in ν-direction at $t = 0$ using Eq. 2.25:

$$\begin{aligned}\phi_{\mu\nu}(t) &= \frac{1}{i\hbar} \mathrm{Tr} \left[\hat{\rho}, \sum_j e_j \hat{x}_{j\mu} \right] \sum_i e_i \dot{\hat{x}}_{i\nu} = \\ &= \int_0^\beta \langle \hat{J}_\mu(-i\hbar\lambda) \hat{J}_\nu(t) \rangle d\lambda \end{aligned} \tag{2.27}$$

where obviously $\langle\cdot\rangle = \mathrm{Tr}\hat{\rho}\cdot$ and

$$\hat{J}_\mu = \sum_i e_i \dot{\hat{x}}_{i\mu}$$

If we consider as flux the spatial average of the density current, $J \to J/V$, then the admittance (in this case the conductivity $\sigma_{\mu\nu}$) is:

$$\sigma_{\mu\nu}(\omega) = \frac{1}{V}\int_0^\infty dt\ e^{-i\omega t}\int_0^\beta \langle \hat{J}_\mu(-i\hbar\lambda)\hat{J}_\nu(t)\rangle d\lambda \tag{2.28}$$

and for a stationary electric field

$$\begin{aligned}\sigma_{\mu\nu} &= \sigma_{\mu\nu}(\omega = 0) = \\ &= \frac{1}{V}\int_0^\infty dt \int_0^\beta \langle \hat{J}_\mu(-i\hbar\lambda)\hat{J}_\nu(t)\rangle d\lambda\end{aligned} \tag{2.29}$$

Finally, we found the Green-Kubo formula to find the transport coefficient of a charge flux in presence of only a perturbation, an applied electric field.

2.2.3 Green-Kubo and heat flux

A heat flux occurs when the temperature is not homogeneous in the sample i.e. when $\nabla T \neq 0$. This situation is outside of the canonical framework where the temperature is fixed for all the material. Also from a theoretical point of view, when we switch on an electric field every particle will feel the force due to H plus the electric one. On the other hand, even if there is a temperature gradient the particles evolve only through H. However, it is still possible to use Green-Kubo theory if we are able with some tricks to describe the perturbed system with a canonical-like matrix density, something like $\exp(-\beta H + \dots)$.

Let us consider a macroscopic system with local temperature $T(\mathbf{r})$. Let us discretize for a moment the problem and let us consider M subsystems each one in local thermal equilibrium $T_{i=1,\dots,M}$. If the subsystems are large enough to be considered independent, then the probability to have the system in a certain global configuration is proportional to the product of their Boltzmann factors $P(\Gamma) = \prod_i e^{-H_i/k_b T_i}$. In the continuous limit we obtain:

$$P(\Gamma) \propto e^{-\int d\mathbf{r}\ \varepsilon(\mathbf{r};\Gamma)/k_b T(\mathbf{r})}, \tag{2.30}$$

where $\varepsilon(\mathbf{r};\Gamma)$ is an energy density of that configuration. Since we are interested in linear response, let us suppose that $T(\mathbf{r}) = T + \Delta T(\mathbf{r})$, with $|\Delta T(\mathbf{r})|/T \ll 1$. Then we can write $\frac{1}{T(1+\Delta T(\mathbf{r})/T)} \approx \frac{1}{T}(1 - \Delta T(\mathbf{r})/T))$. Since by definition $\int d\mathbf{r}\ \varepsilon(r;\Gamma) =$

$H(\Gamma)$, we obtain $P(\Gamma) \propto e^{-\frac{H(\Gamma)+V(\Gamma)}{k_b T}}$, where $V(\Gamma) = -\int d\mathbf{r} \quad \varepsilon(r;\Gamma)\Delta T(\mathbf{r})/T$. Finally, if the inhomogeneity is weak and on long scale we can write $\Delta T(\mathbf{r}) = \nabla T \cdot \mathbf{r}$ and consequently:

$$V(\Gamma) = -\frac{\nabla T \cdot}{T} \int d\mathbf{r}\ \varepsilon(\mathbf{r};\Gamma)\mathbf{r}$$

It is interesting to notice a striking resemblance to the previous electric dipole-potential.

Thanks to this kind of " thermal potential" we can describe the system in equilibrium with a canonical like $\hat{\rho}$. Still this potential is not a perturbation related to a force, which changes the dynamics. The dynamics of the system is still guided only by H. One way of resolving the problem is the following. Assume that we have adiabatically switched on at $t = -\infty$ some thermostats in such a way that at $t = 0$ the system is at equilibrium with them and with a heat flux. At $t = 0$ this system it has the perturbed dynamical matrix with V. Then we isolate the system from any source of heat apart from a thermostat at temperature T, now we have an out of equilibrium system which evolves with H, obeying to Eq. 2.19. This is somehow the opposite case of the charge current example. In that case we have a system at equilibrium and then we switch on an electric field which causes a charge flux. In this case we have a system connected with a forced heat gradient and a heat flux and then we leave the external heat sources and let the system reach thermal equilibrium .i.e. $\hat{\rho}'$ evolves to $\sim e^{-\beta \hat{H}}$.

Since we wrote $\hat{\rho}'(t = 0)$ as a canonical like density matrix Eq. 2.24 can still be used and analogous calculations yields to

$$\kappa_{\alpha\beta} = \frac{1}{VT} \int_0^{1/k_b T} d\lambda \int_0^{\infty} dt\ \langle \hat{J}_\alpha(0) \hat{J}_\beta(t + i\hbar\lambda) \rangle, \tag{2.31}$$

which in the classical case reduces to

$$\kappa_{\alpha\beta} = \frac{1}{V k_b T^2} \int_0^{\infty} dt\ \langle J_\alpha(t) J_\beta(0) \rangle, \tag{2.32}$$

Chapter 3

Green-Kubo theory of heat transport in insulators

This thesis' theoretical foundation is constituted mainly by the Quasi-Harmonic Green-Kubo (QHGK) method presented in *Isaeva et al. (2019)* [9]. In the next chapters such theoretical results will be applyed, their range of validity will be studied and finally they will be extended through a better approximation of the phonons' time-autocorrelation or propagator.

In the aforementioned paper the heat conductivity is calculated using Green-Kubo theory of linear response (GK) (*Kubo, 1957* [11]), which has been re-derived in the previous chapter: Eqs. 2.32-2.31. Just as a reminder, such theory states in the classical case that:

$$\kappa_{\alpha\beta} = \frac{1}{Vk_bT^2}\int_0^\infty dt\ \langle J_\alpha(t)J_\beta(0)\rangle, \tag{3.1}$$

where $\kappa_{\alpha\beta}$ is the heat-conductivity tensor, α, β indicates the spatial axes, V the volume, J is spatial's average of the energy flux and $\langle\cdot\rangle$ is the thermodynamical average. While in the quantal case:

$$\kappa_{\alpha\beta} = \frac{1}{VT}\int_0^{1/k_bT} d\lambda\ \int_0^\infty dt\ \langle \hat{J}_\alpha(0)\hat{J}_\beta(t+i\hbar\lambda)\rangle, \tag{3.2}$$

where now $\hat{J}$ is the operator energy flux and there is an extra integration over an imaginary time. Green-Kubo theory is extremely general, but in this thesis it will be applied to a specific case.

The physical system of our interest is an insulator, amorphous or periodic, described by the temperature and a quasi-harmonic hamiltonian (here explained the name QHGK): an harmonic potential plus plus third-order anharmonicities. In the normal-mode basis of coordinates and momenta ξ_n, π_n , which are found

diagonalizing the Dynamical Matrix, the hamiltonian is

$$H = \sum_n \frac{\omega_n^2}{2}\xi_n^2 + \frac{1}{2}\pi_n^2 + \frac{1}{6}\sum_{mnl} V_{nml}\xi_n\xi_m\xi_l, \tag{3.3}$$

where $V_{nml} = \frac{\partial^3 V}{\partial\xi_n\xi_m\xi_l}$ is the third derivative of the potential calculated with respect of the normal-mode coordinates at equilibrium. Due to Schwarz's theorem it is a symmetric tensor.

Everything can be rewritten using the amplitudes $(\alpha_n, \alpha_n^*) = \sqrt{\frac{\omega_n}{2}}\xi_n \pm \frac{i}{\sqrt{2\omega_n}}\pi_n$, which recall the quantum operators of creation and annihilation. The Hamiltonian becomes

$$H = \sum_n \omega_n\alpha_n^*\alpha_n + \frac{1}{6}\sum_{mnl} V_{nml}\frac{1}{\sqrt{8\omega_n\omega_m\omega_l}}(\alpha_n + \alpha_n^*)(\alpha_m + \alpha_m^*)(\alpha_l + \alpha_l^*), \tag{3.4}$$

It can be demonstrated [9] that in this case the energy flux can written as:

$$J_\alpha = \frac{i}{2}\sum_{mn} v_{nm}^\alpha\omega_m(\alpha_n^* + \alpha_n)(\alpha_m^* - \alpha_m) \tag{3.5}$$

where v_{nm}^β is an antisymmetric "velocity" matrix. The flux is obtained by a simple but lengthy calculation, where the velocity of each atom times its energy is rewritten in the normal-mode basis [9]. To use GK we now need the time evolution of J and then to evaluate the canonical average of $J(t)J(0)$. This task can be done using Wick's Theorem and an approximation for $\langle\alpha_n^*(t)\alpha_n(0)\rangle$.

Indeed, if we neglect the anharmonicities in the evaluation of the average we can use Wick's/ Isserlis' theorem and therefore every average can be expressed as a sum of product of second momenta. For instance, for 4 variables:

$$\langle x_1x_2x_3x_4\rangle = \langle x_1x_2\rangle\langle x_3x_4\rangle + \langle x_1x_3\rangle\langle x_2x_4\rangle + \langle x_1x_4\rangle\langle x_2x_3\rangle$$

Now, only the second moment is needed. At $t = 0$:

$$\langle\alpha_n^*\alpha_m\rangle = \delta_{nm}n_n \tag{3.6}$$
$$\langle\alpha_n^*\alpha_m^*\rangle = \langle\alpha_n\alpha_m\rangle = 0 \tag{3.7}$$

where:

$$n_n = \begin{cases} \dfrac{k_bT}{\omega_n} & \text{(classical)} \\ 1/(e^{\hbar\omega/k_bT} - 1) & \text{(quantal).} \end{cases} \tag{3.8}$$

If the system were perfectly harmonic, then $\langle\alpha_n^*(t)\alpha_n(0)\rangle = n_ne^{i\omega_nt}$. However, for long times the anharmonic part induces a line-width γ_n and consequentially a

finite lifetime:

$$\langle \alpha_n^*(t)\alpha_m \rangle = \delta_{nm} n_n e^{i\omega_n t - \gamma|t|} \tag{3.9}$$
$$\langle \alpha_n^*(t)\alpha_m^* \rangle = \langle \alpha_n(t)\alpha_m \rangle = 0 \tag{3.10}$$

Obviously since we are assuming that our system is quasi-harmonic then the condition $\gamma_n/\omega_n << 1$ must be verified. If we assume that this time-evolution holds also for small times, then we can compute Eq. 2.32. After easy but lengthy calculations one obtains [9] :

$$\langle J^\alpha(t)J^\beta(0)\rangle = -\frac{1}{4}\sum_{nm}\omega_m^2 v_{nm}^\alpha v_{nm}^\beta \times$$
$$\left[\frac{\omega_n-\omega_m}{\omega_m}(g_n(t)g_m(t)+g_n^*(t)g_m^*(t)) - \frac{\omega_n+\omega_m}{\omega_m}(g_n^*(t)g_m(t)+g_n(t)g_m^*(t))\right] \tag{3.11}$$

where $g_n(t) = \frac{\langle \alpha_n^*(t)\alpha_n(0)\rangle}{n_n} = e^{i\omega_n-\gamma_n t}$ (the time integral is defined only for positive times). These expressions are does not depend on the shape of $g_n(t)$, they would hold even if the time evolution were not $e^{i\omega_n-\gamma_n t}$. Moreover, it can be noticed that the final result must be a real number since every complex function in the parenthesis is added to its complex conjugate.

Performing $\int_0^\infty dt \ldots$, we obtain:

$$\kappa_{\alpha\beta} = -\frac{k_b}{4V}\sum_{nm} v_{nm}^\alpha v_{nm}^\beta$$
$$\left[\frac{\omega_n-\omega_m}{\omega_n}\frac{2(\gamma_n+\gamma_m)}{(\omega_n+\omega_m)^2+(\gamma_n+\gamma_m)^2} - \frac{\omega_n+\omega_m}{\omega_n}\frac{2(\gamma_n+\gamma_m)}{(\omega_n-\omega_m)^2+(\gamma_n+\gamma_m)^2}\right] \tag{3.12}$$

Finally, symmetrizing the expression for n and m one has:

$$\begin{aligned}\kappa_{\alpha\beta} &= \frac{k_b}{V}\sum_{nm} v_{nm}^\alpha v_{nm}^\beta \\ &= \left[\frac{(\omega_n+\omega_m)^2}{4\omega_m\omega_n}\frac{\gamma_n+\gamma_m}{(\omega_n-\omega_m)^2+(\gamma_n+\gamma_m)^2}\right. \\ &\qquad \left. + \frac{(\omega_n-\omega_m)^2}{4\omega_m\omega_n}\frac{\gamma_n+\gamma_m}{(\omega_n+\omega_m)^2+(\gamma_n+\gamma_m)^2}\right] \\ &= \frac{k_b}{V}\sum_{nm} v_{nm}^\alpha v_{nm}^\beta \tau_{nm}\end{aligned} \tag{3.13}$$

τ_{mn}, the expression inside [], is composed of a "resonant" part, which has a peak when $\omega_n = \omega_m$ and an "anti-resonant" part which would have a peak for $\omega_n = -\omega_m$,

but since the ω_n are all positive only the tails of this Lorentzian matter. It is quite intuitive, and it will be confirmed numerically later, that the relevant contribution for any mode n is given by the near frequencies, such that $|\omega_n - \omega_m| \sim \gamma_n$. Keeping this in mind, the formulas can be simplified: $\frac{(\omega_n+\omega_m)^2}{4\omega_n\omega_m} \approx 1 + \frac{(\omega_n-\omega_m)^2}{(\omega_m+\omega_n)^2}$ and the $\frac{(\omega_n-\omega_m)^2}{(\omega_m+\omega_n)^2}$ together with the anti-resonant term can be neglected. Thus, the final formula becomes:

$$\kappa_{\alpha\beta} = \frac{k_b}{V} \sum_{nm} v^{\alpha}_{nm} v^{\beta}_{nm} \tau^0_{nm} \tag{3.14}$$

where

$$\tau^0_{nm} = \frac{\gamma_n + \gamma_m}{(\omega_n - \omega_m)^2 + (\gamma_n + \gamma_m)^2} \tag{3.15}$$

3.1 Phonons' lifetimes

The linewidth γ_n, or better its inverse $1/\gamma_n$, gives an estimate of how much time a phonon remains in a certain state before decaying. Since the system's hamiltonian has anharmonicities of third order, physically we are considering 3-phonons process. There are two cases: or a phonon n split up in two phonons, or the viceversa, two phonons joins to create a phonon n. At thermal equilibrium the occupation number for every mode is stationary, but the decay process (and recombination process) introduces a decorrelation. To summarize, $\langle \alpha^*_n(t+t_0)\alpha_n(t)\rangle$ decays, while $\langle \alpha^*_n(t_0)\alpha_n(t_0)\rangle = n_n$.

How can these line-widths be calculated? In the quantum regime the answer is straightforward: **Fermi's Golden Rule**(FGR). For this third-order pertubation FGR yields to:

$$\hbar\gamma_n = \frac{\pi\hbar^2}{8\omega_n} \sum_{jl} \frac{|V_{njl}|^2}{\omega_j\omega_l} \left[\frac{1}{2}(1 + n_j + n_l)\delta(\omega_n - \omega_j - \omega_l) + (n_j - n_l)\delta(\omega_n + \omega_l - \omega_j)\right] \tag{3.16}$$

or after some algebra and noticing that

$$(e^{\beta\hbar(\omega_j+\omega_l)} - 1)\delta(\omega_n - \omega_j - \omega_l) = \frac{1}{n_n}\delta(\omega_n - \omega_j - \omega_l),$$

and

$$(n_j - n_l)\delta(\omega_n + \omega_l - \omega_j) = \frac{n_n n_l}{n_n} e^{\beta\hbar\omega j}\delta(\omega_n + \omega_l - \omega_j),$$

then the line-width expression can be also rewritten as:

$$\hbar\gamma_n = \frac{1}{2n_n}\frac{\pi\hbar^2}{8\omega_n} \sum_{jl} \frac{|V_{njl}|^2}{\omega_j\omega_l} \times \\ \times \left[n_j n_l \delta(\omega_n - \omega_j - \omega_l) + n_j n_l (e^{\beta\hbar\omega_j} + e^{\beta\hbar\omega_l})\delta(\omega_n + \omega_l - \omega_j)\right]. \tag{3.17}$$

For a complete derivation of this formula see *Srivastava, 1990* [14].

The classical γ_n can be obtained performing the classical limit, as explained in the next section. However, it will be shown that the same result of FGR + classical limit can be obtained in the Mori-Zwanzig formalism, which is well defined both for classical and quantum observables.

3.2 Quantum-Classical limit

The classical limit is usually obtained by performing the limit $\hbar \to 0$ and declassing the operators or in simpler words by removing the $\hat{}$. Physically the two descriptions coincide when $T \to \infty$ and the Bose-Eistein (or Fermi-Dirac for fermions) distribution becomes the Maxwell-Boltzmann one.

In this work there are simple mnemonic rules to move from a limit to the other one[9]. Firstly, $\alpha_n \to \sqrt{\hbar}\hat{a}_n$ where $\hat{a}_n$ is the annihilation operator. As a consequence:

$$\begin{cases} \langle \hat{a}_n^\dagger \hat{a}_n \rangle = n_n = \frac{1}{e^{\beta\hbar\omega_n}-1} \to \langle \alpha_n^* \alpha_n \rangle = \frac{k_b T}{\omega_n} \\ \langle \hat{a}_n \hat{a}_n^\dagger \rangle = n_n + 1 = \frac{e^{\beta\hbar\omega_n}}{e^{\beta\hbar\omega_n}-1} \to \langle \alpha_n \alpha_n^* \rangle = \frac{k_b T}{\omega_n}, \end{cases}$$

where we used the commutation rules $[\hat{a}, \hat{a}^\dagger] = 1$ for the second line.

3.3 Quantum Quasi-Harmonic Green-Kubo

Applying the rules as just explained, the generalization to the quantum case is almost trivial. We must use Eq. 2.31 where the operator energy flux is:

$$\hat{J}_\alpha = \frac{i\hbar}{2} \sum_{mn} v_{nm}^\alpha \omega_m (\hat{a}_n^\dagger + \hat{a}_n)(\hat{a}_m^\dagger - \hat{a}_m) \tag{3.18}$$

Following the same path as in the classical case, we define the propagators G_n and $\tilde{G}_n$:

$$G_n(t) = \langle \hat{a}_n^\dagger \hat{a}_n(t) \rangle = \hbar n_n e^{-i\omega_n t} \tag{3.19}$$

$$\tilde{G}_n(t) = \langle \hat{a}_n \hat{a}_n^\dagger(t) \rangle = \hbar(n_n + 1) e^{i\omega_n t} \tag{3.20}$$

It can be noticed that the high-temperature limit of the quantum Green's function reduces to the classical one $\lim_{\hbar\to 0} \tilde{G}_n(t) = \lim_{\hbar\to 0} G_n^*(t) = g_n(t)$. Next, in analogy

with the classical case, we obtain the quantum canonical average:

$$\langle \hat{J}^{\alpha}(0)\hat{J}^{\beta}(\tau)\rangle = -\frac{1}{4}\sum_{nm}\omega_m^2 v_{nm}^{\alpha}v_{nm}^{\beta}\times \left(\frac{\omega_n-\omega_m}{\omega_m}\left(G_n(\tau)G_m(\tau)+\tilde{G}_n(\tau)\tilde{G}_m(\tau)\right) - \frac{\omega_n+\omega_m}{\omega_m}\left(G_n(\tau)\tilde{G}_m(\tau)+\tilde{G}_n(\tau)G_m(\tau)\right)\right), \quad (3.21)$$

where $\tau = t + i\hbar\lambda$. Now, we have to perform the double integration in time and in the inverse temperature λ to obtain the quantum QHGK formula. Again we would have a resonant and an antiresonant contribute, but in the quasi-harmonic regime $\frac{\gamma}{\omega} \to 0$ the latter can be neglected, in perfect analogy with the classical case. Finally, after all these considerations, we would find that:

$$\kappa_{\alpha\beta} = \frac{1}{V}\sum_{nm} c_{nm} v_{nm}^{\alpha} v_{nm}^{\beta} \tau_{nm}^{0}, \quad (3.22)$$

where $c_{nm} = \frac{\hbar\omega_n\omega_m}{T}\frac{n_n - n_m}{\omega_m - \omega_n}$. For $n = m$ this matrix reduces to the modal heat capacity $c_n = k_b\left(\frac{\hbar\omega_n}{k_b}\right)^2 \frac{e^{\hbar\omega_n/k_bT}}{(e^{\hbar\omega_n/k_bT}-1)^2}$. Furthermore, for high temperatures $\lim_{T\to\infty} c_{nm} = k_b$ for any n, m and therefore the classical formula and the quantum one coincide.

The obtained heat conductivity $\kappa_{\alpha\beta}$ is a 3×3 tensor. However, for sake of simplicity in the next chapters we will often consider the corresponding isotropic heat conductivity κ:

$$\kappa = \frac{1}{3}\sum_{\alpha}\kappa_{\alpha\alpha} \quad (3.23)$$

3.4 Quasi-Harmonic Green-Kubo method on crystals

One of the most fascinating achievement of QHGK method is unifying the description of heat transport for both amorphous and crystalline solid insulators. However, the latter one was already described with BTE, so let us show that indeed in the crystal case QHGK reduces to BTE. For details see Ref. [9].

In crystals, equilibrium positions $\mathbf{R}_i^0$ are characterised by a discrete lattice position , $\mathbf{a_i}$, and by an integer label, s_i, indicating different atomic sites within a unit cell, $\mathbf{d}_s$: $\mathbf{R}_0^i = \mathbf{a_i} + \mathbf{d}_{s_i}$. Likewise, in the Bloch representation, normal modes can be labelled by a quasi-discrete vector, $\mathbf{q}$, belonging to the Brillouin

Zone (BZ), and by a index band ν: $n \to (\mathbf{q}, \nu)$. It is well-known that due to the periodicity the Dynamical Matrix $\mathbf{D}(\mathbf{q})$ becomes a block matrix, with a block for every $\mathbf{q}$. This fact and the choice of taking the eigenvectors of $\mathbf{D}(\mathbf{q})$, the normal modes, real or complex affects the velocity matrix. For a real basis, $v^{\alpha}_{\nu\mathbf{q},\mu\mathbf{p}}$ is real and antisymmetrical. Therefore the diagonal terms are null and the heat conduction is due to (quasi-) degenerate normal modes. Instead, in the Bloch basis the matrix v^{α} is anti-hermitian and block-diagonal with respect to the wave vector $\mathbf{q}$. As a consequence, the diagonal terms are imaginary and not necessary null and moreover only phonons with the same $\mathbf{q}$ contribute to the conductivity. Still, they can have different band index i.e. $v^{\alpha}_{\mathbf{q}\nu,\mathbf{q}\mu} \neq 0$ in general even if $\nu \neq \mu$. However, the Lorentzian τ_{nm} selects only modes that are almost degenerate within the sum of their linewidths, $|\omega_{\mathbf{q}\nu} - \omega_{\mathbf{q}\mu}| \lesssim \gamma_{\mathbf{q}\nu} + \gamma_{\mathbf{q}\mu}$. Since the number of bands is discrete even in the thermodynamic limit and in practice the distance between band is usually much greater than the sum of linewidths, the contribute to conductivity is not null only when $\mathbf{q} = \mathbf{p}$ and $\nu = \mu$.

To summarize, in the Bloch basis and with the hypothesis of well-spaced bands, only the diagonal terms of v^{α} and τ, $\tau_{\mathbf{q}\nu,\mathbf{q}\nu} = \frac{1}{2\gamma_{\mathbf{q},\nu}}$, contribute. Thus, the final formula for heat conductivity can be rewritten as:

$$\kappa_{\alpha\beta} = \frac{1}{2V} \sum_{\mathbf{q}\nu} c_{\mathbf{q}\nu,\mathbf{q}\nu} v^{\alpha}_{\mathbf{q}\nu} v^{\beta}_{\mathbf{q}\nu} \frac{1}{\gamma_{\mathbf{q}\nu}} \tag{3.24}$$

which remarkably coincides with the solution of BTE-RTA [15](RTA stands for Relaxation Time Approximation).

3.5 Results

In the following figures there are some of the numerical tests presented in *Isaeva et. al, 2019* [9]. QHGK formula, quantum or classical, has been applied for an amorphous silicon of 1728 and 13824 atoms. The former physical system, together with a smaller a-Si of 512 atoms, will be the benchmarks of most of our numerical experiments.

In Fig. 3.1 we can see a comparison between classical QHGK and a Green-Kubo Molecular Dynamics approach. There is a good agreement until high temperatures $\sim 800 - 1000$ K. Such behaviour was expected, because at higher temperatures, the higher order anharmonicities can not be neglected anymore for QHGK (the average quadratic displacement from the equilibrium position does increase with temperature). On the other hand, the molecular dynamics approach works with all the potential, not its truncated expansion.

In Fig. 3.2 we can observe a similar comparison between quantum QHGK, Allen-Feldman approach [[1],[5]] and experimental results. On overall quantum QHGK seems to give a good estimate of the conductivity. However, at low temperature ($\lesssim 100K$) the different experimental data sets overlap and it can be noticed that QHGK is underestimating the experimental results. On the other hand, for higher temperature the experimental data are quite scattered, therefore even if all the QHGK results are between experimental points, it is hard to obtain definitive conclusion on the accuracy of the method. For instance, it seems that for higher temperatures QHGK tends to overestimate most experimental data. This spread of experimental data is usually due to impurities in the production of the glasses. It is almost impossible to reproduce twice exactly the same glass through the usual process of melting and quickly cooling off. On the other hand, some of the discrepancies in theoretical and experimental data could be due to some approximations in QHGK formulation that will be discussed later.

In the plot is also shown the Allen-Feldman approach. In this case, such approach reduces to an QHGK where all the linewidths are equal to η. In general, it can be noticed that the result depends strongly on the choice of η and it is usually worse than quantum QHGK. The fact that in QHGK method the γ_n are obtained by first-principles, the FGR, and they can be all different proves how more general is this theory in comparison to the Allen-Feldman approach where the choice of the parameter η is usually suggested by experiments.

Finally, in Fig. 3.3 it can be observed what do we mean when we talk about classical limit at high temperature. The differences between the results of the two version of QHGK seems to disappear for temperatures of order $\sim 800K$.

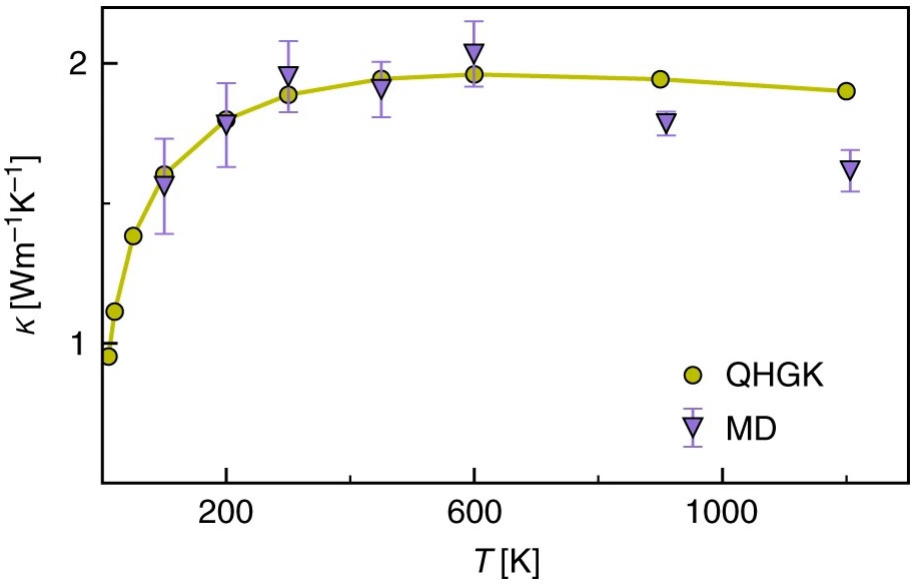

Figure 3.1: Comparison between the thermal conductivity of a-Si 1728 atoms supercell computed by classical QHGK or by classical Green-Kubo using molecular dynamics. The κ_{xx}, κ_{yy}, κ_{zz} are averaged to obtain a value corresponding to an isotropic amorphous media. Picture drawn from *Isaeva et. al, 2019* [9]

3.5.1 Software: kALDO

All the previous results can be reproduced using kALDO. All the necessary documentation in the link. This same program, with little changes, has been used for most of the calculations of this thesis.

3.5.2 Benchmark: a-Si

Since most of the tests will be performed over this sample of a-Si of 1728 atoms, let us show some features of this material. In Fig. 3.4 it is represented the spatial configuration of the system.

To obtain the amorphous silicon with its configuration and potential at equilibrium the "recipe" is the usual for a glass: melting and then slowly cooling a Si-crystal. The simulation can be done using, for instance, LAMMPS. For the interested reader Here there is an example of how to create the second and third order matrix using LAMMPS.

In all of our discussions, the main parameters are ω_n and their linewidths γ_n, and especially their ratio γ_n/ω_n is important since it is what confirm or not that

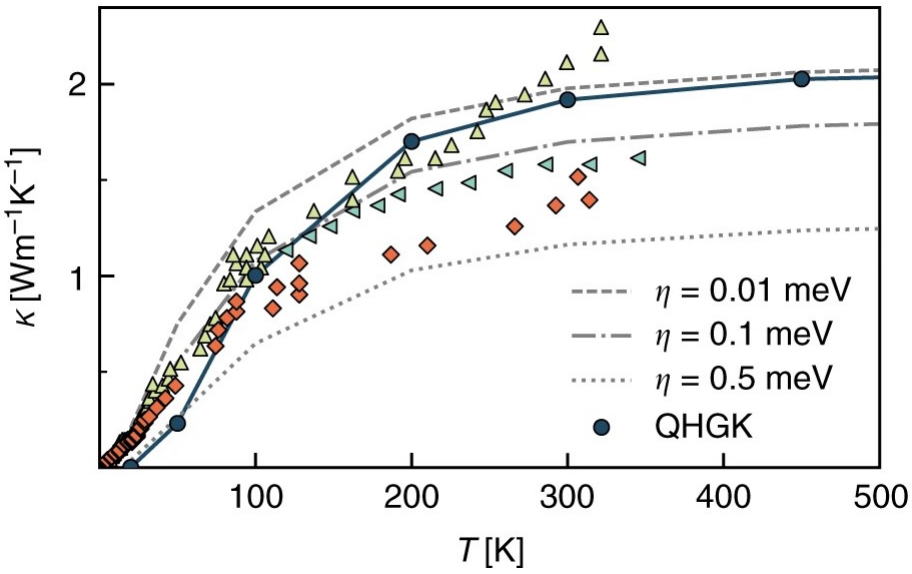

Figure 3.2: Thermal conductivity of a-Si 13824 atoms supercell computed by quantum QHGK approach compared to Allen-Feldman [[1],[5]] approach for various line-widths η and experimental data (Ref. [16] green triangles- rhombus)(Ref. [4] blue triangles). Picture drawn fro, *Isaeva et al, 2019*[9]

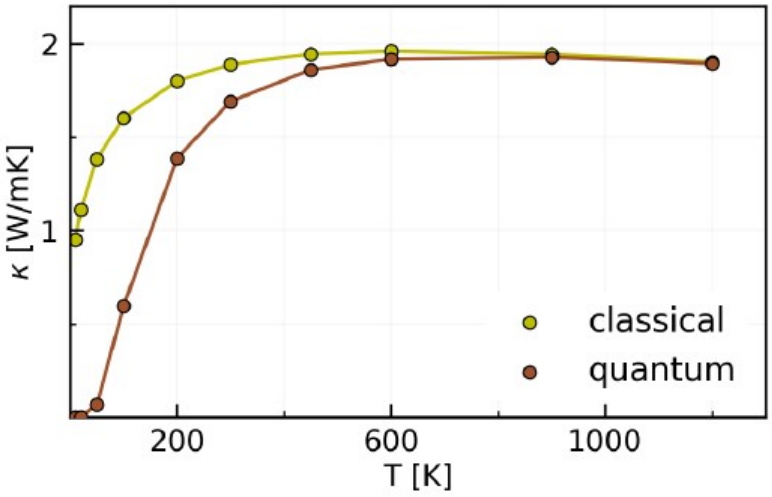

Figure 3.3: Thermal conductivity of a-Si 13824 atoms supercell computed by quantum and classical QHGK approach. Picture drawn from *Isaeva et al, 2019* [9]

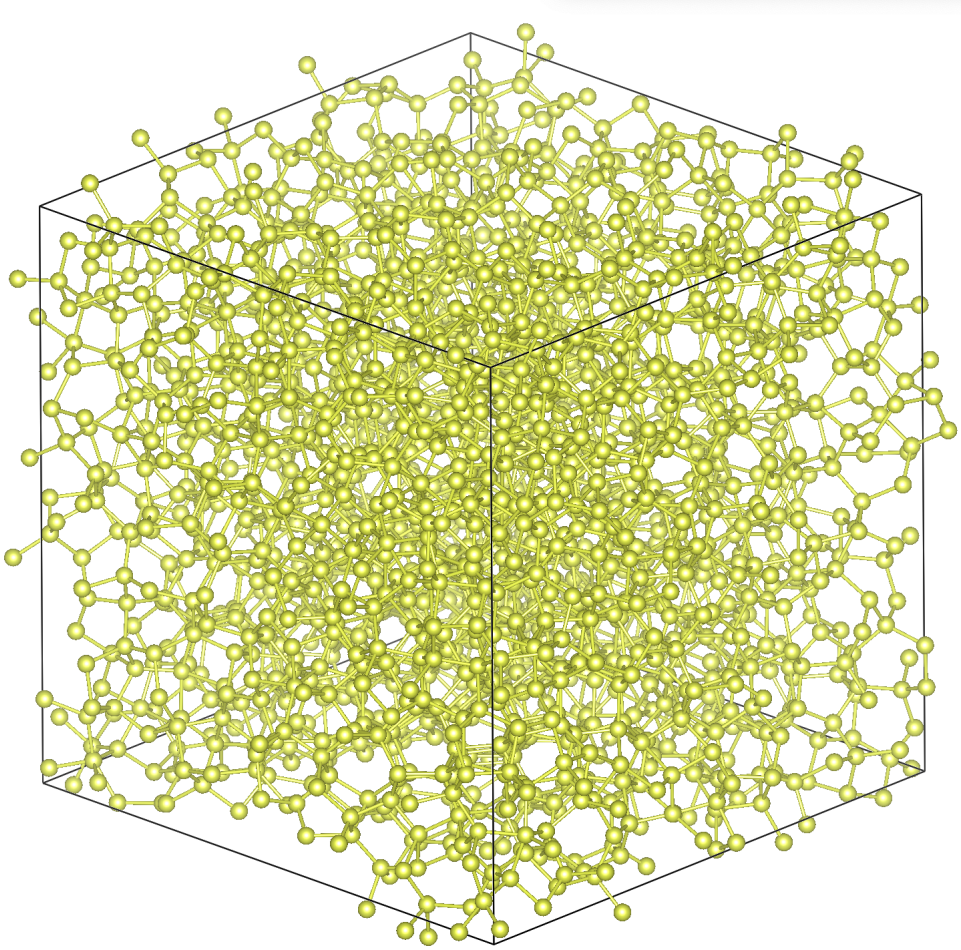

Figure 3.4: Spatial configuration of a-Si 1728. Image done with VESTA.

we are in the quasi-harmonic regime. In Fig. 3.5 there is a plot of the inverse-life times and the frequencies. First, it can be noticed how such γ are indeed far smaller than the frequencies, but they increase monotonically with T.

This positive correlation between γ and T can be understood by studying Eq. 3.17. In such equation all the dependence on temperature is given by the product of bose-eistein functions $\frac{n_j n_l}{n_n}$, which are increasing functions in respect of the temperature. In the large-temperature limit we can find even an accurate estimate of the dependence. Since $\lim_{T\to\infty} n_n = \frac{k_b T}{\hbar\omega_n}$, after the product $\frac{n_j n_l}{n_n}$ it remains a linear dependence on T.

Another important features is the density of modes or states (DOS), which we can see in Fig. 3.6. The range in THz is between 0 and ~ 18. The low-frequencies behaviour is worth some words. For any crystal, or in general for a material that

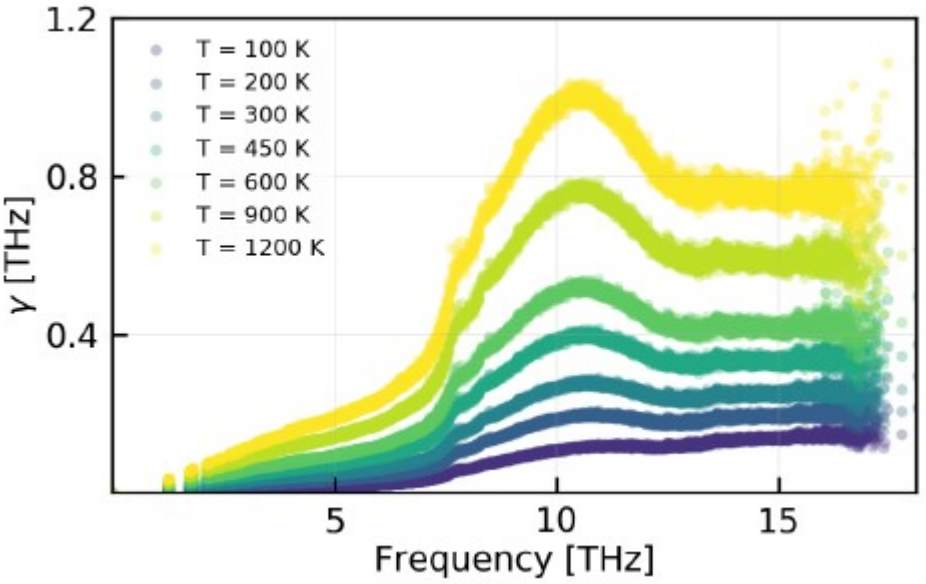

Figure 3.5: Linewidths and frequencies for different temperatures for a-Si 1728. Picture drawn from Ref. [9]

after a certain scale is homogeneous, it is well known that in 3-dimension the density of modes near the origin should be $\sim \omega^2$. Such feature can be proved in a crystal using the common formula for density of and the linear dispersion $\omega = c_s \mathbf{q}$, which holds for small wave-vector $\mathbf{q}$ and where c_s is the speed of sound. In Fig. 3.6 such ω^2 behaviour is not shown, or at least it seems there are some empty intervals without frequencies. This matter will be treated later, when size effects will be discussed. Indeed, the number of modes is proportional to the number of atoms (times the dimension), therefore with few atoms there are few frequencies and the density of modes can be flawed.

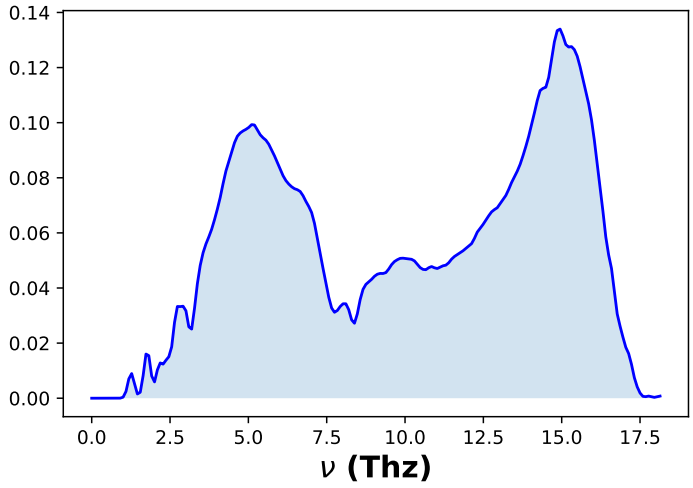

Figure 3.6: Density of modes a-Si 1728. On the x-axis there are the frequencies $\nu = \omega/2\pi$.

Last but not least, we are going to talk about the flux v^{α}_{nm}. Since in Eq. 3.22 there is a product of flux, we are going to watch the quadratic term $(v^{\alpha}_{nm})^2$. As α it has been chosen the axis x, but it has been verified that it makes little difference, since the material is in first approximation isotropic.

For a better visualization a log scale has been used. In Fig. 3.7 all the flux matrix has been rappresented. Apart from the diagonal, which must be zero since the flux in this basis is antisymmetric, there is not a clear pattern, even if it seems that there is a certain concentration of high flux near the diagonal, especially for the first half of frequencies. Indeed, a closer look shows that if we restrict our range to the first 100 frequencies (Fig. 3.8), which have $\nu < 2.8THz$, there is an interesting trend. Apart from the zero diagonal, all the higher values are near the diagonal. This means that v_{nm} is higher when n, m have similar energies. This pattern is more visible for smaller frequencies, which are also the most occupied, especially for low temperatures. This property of of the flux could provide, together with τ_{nm}, another filter for contributes from modes with great difference in frequency/energy.

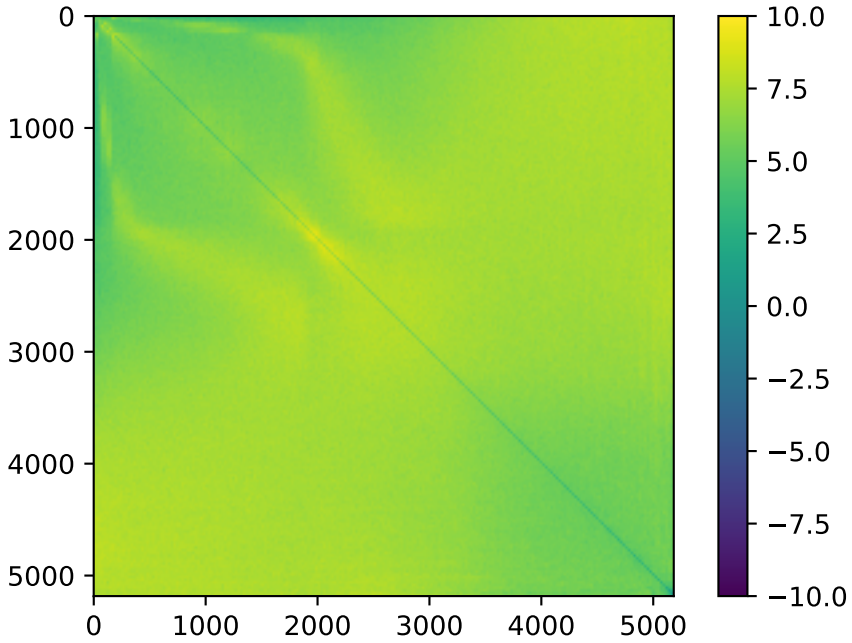

Figure 3.7: $(v^x_{nm})^2$ in log scale with all the 5184 $(1728 * 3)$ frequencies. Notice the blue diagonal line due to v_{nm} antisymmetry.

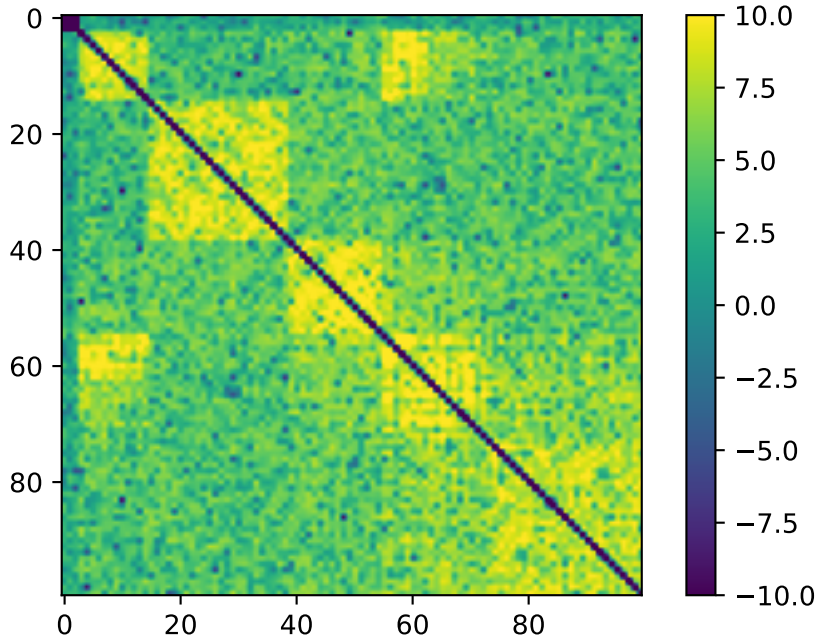

Figure 3.8: $(v_{nm}x)^2$ in log scale but with only the first 100 frequencies ($\nu < 2.8THz$).

Chapter 4

Long-tail effects, finite-size effect and other approximations

In the previous section, we briefly discussed the derivation of QHGK and some of its results. While the results seems promising, there are some approximations and hypothesis in the derivation and/or application of the formulas that are worth a discussion:

- Short-time behaviour of the Green's function $g(t)$
- orthogonality of the modes/ off-diagonal terms of the density matrix: $\langle \alpha_n \alpha_m \rangle = 0 + \dots$
- antiresonant term
- Size effect: how big should be our simulated system and does QHGK scales correctly with size?

Some of these arguments, like the antiresonant one and the orthogonality, are just a consequence of the quasi-harmonic limit $\gamma/\omega \to 0$. While these approximations are mathematically rigorous it is interesting to see when, for which range of temperatures for instance, and how much this quasi-harmonic limit is respected in a real material.

Estimating the size effect is a common problem when simulating materials, especially amorphous ones where one cannot use periodicity and its consequences i.e. the Bloch theorem .

A more subtle problem, and also the one that will be most studied in this thesis, is the short-term behaviour of $g_n(t)$. Until now, the correct first order large-time behaviour $e^{i\omega_n t - \gamma_n |t|}$ has been extended to short time. However, we do not studied when this large time behaviour kicks in and how different the real time-evolution and the extended large-time limit really are.

4.1 Sum rules

The first hint about if we should change or not the Green-function is given by the sum rules, which are usually the zero-time derivatives of the correlation/response-functions, or in the frequency representation the momenta of the spectrum. For instance:

$$g_n(t=0) = \frac{1}{n_n}\langle \hat{a}_n^\dagger(t)\hat{a}\rangle|_{t=0} = 1 = \int_{-\infty}^{\infty} d\omega \tilde{g}_n(\omega) \tag{4.1}$$

where with $\tilde{g}(\omega)$ I intend the Fourier Transform (FT) defined as:

$$\tilde{f}(\omega) = \int_{-\infty}^{\infty} dt\ f(t)e^{-i\omega t}$$

$$f(t) = \frac{1}{2\pi}\int_{-\infty}^{\infty} d\omega\ f(t)e^{i\omega t}$$

Surely, $g(t) = e^{i\omega t - \gamma|t|}$, or its FT $\frac{2\gamma}{\omega^2+\gamma^2}$, obeys to the zero-th sum-rule.

Second sum rule

However, the Lorentzian function $\frac{2\gamma}{\omega^2+\gamma^2}$ does not respect the second sum rule. Indeed, the second derivative in $t = 0$ should be the harmonic part ω_n^2 plus a small correction, something like:

$$-\partial_t^2 g_n(t)|_{t=0} \approx \omega_n^2 + \mathcal{O}(V_{nml}). \tag{4.2}$$

Instead of this finite quantity with the Lorentzian we obtain:

$$-\partial_t^2 g_n(t)|_{t=0} = \int_{-\infty}^{\infty} d\omega\omega^2 \tilde{g}_n(\omega) \tag{4.3}$$

$$= \int_{-\infty}^{\infty} d\omega\omega^2 \frac{2\gamma}{\omega^2+\gamma^2} = +\infty. \tag{4.4}$$

This second sum rule is **clearly** not respected.

Another hint about the problems of the Lorentzian can arrive from stationarity. Since:

$$\langle \alpha_n(t_0)^* \alpha_n(t_0)\rangle = constant$$

then

$$2\,\mathrm{Re}\langle \partial_t \alpha_n(t+t_0)^* \alpha_n(t_0)\rangle_{t=0} = 0. \tag{4.5}$$

Which means that the first derivative in zero should be only imaginary but $e^{i\omega t-\gamma|t|}$ does respect only in "principal value", i.e. the average of the right and left derivative is imaginary, but they are different and not totally imaginary.

4.2 Long tails

The mathematical problem with the second sum rule is the slow decay of the Lorentzian function. To obtain a finite value, $\tilde{g}_n(\omega)$ should decays asymptotically faster than $1/\omega^3$. In genereal, to have all the sum rules finite, the spectrum of the propagator should decays faster than any inverse polinomial.

To summarize, a possible correct ansatz for $\tilde{g}_n(\omega)$ should have a Lorentzian behaviour for small- frequencies (long-times), an asymptotic "faster than any inverse polynomial" decay and still be peaked near ω_n.

How would change QHGK formulas if we modify the Green-Function? Only the calculation of τ_{nm}. Indeed its resonant part was obtained computing :

$$\tau_{nm} = \frac{1}{2}\int_0^\infty dt\ g_n^*(t)g_m(t) + g_n(t)g_m^*(t) = \frac{1}{2}\int_0^\infty dt\ 2\,\mathrm{Re}(g_n^*(t)g_m(t)) =$$

Using the convolution theorem and time-reversal symmetry, τ_{nm} can be rewritten as:

$$\tau_{nm} = \frac{1}{4\pi}\int_{-\infty}^\infty d\omega'\ \mathrm{Re}(\tilde{g}_n^*(-\omega')\tilde{g}_m(\omega')) = \frac{1}{4\pi}\int_{-\infty}^\infty d\omega'\ \mathrm{Re}(\tilde{g}_n(\omega')\tilde{g}_m(\omega')), \quad (4.6)$$

where we used that for generic functions f, h:

$$FT[f * h, \omega] = \frac{1}{2\pi}\int_{-\infty}^\infty d\omega'\ f(\omega - \omega')h(\omega')$$

and

$$FT[f(t), \omega = 0] = \int_{-\infty}^\infty dt\ f(t)$$

Preliminary tests

In the next chapters it will be discussed how finding an ansatz for the propagator which satisfies all of our requests. But before that, it is worth doing some tests to see, or at least have an hint, of what could happen and if the result could be relevant.

The tests consisted of modifying the matrix τ_{nm} and then studying how this change affected the value of the conductivity.

I have tried:

- a truncated Lorentzian
- a Gaussian τ_{nm}

The first test consisted of imposing a threshold over the Lorentzian τ_{nm}. The aim of this test was seeing hom much the off-diagonal (in energy) terms contribute. This analysis involves also the form of c_{nm} and v_{nm} (see Eq. 3.22). For instance if v_{nm} were practically diagonal in energy, the tail of Lorentzian would not matter in any case.

The second test is imposing a Gaussian shape to τ_{nm}. This ensures that the tails falls fast enough to have all the momenta/sum rules finite (not necessarily with the correct values, but finite). Since the spectrum is normalized, zero-th sum rule, what we take from the tails goes to the peak. Therefore, a Gaussian-kind τ_{nm} would prioritize the near diagonal contribute and as a consequence would further justify the neglecting of the anti-resonant term.

Test 1: threshold

The Lorentzian τ_{nm} has been substituted with:

$$\tau_{nm}^{th} = \begin{cases} \frac{\gamma_n+\gamma_m}{(\omega_n-\omega_m)^2+(\gamma_n+\gamma_m)^2} & |\omega_n - \omega_m| < M_{th}(\gamma_n + \gamma_m) \\ 0 & elsewhere \end{cases} \tag{4.7}$$

where M_{th} is the threshold parameter.

In Fig. 4.1 there is an example of the importance of the off-diagonal contribution to κ. However the threshold needed for convergence is not equal for all the temperatures, is smaller for higher temperature. While analyzing this trend, we must remember the results presented in the benchmark part of Sec. 3.3: $\gamma_n(T)$ is an increasing function and v_{nm}^2 is not homogeneous, but in certain frequency intervals it is dominated by the near diagonal terms. Combining these two facts, if only frequencies with $|\omega_n - \omega_m| < \Delta\omega$ contribute to the conductivity, then the convergence tolerance M_{th} is:

$$M_{th}(T) \approx \frac{\Delta\omega}{\gamma(T)} \tag{4.8}$$

and since γ-s increase with temperature, then M_{th} decreases. Truth to be told, we oversimplified a little the discussion, since the $\Delta\omega$ can be also a function of the frequency in the following sense: $\kappa = \sum_n \kappa_n$ and every conductivity per mode could have its own $\Delta\omega_n$. However, this should not affect the previous qualitative speech about increasing γ and decreasing number of γ needed to cover the relevant frequency range.

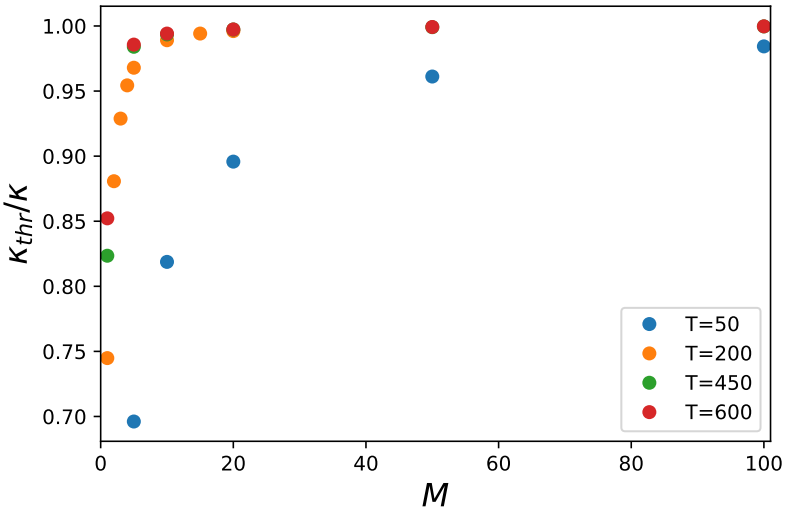

Figure 4.1: Ratio $\kappa_{thr}(M)/\kappa$ for different temperatures.

Test 2: Gaussian

In the second test the Lorentzian function:

$$\tau_{nm} = \frac{\gamma}{(\Delta\omega)^2 + \gamma^2}, \tag{4.9}$$

where $\gamma = \gamma_n + \gamma_m$ and $\Delta\omega = \omega_n - \omega_n$, it has been substituted with a function with the same normalization:

$$\tau^g_{nm} = \pi\sqrt{\frac{1}{\pi\gamma^2}}e^{-(\Delta\omega)^2/\gamma^2}. \tag{4.10}$$

The Gaussian function decays faster but for small $\Delta\omega$ has a larger value, indeed $\frac{\tau^g_{nn}}{\tau_{nn}} = \sqrt{\pi} \approx 1.77$. In Fig. 4.2 it is shown a plot of τ^g_{nm}/τ_{nm} for an a-Si 512 for any couple n, m of modes. As expected, the Gaussian kernel is higher near the diagonal, where $\Delta\omega$ is small, with a maximum of $\sqrt{\pi}$. Off the diagonal, the ratio between the two kernels goes to zero. However, it is worth noticing that the broadness of the near-diagonal/off-diagonal is not constant, it is an increasing function of the frequency. This was expected, because the broadness of the Gaussian is given by the γ_n and on average they do increase together with frequency.

In Fig. 4.3 it can be observed the effect of this "squeezing" of the kernel, for small temperatures there is almost no effect while for higher ones the "gauss-conductivity" surpasses the original one.

A possible explanation of this trend could be that in a certain range of difference of energy all the modes gives somehow the same values of $c_{nm}v^\alpha_{nm}v^\beta_{nm}$, therefore

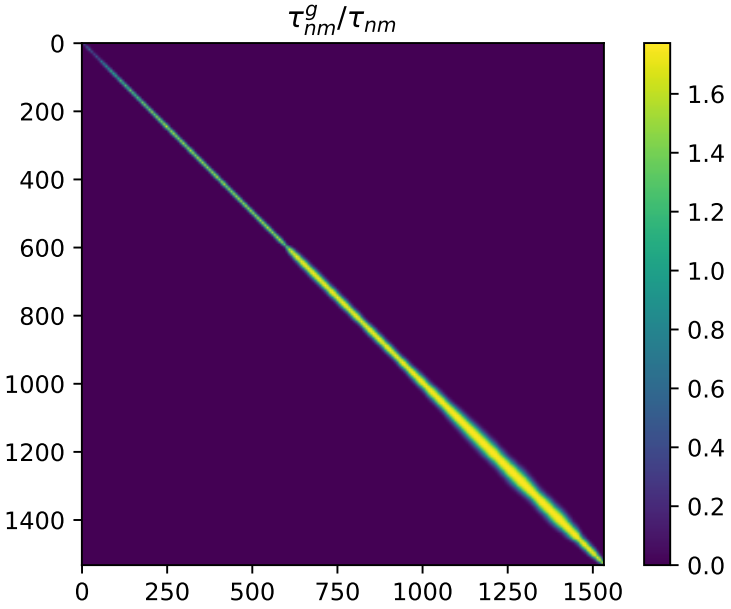

Figure 4.2: τ^g_{nm}/τ_{nm} for a-Si 512 at $T = 600$. In the axis, the n and m-th indices of the $512 * 3 = 1536$ modes. The maximum is indeed $\sqrt{\pi}$.

as long the Gaussian decays inside this range, the increase of the peak and the decrease of the tail, in comparison to the Lorentzian, compensate each other. However, when γ increases at high temperatures, the Gaussian gets broader and all the relevant modes are inside the range where the Gaussian is larger than the Lorentzian. Moreover, as seen in Fig. 4.2 the "larger-than-Lorentzian-zone" is broader for higher frequencies which are more occupied at higher temperatures, and almost empty at low temperatures.

All this reasoning could be explained by the structure of other matrices in Eq. 3.22. For instance, in c_{nm} there is $\frac{n_n - n_m}{\omega_m - \omega_n}$ which decreases when $|\omega_n - \omega_m|$ grows because n_n is a convex function. Another guess could be that v_{nm} decreases when the modes have too different energy, which indeed it happens for small energies, as seen in Sec. 3.3

To summarize the results of these tests, there is a relevant contribute of off-diagonal modes and substituting the Lorentzian with a squeezed function, faster decay but higher peak, can have relevant effects.

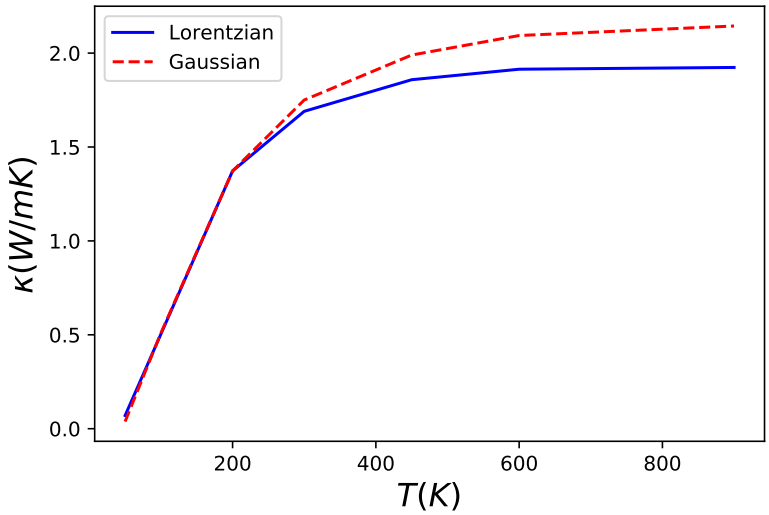

Figure 4.3: The heat conductivity with a Lorentzian and Gaussian kernel for different temperatures. a-Si 1728.

4.3 Antiresonant term

As seen in Eq. 3.13 classically and accordingly in the quantum case, the complete τ_{mn} should contain a resonant, but also an antiresonant term, proportional to:

$$\tau_{nm}^{ar} = \frac{(\omega_n - \omega_m)^2}{4\omega_m\omega_n} \frac{\gamma_n + \gamma_m}{(\omega_n + \omega_m)^2 + (\gamma_n + \gamma_m)^2} \tag{4.11}$$

Since the antiresonant condition can not be satisfied because all the ω_n are positive, only the tail of this Lorentzian matters. Not only in the quasi-harmonic regime these tails are neglectable, but there is also a prefactor that we could estimate of order $(\gamma/\omega)^2$ for the relevant range of frequencies. Furthermore, correcting the Lorentzian spectrum with another one with faster decay would further decrease this antiresonant contribute .

Let us verify our suppositions. The easiest way to do it is to define:

$$\tau'_{nm} = \tau^0_{nm} + \frac{\gamma_n + \gamma_m}{(\omega_n + \omega_m)^2 + (\gamma_n + \gamma_m)^2}. \tag{4.12}$$

This will **overestimate** the effect of the antiresonant term, since we are omitting the (generally very small in the relevant near-diagonal zone) prefactor $\frac{(\omega_n-\omega_m)^2}{4\omega_m\omega_n}$.

In Fig. 4.4 there is a plot of the relative error $\frac{\kappa_{ar}-\kappa}{\kappa}$. The correction is of order $0.01\% - 0.1\%$ and it does increase with temperature. Also in this case, this trend

can be explained through $\gamma_n(T)$. We are just adding the tails of a Lorentzian, and the larger is γ, the bigger is the weight of the tails.

Since even this overestimate of the antiresonant term is small, it confirms in first approximation we can neglect such antiresonant contribute.

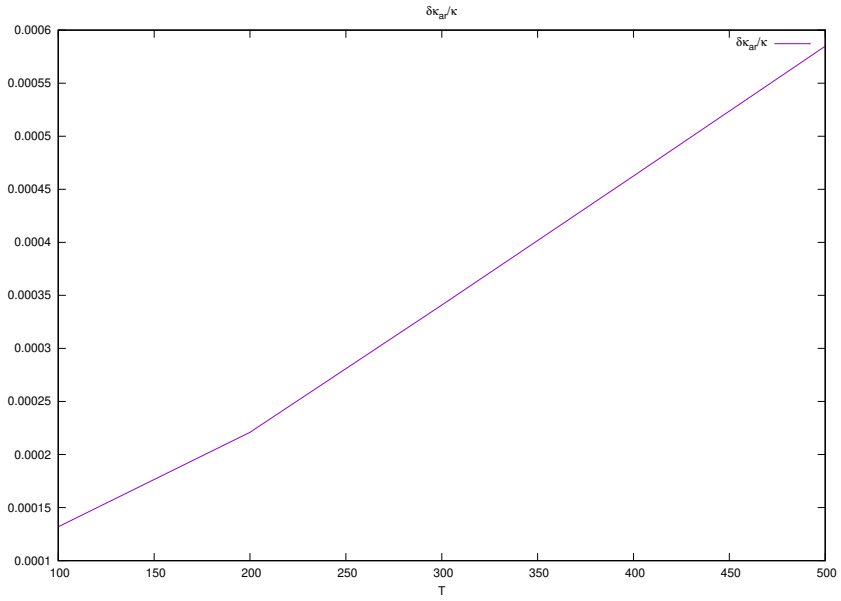

Figure 4.4: Relative error between the conductivity and the conductivity calculated with τ'_{nm}.

4.4 Anharmonic effects on canonical averages

Off-diagonal occupation: $\langle \alpha_n^* \alpha_m \rangle$

Until now, we did the expectation value of same-time observables just like we were in a pure harmonic system. But we are not. Since the hamiltonian has some anharmonicities, the canonical average should have been done with both the harmonic part H_0 and the anharmonic one H_A. Only for this discussion I will introduce the following notation: $\langle \cdot \rangle_{eq}$ and $\langle \cdot \rangle_A$ are respectively the canonical average for a pure harmonic system and for the system with also anharmonicities.

Since we are interested in the quasi-harmonic regime, and for vanishing V_{nml} the system becomes a pure harmonic one, we will try a perturbative approach, approximating the $\langle \cdot \rangle_A$ with a sum of $\langle \cdot \rangle_{eq}$. All the discussion will be done for a classical system, but the corresponding quantum one is very similar and gives qualitatively the same results.

Firstly, let us remind that the canonical average for an hamiltonian H is defined as:

$$\langle A \rangle = \frac{1}{Z} \int d\boldsymbol{\xi} d\boldsymbol{\pi} \; e^{-\beta H(\boldsymbol{\xi},\boldsymbol{\pi})} A(\boldsymbol{\xi},\boldsymbol{\pi}), \tag{4.13}$$

where Z is the partition function. Let us enunciate the expectation values for some key quantities in the harmonic case:

$$\langle \xi_n \xi_m \rangle_{eq} = \delta_{nm} \frac{k_b T}{\omega_n^2} \tag{4.14}$$

$$\langle \pi_n \pi_m \rangle_{eq} = \delta_{nm} k_b T \tag{4.15}$$

$$\langle \alpha_n^* \alpha_m \rangle_{eq} = \delta_{nm} \frac{k_b T}{\omega_n} \tag{4.16}$$

To evaluate $\langle \alpha_n^* \alpha_m \rangle_A$ let us start with the partition function:

$$\begin{aligned} Z_A &= \int d\boldsymbol{\xi} d\boldsymbol{\pi} \; e^{-\beta(H_0 + \frac{1}{6}\sum_{pqr} V_{pqr}\xi_p\xi_q\xi_r)} \approx \\ &\approx \int d\boldsymbol{\xi} d\boldsymbol{\pi} \; e^{-\beta H_0} \left(1 - \beta \frac{1}{6} \sum_{pqr} V_{pqr}\xi_p\xi_q\xi_r + \frac{\beta^2}{2} \left(\frac{1}{6} \sum_{pqr} V_{pqr}\xi_p\xi_q\xi_r) \right)^2 \right). \end{aligned} \tag{4.17}$$

While the hamiltonian is purely harmonic, we are evaluating Gaussian momenta and it is well-known that all the odd momenta of the Gaussian are null, therefore the corrections up to first order are null. Instead, up to second order we have:

$$Z_A = Z_{eq} \left(1 + \frac{\beta^2}{2} \left\langle \left(\frac{1}{6} \sum_{pqr} V_{pqr}\xi_p\xi_q\xi_r) \right)^2 \right\rangle \right) \tag{4.18}$$

Expanding $\frac{1}{Z_A} \approx \frac{1}{Z_{eq}} \left(1 - \frac{Z_A - Z_{eq}}{Z_{eq}} \right)$ and performing similar calculation we obtain that:

$$\begin{aligned} \langle \alpha_n^* \alpha_m \rangle_A &= \frac{1}{Z_A} \int d\boldsymbol{\xi} d\boldsymbol{\pi} \; e^{-\beta(H_0 + \frac{1}{6}\sum_{pqr} V_{pqr}\xi_p\xi_q\xi_r} \alpha_n^* \alpha_n \approx \\ &\approx \int d\boldsymbol{\xi} d\boldsymbol{\pi} \; e^{-\beta H_0} \left(1 - \beta \frac{1}{6} \sum_{pqr} V_{pqr}\xi_p\xi_q\xi_r + \frac{\beta^2}{2} \left(\frac{1}{6} \sum_{pqr} V_{pqr}\xi_p\xi_q\xi_r \right)^2 \right) (\alpha_n^* \alpha_n). \end{aligned} \tag{4.19}$$

Then, with further simplifications we obtain:

$$\langle \alpha_n^* \alpha_m \rangle_A \approx \frac{1}{Z} \left(1 - \frac{\beta^2}{2} \left\langle \left(\frac{1}{6} \sum_{pqr} V_{pqr} \xi_p \xi_q \xi_r \right)^2 \right\rangle \right) \times$$
$$\int d\boldsymbol{\xi} d\boldsymbol{\pi} \; e^{-\beta H_0} \left(1 - \beta \frac{1}{6} \sum_{pqr} V_{pqr} \xi_p \xi_q \xi_r + \frac{\beta^2}{2} \left(\frac{1}{6} \sum_{pqr} V_{pqr} \xi_p \xi_q \xi_r \right)^2 \right) \alpha_n^* \alpha_n \quad (4.20)$$

In the end, since the fifth momenta is odd and therefore its average is null, the correction to $\langle \alpha_n^* \alpha_m \rangle$ is of order $|V_{nml}|^2$ (also γ_n is proportional to $|V_{nml}|^2$). To summarize, it is safe to assume that when $\gamma/\omega \to 0$ also these off-diagonal terms can be neglected.

4.4.1 Equilibrium position at finite temperature

In this paragraph it will be shown that $\langle \alpha_n \rangle \neq 0$ at finite temperature. This obligate us to redefine partially $g_n(t)$. Indeed, we want $g_n(t)$ to goes to zero for large times, but $\lim_{t\to\infty} \langle \alpha_n^*(t) \alpha \rangle = \lim_{t\to\infty} \langle \alpha_n^*(t) \rangle \langle \alpha_n \rangle = \langle |\alpha_n|^2 \rangle \neq 0$. For this reason, as it is commonly done, the product of the averages will be subtracted from the autocorrelation.

However, let us understand what are the causes and the magnitude of not null average $\langle \alpha_n \rangle$. It is well-known that the diffusion of the (quasi-)harmonic approximation is due the ability to describe the dynamics near the equilibrium. However, while the average position at $T = 0$ coincides with the minimum of the potential, this is not true anymore for $T > 0$. Indeed

$$\langle \xi_n \rangle_A \approx \frac{1}{Z} \int d\pi \int d\xi e^{-\beta H_{har}} \left(1 - \beta \frac{1}{6} \sum_{mjl} V_{mjl} \xi_m \xi_j \xi_l \right) \xi_n = -\frac{1}{2} \frac{1}{\omega_n^2} \sum_j V_{njj} \frac{k_b T}{\omega_j^2} \quad (4.21)$$

There is a simple physical explanation for these translation, for any finite temperature the average of the anharmonic part is no zero and the equilibrium position is translated in the material. The $\xi_{n,o}$ can be found by an equilibrium of the forces (let us imagine a spring in a constant gravitational field):

$$\omega_n^2 \xi_{n,0} = -\sqrt{2\omega_n} \langle F_{A,n}^* \rangle = -\frac{1}{2} \sum_{jl} V_{njl} \langle \xi_j \xi_l \rangle = \quad (4.22)$$
$$= -\frac{1}{2} \sum_j V_{njj} \frac{k_b T}{\omega_j^2}. \quad (4.23)$$

where $F_{A,n}$ is the anharmonic part of $\partial_t \alpha_n$:

$$F^*_{A,n} = \frac{i}{2\sqrt{2\omega_n}} \sum_{jl} V_{njl} \left(\frac{\alpha^*_j + \alpha_j}{\sqrt{2\omega_n}} \right) \left(\frac{\alpha^*_l + \alpha_l}{\sqrt{2\omega_n}} \right) \tag{4.24}$$

To summarize, due to the anharmonic part of the potential, at finite temperature the phonon oscillates near an equilibrium position which does not coincide with the minimum of the potential. Obviously a translation should not affect the fluctuations, which are always implicitly defined as the difference from the average value.

Then, there are two equivalent solutions. The first one consists of subtracting the average value which now is not zero. This is the standard procedure when the average is not zero. Thus $g_n(t) = \frac{1}{n_n}(\langle \alpha^*_n(t)\alpha_n \rangle) - \langle \alpha^*_n(t) \rangle \langle \alpha_n \rangle)$ and doing similarly for the energy flux and Eq. 2.32. The second solution would be of translating the phonons' position at every temperature. In other words, let us re-define α as:

$$\alpha'_n = \sqrt{\frac{\omega_n}{2}}(\xi_n - \xi_{n,0}) + \frac{i}{\sqrt{2\omega_n}}\pi_n \tag{4.25}$$

With this definition, now $\langle \alpha_n \rangle = 0$. With this translation the energy flux , Eq. 3.5, would change in the following way:

$$\begin{aligned} J'_\alpha &= J_\alpha + \frac{i}{2} \sum_{mn} v^\alpha_{nm} \omega_m \sqrt{2\omega_n} \xi_{0,n} (\alpha^*_m - \alpha_m) = \\ &= J_\alpha + \frac{d}{dt} \frac{}{2} \sum_{mn} v^\alpha_{nm} \sqrt{2\omega_n} \xi_{0,n} (\alpha^*_m + \alpha_m), \end{aligned}$$

where in the last equivalence I used $\partial_t(\alpha^*_m + \alpha_m) = i\omega_m(\alpha^*_m - \alpha_m)$. A recently established *gauge invariance* [12] states that adding a total derivative to the flux does not change the conductivity. So we could implicitly work in this translated basis and assume that $\langle \alpha_n \rangle = 0$. Furthermore even without this *gauge invariance* it would be easy to prove that extra part in the energy flux is neglectable. Firstly, because it is proportional $\propto \xi_{0,n} \propto V_{nml}$ and secondly since it depends on time only through α_m , α^*_m because the n part is constant, there is no possibility of a resonance. In the worst case it would contribute as an antiresonant term.

In conclusion, we proved that the not zero average of the anharmonic force causes no harm, since it can always be absorbed by a translation of the modes, which does not change the conductivity. For simplicity, we will keep working with the original basis, implicitly considering $g_n(t)$ as the autocorrelation minus the product of averages.

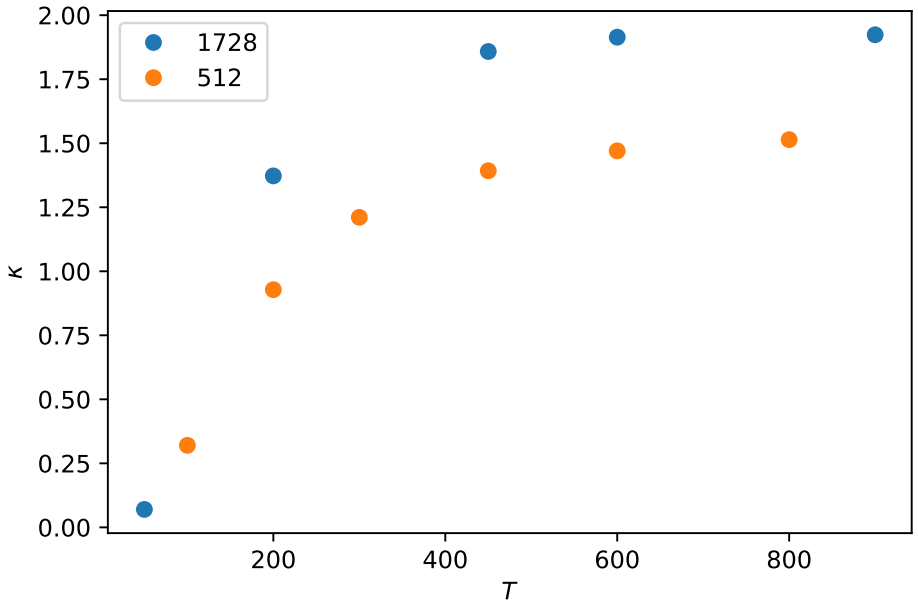

Figure 4.5: Caption

4.5 Size effect

The size of the simulated sample is always a compromise between the desire of having a sample as similar as possible as the real one, which usually has trillion of particles, and the necessity of limiting the computational weight and time of the simulation. In particular, while using QHGK on kALDO the bottleneck is given by the calculation of the γ_n, which for an amorphous costs $(3N)^3$, where N is the number of atoms. On the other hand, if there are not enough atoms, it is likely that the DOS will not be accurate.

Taking these two necessities in account, in this section we will discuss how the DOS and the results changes with the size, and then how using replicas of the supercell to speed up the calculation of the line-widths γ_n for larger systems.

Firstly, let us observe the importance that size can have. In Fig. 4.11 there is a plot of $\kappa(T)$ for the a-Si 512 and 1728 system. The larger system has an higher conductivity. This considerable difference proves that the 512 is still not at convergence in size. This is probably due to the DOS. The number of modes should be almost infinite in a real system and consequently the DOS should be dense, instead in our case we have few hundreds or thousands of modes and therefore the DOS is discrete and not at convergence. Such different DOS can be seen in

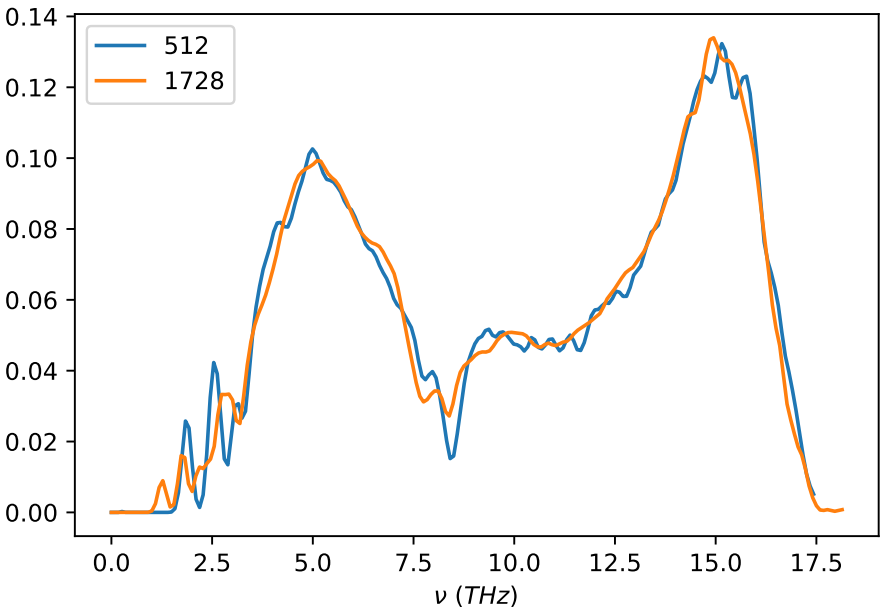

Figure 4.6: Density of states for a-Si 1728 and 512.

Fig. 4.6 and it can be noted that especially the low frequency regime is different: the 512 system is emptier there. Reasoning about crystals, this behaviour for low frequencies is perfectly natural. In a crystal that range is populated by small $q-$vectors since $\omega \propto q$ and small wavevectors are connected to long wavelengths. Indeed, for a finite sample the smallest $q \sim 2\pi/L$ where L is the length of the sample.

What are the consequences of a too empty DOS? Well, the γ_n are calculated with Eq. 3.17, where the DOS plays an important role through the presence of the δ function. Roughly speaking, the δ counts how many channels a mode can decay while satisfying the resonance condition. Numerically, the δ function is approximated with a peaked function (Gaussian, triangular, etc...) with a peak of order $\sim 1/\Delta\omega$ and a broadness of order $\Delta\omega$, where $\Delta\omega$ is the distance between two consecutive frequencies and obviously it is itself a function of the frequency. Mathematically, the δ function is well defined when the frequencies are dense, i.e. $\Delta\omega \to 0$. This explain why having a large sample and consequently a good DOS is important to compute correctly the life-times. In Fig. 4.7 there is a comparison of $\gamma_n - \nu_n$ for a-Si 512 and 1728. It can be observed that the shape of the function is very similar, but the larger system have higher γ_n. This proves 512 is not large enough to have a reliable $\gamma_n - \omega_n$ plot.

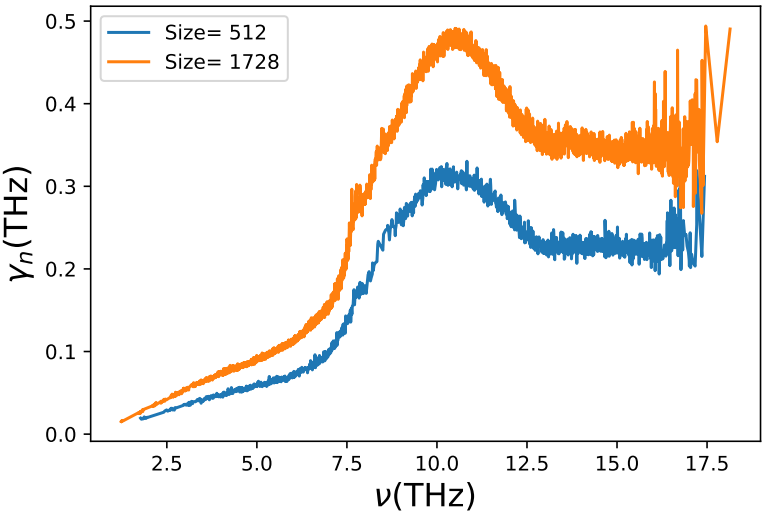

Figure 4.7: γ_n and $\nu = \omega/2\pi$ for a-Si 512-1728. $T = 600$ for both.

Is instead 1728 large enough? Fig. 4.8, drawn from *Isaeva et al.* [9], shows that there is indeed a difference between a-Si 1728 and its larger version 13824, but such difference is significant only at $T \lesssim 100K$ and its due to the low frequencies. To understand the plots, let us define a couple of quantities: the differential $\kappa'(\omega)$ and the conductivity accumulation function $\kappa(\omega)$.

The first quantity gives the contribute of every frequency to the conductivity. It is defined as:

$$\kappa'(\omega) = \frac{1}{3V} \sum_{\alpha} \sum_{nm} \Delta(\omega - \omega_n) c_{nm} (v_{nm})^2 \tau^0_{nm} \tag{4.26}$$

where $\Delta(\omega - \omega_n)$ is a broadened approximation of a delta function. The accumulation function is just the integral of κ':

$$\kappa(\omega) = \int_0^{\omega} d\omega' \; \kappa'(\omega'). \tag{4.27}$$

Obviously $\kappa(\omega \to \infty) = \kappa$.

Now, we can analyze Fig. 4.8. Looking at the accumulation function, it is clear that at $100K$ the difference is far greater that at $600K$, but apart from the first part of the plot the accumulation function are parallel. This is easily explained looking at $\kappa'(\omega)$. The contribute of the 13824 system is bigger just for the low frequency regime, which is reasonable since it is the zone where the 1728-DOS is emptier. The lack of low frequency also explain the temperature trend. At low temperatures, the low frequencies dominate due to their higher occupation n_n.

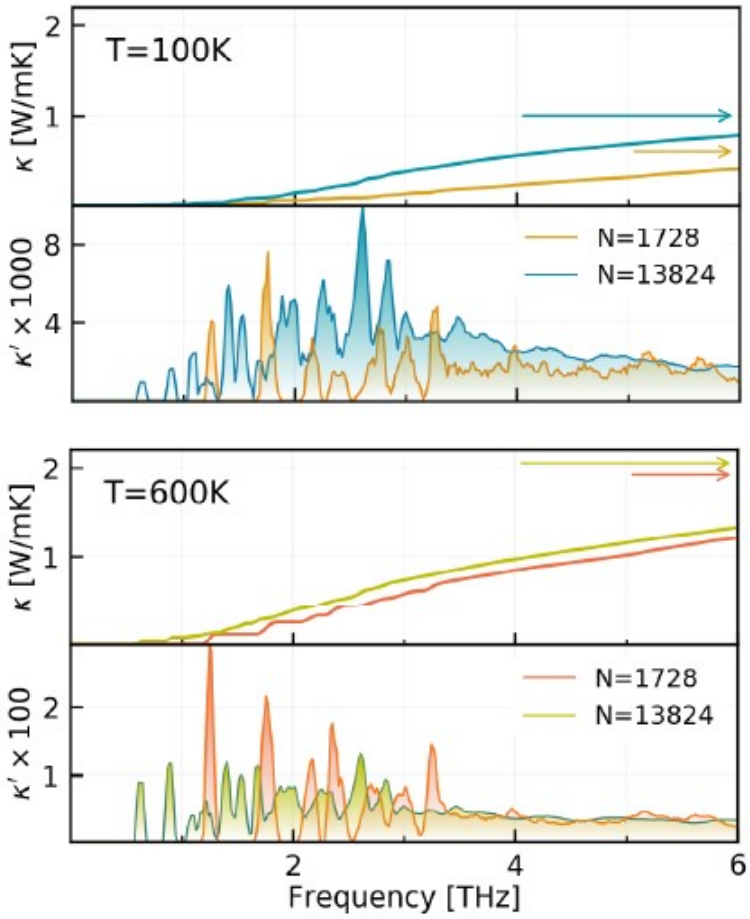

Figure 4.8: The differential and cumulative κ for a-Si 1728 and 13824 at $T = 100$ and $600K$. Figure drawn from [9].

How can we improve the DOS and the results avoiding the time-expensive brute force method of truly simulating very large systems? An intelligent use of replicas of the supercell can help. With that, I meant treating the amorphous like a crystal, replicating the 1728 atoms supercell few times, and then using all the usual periodic tools (bloch states et cetera). For details see kALDO's documentation. One of the advantages of this approach is that when the system is periodical the dynamical matrix, whose eigenvalues are the frequencies, is a block matrix, where every block has the dimension of an elementary cell. For instance, if my system is obtained replicating k times a cell with N atoms, then I have to diagonalize k times a $N \times N$ matrix, instead of diagonalizing once a $kN \times kN$ matrix.

In Figs. 4.9-4.10 the DOS of a $(3, 3, 3)$ and $(5, 5, 5)$ replicas is plotted, where with (a, a, a) I meant that the 1728 atoms elementary cell has been replicated a times in each direction. Comparing these figures with Fig. 3.6 we see major differences only in the low frequencies range, while the other part of the plot remains pretty much unchanged. It is important to notice that now the low frequency regime of the DOS has a parabolic $\propto \nu^2$ or, as it should be.

This quadratic behaviour is a well-known effect of spatial periodicity. However quite often the glasses are homogeneous after a certain scale, so we could expect that the small wavelength q and small ω limit ($\omega \sim c_s q$) of the periodic system would coincide with the low frequency behaviour of the large-size amorphous system.

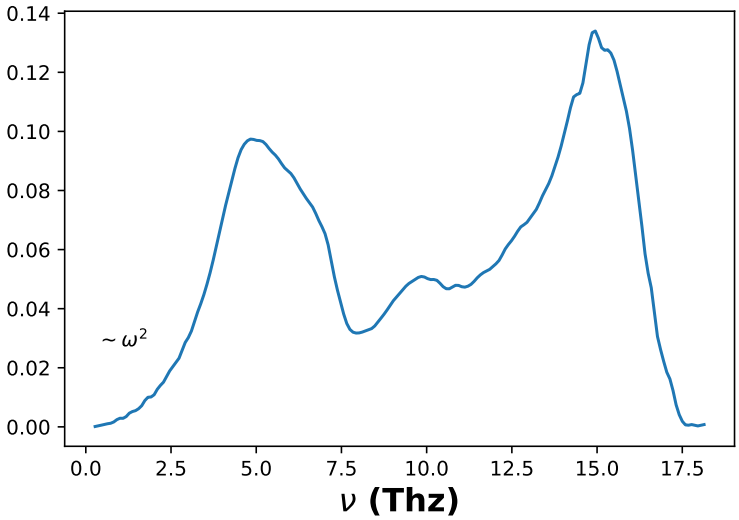

Figure 4.9: a-Si 1728 replicated $(3, 3, 3)$

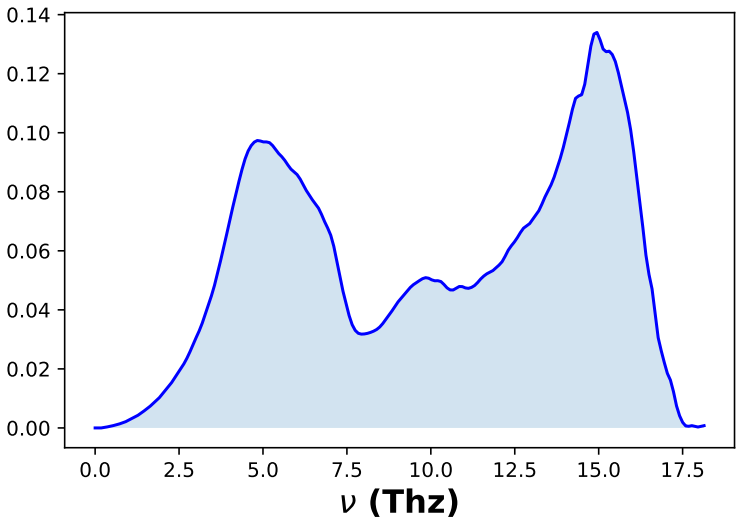

Figure 4.10: a-Si 1728 replicated $(5, 5, 5)$

Fitting decay rates γ_n from a small sample

With few replicas we obtained more physically reliable DOS, speeding up of a factor k in comparison of an amorphous with Nk atoms, where k is the number

of replicas. Just to say some numbers, for the $(5, 5, 5)$ case we gained a factor $5^3 = 125$.

However, as said before, the biggest computational problem when growing in size, it is the calculation of all γ_n, which has a cost proportional to N^3. The replicas could help, but the cost would remain of order $N^3 * k^2$. Luckily, periodicity and a fit can still save the day. At the moment we, the authors of [9] and me, are working to this project.

The idea is to fit the γs as a function of the frequency $\gamma_n = \gamma(\omega_n)$ for a system of reasonable size and then use this function $\gamma(\omega)$ for a larger system of the same kind. For instance if we assume that a-Si 1728 has a $\gamma_n - \omega_n$ plot pretty much at convergence in size, we could use it to fit the function $\gamma(\omega)$. Then we would use such function over the frequencies calculated with the replicas and magically we would obtain the γ_n for the replicated system. In this way we could fill the "holes" in the *DOS* of Fig. 3.6 and obtain the γ_n of these extra frequencies almost for free. To summarize, the procedure is:

- Simulate a system of size N and compute the γ_n
- use the γ_n to obtain a fit $f(\omega) = \gamma_n(\omega)$
- calculate the frequencies for a replicated system kN (not the line-widths, which are expensive!)
- Compute the γ_n for the replicated system applying the $f(\omega)$ on the frequencies. This scales as Nk.
- then calculate the conductivity for the replicated system

Fitting γ_n: results

The fit-and-replica method has been applied for the a-Si 1728 system. The system has been replicated $(3, 3, 3)$ times, so we have $3^3 = 27$ times more modes. Indeed we have previously seen that Figs. 4.9-4.10 have pratically the same DOS, so it is safe to assume that we have a convergence in size for the DOS.

The important points of the simulation have been the following ones. Firstly, simulating in the usual way a-Si 1728. Then, using Python3 library **scipy.interpolate** the linewidths have been interpolated. For building the interpolating function it has been used :

```
spl = scipy.interpolate.splrep(x, y),
```

where x are the frequencies and y the γ. This command finds the coefficient for a polynomial interpolation, then to calculate the γ of the replicated system it has been used:

```
gamma_k[phonons_with_k.physical_mode] =\
scipy.interpolate.splev(\
phonons_with_k.frequency[phonons_with_k.physical_mode], spl),
```

where physical mode is mask of $True$ and $False$ that can be potentially used to impose some cut-off. Since the plot $\gamma_n - \omega_n$ is quite noisy, Fig. 3.5, before fitting it have been implemented also an average by blocks, in order to have a smoother plot. For details see App. 8.2. Finally, the program with the replicated system has been launched as usual, but instead of calculating the linewidths from scratch, it used the γ_ns computed by interpolation.

In Fig. 4.11 there is a plot of the ratio between the extended (through replication system's heat conductivity and the normal a-Si 1728. While it is clear that the relative difference can be neglected for higher temperatures (3% at $100K$ and $\sim 1\%$ at $300K$), on the other hand it is notable for very low temperatures: at $T = 25$ the ratio κ_{ext}/κ is of order 3! This proves the importance of having a good DOS also for small frequencies. At low temperatures, the less energetic modes , low frequencies, are by far the most occupied ones and can dominate the conductivity. Up until now, we had an "empty" DOS for low frequencies, which was not a problem for large temperatures, but it is for low ones. Another positive point is that the value of κ has increased with this fit-and-replica technique and indeed Fig. 3.2 had shown that QHGK gives a lower conductivity than the experiments, for small temperatures.

Finally, we should compare our results of the replicated system with the a-Si 13824 studied by *Isaeva et al.* [9]. In Fig. 3 of such article (here reported as Fig. 4.8) it was shown how the 13824 system had a larger conductivity than the 1728 one, but the difference was very small for $T = 600$ and quite import for $T = 100$ and the difference were given mainly by the low frequencies. This is exactly what is happening with the replicas. This strongly suggests that there is indeed a size of the amorphous such that replicating that sample or studying a bigger amorphous sample of the same material gives the same result.

The effect of long tails on larger size

During the numerical experiments with τ_{nm} we observed the weight of off-diagonal term, for instance in Fig. 4.1. It is reasonable asking if such behaviour also changes with size, or if with an higher density of modes the diagonal terms become more dominant or if nothing changes. Fig4.12 seems proving that even if the the DOS is densier, the off-diagonal terms have pretty much the same contribute.

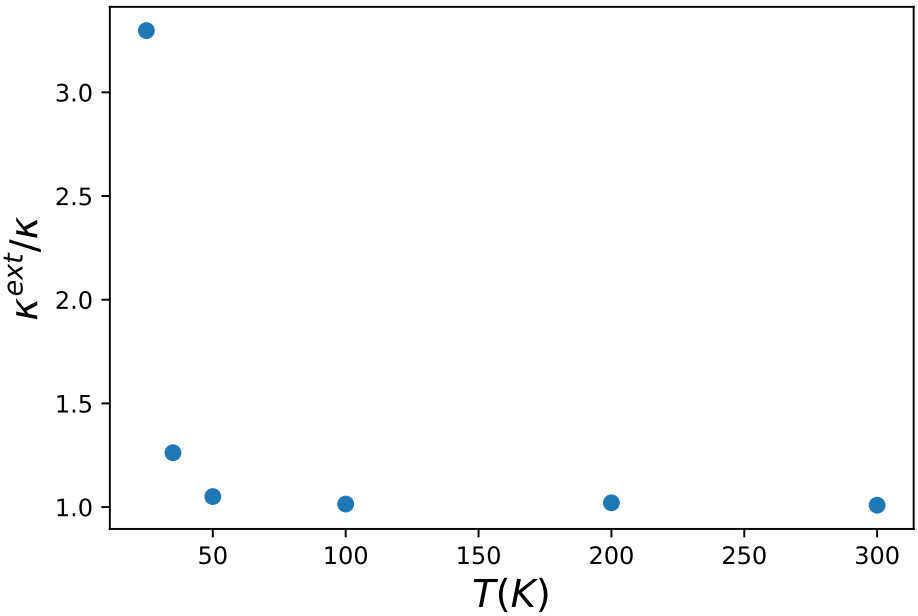

Figure 4.11: The ratio of κ_{ext}/κ for a-Si 1728 and its replicated $(3, 3, 3)$ system.

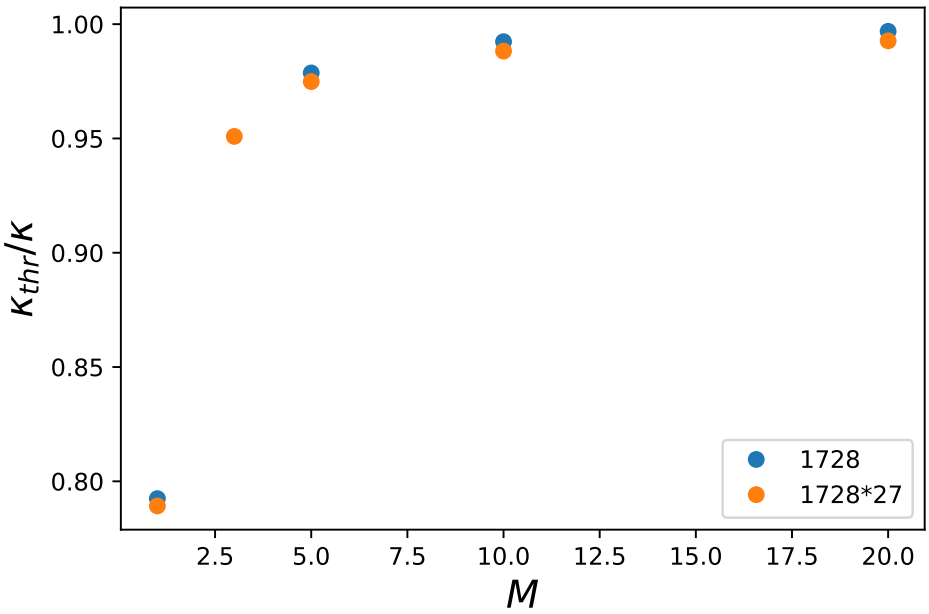

Figure 4.12: The effect of threshold at $T = 300K$ for a-Si 1728 and its replicated $(3, 3, 3)$-version

Chapter 5

Memory Function Formalism

In this chapter a new, more physical, phonon propagator will be suggested and studied. In order to obtain that, I will use the Mori function formalism (*Mori 1965* [13]). Using such a formalism it can be demonstrated that for a dynamical variable A the average autocorrelation $C_A(t) = \langle A(t)A(0)\rangle = \langle A(t+t_0)A(t_0)\rangle$ obeys to the following time evolution:

$$[\partial_t + i\Omega]C_A(t) + \int_0^t dt'\ \Gamma(t-t')C_A(t') = 0 \tag{5.1}$$

where there is an harmonic part given by the frequency Ω and a memory contribute given by the convolution of $C_A(t)$ and the memory function $\Gamma(t)$. The memory function is also called the damping function for reasons that will be clearer later.

Before explaining the theory, how the physics of the systems gives Γ and Ω and the consequences, let us notice immediately some advantages of this formalism. If $\Gamma(t)$ is a regular function, then

$$[\partial_t + i\Omega]C_A(t=0) = 0$$

the first derivative in zero is imaginary, which is a condition requested by stationarity (Eq. 4.5) and that was not respected by the $e^{i\omega t-\gamma t}$ model. Also the second derivative at $t = 0$ is finite, indeed:

$$\partial_t^2 C_A(t) = -(\Omega^2 + \Gamma(t=0))C_A(t) \tag{5.2}$$

Using the correct memory function, all the derivatives would be correct. However, the last expression shows that for having a correct zero-time second derivative only $\Gamma(t=0)$ is needed, not the entire memory function. This will be useful for approximations of the memory function.

At this moment, this model seems full of promises. It seems capable of describing the long term damping and also the short time behaviour.

5.1 The memory function formalism

I will partially follow the discussion in [6] Ch.5. I will start with the classical case for a generic variable A, but the conversion to the quantum case is trivial. Finally, the theory will be applied on the observable of our interest : $\hat{a}_n$.

There are two main ingredients of the theory: the Liouvillian operator L and the projectors P, Q.

The Liouvillian operator is the operator responsible for time evolution:

$$\partial_t A(t) = \{A(t), H\} = iLA(t)$$

where , indicates the Poisson Brackets. For the Quantum case there is the commutator $[,]$ instead. The formal solution is $A(t) = e^{iLt}A(0)$. If we insert it in the correlation definition we obtain:

$$C_A(t) = \langle A(t)A\rangle = \langle A(0)A(-t)\rangle = \langle A(0)e^{-iLt}A(0)\rangle \tag{5.3}$$

where we used time translation invariance, which always holds for equilibrium averages. Applying a Laplace transform defined as:

$$C(z) = \int_0^\infty dt\ C(t)e^{izt}$$

we obtain

$$C(z) = \langle A\frac{1}{z-L}A\rangle \tag{5.4}$$

where z is a complex variable. It is tempting to interpret this expression as a matrix element of the operator $(z-L)^{-1}$ and the vector $|A\rangle$. We can do it, we just have to define a scalar product. The easiest one would be $\langle A|B\rangle = \mathrm{Tr}\hat{\rho}^0 A^\dagger B$ or for classical variables $\langle A^* B\rangle_{eq}$, but since we are interested in when the fluctuations disappear, it is better to work with zero average quantities or to define the following scalar product:

$$\langle A|B\rangle = \langle A^\dagger B\rangle_{eq} - \langle A^\dagger\rangle_{eq}\langle B\rangle_{eq}, \tag{5.5}$$

where $\langle A^\dagger B\rangle_{eq} = \mathrm{Tr}(\rho^0 A^\dagger B)$. For the quantum case instead is often more useful the following product:

$$\langle\hat{A}|\hat{B}\rangle = \frac{1}{\beta}\int_0^\beta d\lambda\ [\langle\hat{A}^\dagger\hat{B}(i\hbar\lambda)\rangle_{eq} - \langle\hat{A}^\dagger\rangle_{eq}\langle\hat{B}(i\hbar\lambda)\rangle_{eq}] \tag{5.6}$$

where as usual:

$$\hat{B}(i\hbar\lambda) = e^{-\lambda\hat{H}}\hat{B}e^{\lambda\hat{\hat{H}}}$$

In any case, most of Mori formalism is independent of the chosen scalar product. All these scalar products satisfy the defining properties of an Hilbert space:

$$\langle A|A\rangle \geq 0 \tag{5.7}$$
$$\langle A|bB + cC\rangle = b\langle A|B\rangle + c\langle A|C\rangle \tag{5.8}$$
$$\langle A|B\rangle^* = \langle B|A\rangle \tag{5.9}$$

These description is useful to give a "geometrical" representation of the auto-correlation. Apart from a normalization, $C_A(t)$ is the projection of $A(t)$ along the direction $A(0)$. With this in mind, it is understandable why we should define the projector P and its complementary Q:

$$P = |A\rangle \frac{1}{\langle A|A\rangle}\langle A| = 1 - Q \tag{5.10}$$

These projectors have the usual properties:

$$\begin{aligned} P^\dagger = P \qquad & Q^\dagger = Q \\ P^2 = P \qquad & Q^2 = Q \\ PQ = QP = 0 & \end{aligned}$$

and inside their subspace they act as the identity matrix (of that subspace).

Mori's brilliant idea is to divide the effect of L into the part that leaves A parallel to itself and the orthogonal one. Let us therefore write $L = LP + LQ$, since $P + Q = 1$. Then it is convenient to use this algebraic operator identity:

$$\frac{1}{X+Y} = \frac{1}{X} - \frac{1}{X}Y\frac{1}{X+Y}. \tag{5.11}$$

With this, we obtain:

$$C(z) = \langle A|\frac{i}{z-L}|A\rangle = \langle A|\frac{i}{z-LP-LQ}|A\rangle = \tag{5.12}$$
$$= \langle A|\frac{i}{z-LQ} + \frac{i}{z-LQ}LP\frac{i}{z-LQ}|A\rangle \tag{5.13}$$

Let us consider the first term in Eq. 5.12, it is just:

$$\langle A|\frac{i}{z-LQ}|A\rangle = \frac{i}{z}\langle A|A\rangle = \frac{i}{z}C(t=0). \tag{5.14}$$

This result can be obtained reminding that $P|A\rangle = A\ Q|A\rangle = 0$ and through the expansion:

$$\frac{i}{z-LQ} = \frac{i}{z}[1 + \frac{1}{z}LQ + \frac{1}{z^2}LQLQ + \dots]. \tag{5.15}$$

All the terms, apart from the first one, finish with a Q, so they disappear when applied on $|A\rangle$. Now we use the definition of P (Eq. 5.10) on the second term of Eq. 5.12:

$$P\frac{i}{z-L}|A\rangle = |A\rangle\frac{1}{\langle A|A\rangle}\langle A|\frac{i}{z-L}|A\rangle = |A\rangle C^{-1}(t=0)C(z). \tag{5.16}$$

Now, if we put everything together, we obtain:

$$C(z) = \frac{i}{z}C(t=0) + \langle A|\frac{i}{z-LQ}L|A\rangle C(t=0)^{-1}C(z) \tag{5.17}$$

It is still missing a last trick, let us multiply by z and use again the operator identity Eq. 5.12:

$$\langle A|\frac{z}{z-LQ}L|A\rangle = \langle A|[1+LQ\frac{1}{z-LQ}]L|A\rangle = \tag{5.18}$$

$$= [\Omega - \tilde{\Gamma}^L(z)]C(t=0) \tag{5.19}$$

where

$$\Omega = C(t=0)^{-1}\langle A|L|A\rangle = iC(t=0)^{-1}\langle \dot{A}|A\rangle \tag{5.20}$$

and

$$\tilde{\Gamma}^L(z) = \langle A|LQ\frac{1}{z-LQ}L|A\rangle = \langle \dot{A}|\frac{Q}{z-LQ}|\dot{A}\rangle = \tag{5.21}$$

$$= \langle \dot{A}|Q\frac{1}{z-LQ}Q|\dot{A}\rangle. \tag{5.22}$$

In the previous equations we used the definition of L and the property of $Q^2 = Q$. After all this manipulation we, finally, find that:

$$C(z) = \frac{iC(t=0)}{z - \Omega + i\tilde{\Gamma}^L(z)} \tag{5.23}$$

where $\tilde{\Gamma}^L(z)$ is the Laplace transform of the memory function. If z is restricted to imaginary values $z = i\omega$, then the Laplace transform reduces to the Laplace-Fourier one and the previous expression becomes:

$$\tilde{C}(\omega)^{LF} = \frac{C(t=0)}{i(\omega+\Omega) + \tilde{\Gamma}^{LF}(\omega)}. \tag{5.24}$$

both this and the previous one are , respectively, the Laplace and Laplace-Fourier transform of Eq. 5.1. To summarize, we have proven that $C(t)$ follows Eq. 5.1, where the Ω and the memory function in the time domain are obtained computing:

$$\Omega = \frac{i}{\langle A|A\rangle}\langle \dot{A}|A\rangle \tag{5.25}$$

$$\Gamma(t) = \frac{1}{\langle A|A\rangle}\langle \dot{A}|Qe^{-iQLQt}Q|\dot{A}\rangle. \tag{5.26}$$

Let us analyze the second expression. If we forgot the projector, then $\Gamma(t)$ would be just the autocorrelation of $\dot{A}$, which can be interpreted in many cases as a "force". But what matters in the memory/damping is the orthogonal part of this "force". In other words, the correlation decreases in time because the observable A "decays" in the orthogonal space. This phrase remind the Fermi Golden Rule and it is not a case, as we will see. All the previous discussion can be repeated in the quantum case, substituting the classical Liouville operator with the quantum corresponding one (defined with the commutator instead that with the Poisson's brackets) and using the scalar product defined in Eq. 5.6.

5.2 Phonon propagator

Let us treat the phonon case now. Since it is easy to move from quantum to classical, let us do only the former one. The time derivative of $\hat{a}_n$, using Heisenberg equation, is

$$\dot{\hat{a}}_n = -i\omega_n\hat{a}_n - \frac{i\hbar^{1/2}}{2}\sum_{jl}\frac{V_{njl}}{\sqrt{8\omega_n\omega_j\omega_l}}(\hat{a}_j^\dagger + \hat{a}_j)(\hat{a}_l^\dagger + \hat{a}_l) \tag{5.27}$$

where we can identify an harmonic part, which keeps $\hat{a}_n$ in the original subspace, and an anharmonic part, which projects in the orthogonal subspace. Reminding the definition of the scalar product and that all the odds momenta are null we obtain that:

$$\Omega = -\omega_n$$

and

$$\Gamma_n(t) = \frac{1}{2n_n}\frac{\hbar}{8\omega_n}\sum_{jl}|V_{njl}|^2\frac{1}{\omega_j}\frac{1}{\omega_l}\times$$
$$\times\left[(\langle\hat{a}_j^\dagger(t)\hat{a}_j(0)\rangle + \langle\hat{a}_j(t)\hat{a}_j^\dagger(0)\rangle)(\langle\hat{a}_l^\dagger(t)\hat{a}_l(0)\rangle + \langle\hat{a}_l(t)\hat{a}_l^\dagger(0)\rangle)\right], \tag{5.28}$$

where in the second expression we used the properties of Q such that $Q^2 = Q$ and the projector acts as the identity in its own subspace. Everything on an higher order than V_{nml}^2 has been neglected. A similar discussion, with Mori formalism applied to another glassy system, can be found in *Gotze, 2000* [8].

Let us make the point of the situation. We started with a system of coupled dynamical equations, since the Heisenberg equations for $\hat{a}_n$ are coupled by the

anharmonic part. Then, with Mori formalism we wrote N dynamical equation for the autocorrelator, however they are still coupled through the memory function. At least, now we have a self consistent problem. While having a self consistent problem is often an advantage, this does not look like a huge step-forward in the resolution of the problem. Indeed, a real progress will come after an introduction of a simple ansatz for the memory function.

Before approximating, let us evaluate the potential of Mori equation of motion. At least, it must give us more than the Fermi approximation. In order to do so, we will recover the Fermi limit and we will compute the zero-time second derivative.

5.3 Golden Rule Limit

Fermi Golden Rule is nothing else than the long-time limit of first order time-dependent perturbation theory. Which means that we should use the unperturbed time evolution, $g_n(t) \propto e^{i\omega_n t}$, in the calculations and then perform a $\lim_{t\to\infty}$.

The long time limit is fundamental, because in Eq. 5.1 the memory function acts in a convolution:

$$\int_0^t dt' \ \Gamma(t-t')C_{\hat{a}_n}(t') = \int_0^t dt' \ \Gamma(t')C_{\hat{a}_n}(t-t')$$

where we used the symmetry property of convolution (a simple change of variables is enough to prove it). Now, let us use the unperturbed propagator, omitting the normalization, : $C_{\hat{a}_n} = g_n^0(t) = e^{i\omega_n t}$. Thus:

$$\lim_{t\to\infty} \int_0^t dt' \ \Gamma(t')e^{i\omega_n(t-t')} = e^{i\omega_n t}\tilde{\Gamma}^{LF}(\omega_n) = \tilde{\Gamma}^{LF}(\omega_n)g_n^0(t) \tag{5.29}$$

From a physical point of view, we could say that for long times, the convolution is a frequency filter. If the autocorrelation oscillates at a certain frequency, after enough time all that matters is the part of memory which oscillates in resonance. Now, if we have to compare this result to the one to obtain an exponential decay :

$$\begin{cases} \partial_t g_n(t) = [i\omega_n - \gamma_n]g_n(t) \\ g_n(t=0) = 1 \end{cases} \tag{5.30}$$

it is clear that we should compare:

$$\mathrm{Re}\,\tilde{\Gamma}^{LF}(\omega_n) \Leftrightarrow \gamma_n$$

where γ_n is as usual is the line-width obtained by FGR. To summarize, the real part of the memory function transform acts like a damping constant, while its imaginary part produces a shift in the oscillation frequency.

Now we must compute Eq. 5.28 and its transform using the purely harmonic propagator. We should perform the Laplace-Fourier transform, but since I am more used to the Fourier transform, let us rewrite the former using the latter. As it is shown in App. 8.1, the LF transform can be seen as a Fourier transform of a function which is zero for $t < 0$. Thanks to that, there are simple equations between the LF transform of a function $f(t)$ and the Fourier transform of a conjugated function $f(-t)^* = f(t)$. Therefore

$$\mathrm{Re}\,\tilde{\Gamma}^{LF}(\omega) = \frac{1}{2}\tilde{\Gamma}(\omega) \tag{5.31}$$

$$\mathrm{Im}\,\tilde{\Gamma}^{LF}(\omega) = \frac{1}{2\pi i}\int_{-\infty}^{\infty} d\omega' \frac{1}{\omega'}\tilde{\Gamma}(\omega-\omega') \tag{5.32}$$

Furthermore, since $\Gamma(t)$ has been extended for $t < 0$ with the hypothesis that $\Gamma(-t)^* = \Gamma(t)$, the Fourier Transform $\tilde{\Gamma}(\omega)$ is real. However, it is important to remind that this is only a trick to perform the LF transform, the physical memory function is a causal function $\Gamma(t<0) = 0$, since only events in the past, $t - t' > 0$, can influence the dynamics.

Finally, let us compute $\tilde{\Gamma}(\omega)$, reminding that $FT[e^{i\omega_n t}, \omega] = 2\pi\delta(\omega - \omega_n)$:

$$\begin{aligned}\tilde{\Gamma}_n(\omega) = \frac{1}{n_n}\frac{\pi\hbar}{8\omega_n}\sum_{jl}\frac{|V_{njl}|^2}{\omega_j\omega_l}\times \\ \times\Big[n_j n_l\delta(\omega-\omega_j-\omega_l) + n_j n_l(e^{\beta\hbar\omega_j}+e^{\beta\hbar\omega_l})\delta(\omega+\omega_l-\omega_j)+ \\ +(n_j+1)(n_l+1)\delta(\omega+\omega_j+\omega_l)\Big]\end{aligned} \tag{5.33}$$

and after some algebra it can be noticed that indeed:

$$\mathrm{Re}\,\tilde{\Gamma}^{LF}_n(\omega_n) = \frac{1}{2}\tilde{\Gamma}_n(\omega_n) = \gamma_n, \tag{5.34}$$

where we used that $\delta(\omega_n + \omega_l + \omega_j)$ is never satisfied. This is a comforting result since it proves that indeed in the quasi-harmonic regime the long-time propagator is the same, whether we use FGR or Mori formalism.

5.3.1 Classical limit of Fermi Golden Rule

In the previous paragraph it has been shown that in the right conditions Mori Memory function formalism leads to FGR. However, while FGR has been introduced in the quantum framework, Mori memory formalism is well defined also in

the classic case. This suggests an important possibility: the exponential decay in the long time limit can be found with just the classical mechanics. Instead, it is usually derived doing the classical limit of the purely quantum expression.

Let us try to apply classic Mori theory in the Golden Rule regime. After similar calculations, we obtain the classical $\Gamma_n(t)$:

$$\Gamma_n(t) = \frac{1}{2n_n}\frac{1}{8\omega_n}\sum_{jl}|V_{njl}|^2\frac{1}{\omega_j}\frac{1}{\omega_l}\times \\ \times\left[(\langle\alpha_j^*(t)\alpha_j(0)\rangle + \langle\alpha_j^*(0)\alpha_j(t)\rangle)(\langle\alpha_l^*(t)\alpha_l(0)\rangle + \langle\alpha_l^*(0)\alpha_l(t)\rangle)\right], \quad (5.35)$$

which is the analogous of Eq. 5.28. Then, if we perform the Golden Rule limit, which means assuming $\langle\alpha_j^*(t)\alpha_j(0)\rangle = e^{i\omega_j t}$, Fourier transforming and considering only $\omega = \omega_n$. Thus, we obtain:

$$\frac{1}{2}\tilde{\Gamma}_n(\omega) = \frac{1}{n_n}\frac{\pi}{8\omega_n}\sum_{jl}\frac{|V_{njl}|^2}{\omega_l\omega_j}\frac{1}{2}n_j n_l\times \\ [\delta(\omega-\omega_j-\omega_l)+\delta(\omega+\omega_j+\omega_l)+\delta(\omega-\omega_j+\omega_l)+\delta(\omega+\omega_j-\omega_l)] \quad (5.36)$$

and consequently

$$\frac{1}{2}\tilde{\Gamma}_n(\omega_n) = \frac{1}{n_n}\frac{\pi}{8\omega_n}\sum_{jl}\frac{|V_{njl}|^2}{\omega_l\omega_j}n_j n_l\times \\ \left[\frac{1}{2}\delta(\omega_n-\omega_j-\omega_l)+\delta(\omega-\omega_j+\omega_l)\right], \quad (5.37)$$

where now we have $n_n = k_bT/\omega_n$. Indeed, this is Eq. 3.17 in the classical limit i.e. when $\hbar\omega/k_bT \ll 1$ and therefore $e^{\beta\hbar\omega_n} \approx 1 + \hbar\omega_n/k_bT$.

These few lines prove that also in the classical regime the autocorrelation decays and that the exponent of such decay is indeed given by the classical limit of FGR.

5.4 Zero-time derivatives

Since the long-time limit has been checked, let us see move to the short time one. Now we should compare the second sum zero-time derivative calculated with Heisenberg equation and the one obtained with the memory function. For the latter case, Eqs. 5.2-5.28 yield to:

$$-\partial_t^2 g_n(t=0) = (\omega_n^2 + \Gamma_n(0))g_n(t=0) \quad (5.38)$$

where

$$\Gamma_n(t=0) = \frac{1}{2n_n}\frac{\hbar}{8\omega_n}\sum_{jl}|V_{njl}|^2\frac{1}{\omega_j}\frac{1}{\omega_l}(2n_j+1)(2n_l+1) \tag{5.39}$$

Now, let us evaluate the second derivative in the usual Heisenberg way, using Eq. 5.27 and computing:

$$-\partial_t^2 g_n(t=0) = -\partial_t^2\left(\frac{1}{n_n}\langle\hat{a}_n^\dagger(t)\hat{a}_n(0)\rangle - \langle\hat{a}_n^\dagger(t)\rangle\langle\hat{a}_n(0)\rangle\right)|_{t=0} \tag{5.40}$$

$$= \left(\langle\dot{\hat{a}}_n^\dagger(t)\dot{\hat{a}}_n(t)\rangle - \langle\dot{\hat{a}}_n^\dagger(t)\rangle\langle\dot{\hat{a}}_n(t)\rangle\right)|_{t=0} \tag{5.41}$$

where also $\langle\dot{\hat{a}}_n^\dagger(t)\rangle\langle\dot{\hat{a}}_n(0)\rangle$ is included because we are considering the difference between the correlation and the average value, as it was specified in the choice of the scalar product. In this case $\langle\dot{a}\rangle \neq 0$ because of the anharmonic part of Eq. 5.27. Moreover, the equivalence between the second and third term is obtained by using properties of time-correlations. To be more specific, for a general variable A:

$$\partial_t^2\langle A(t)A(0)\rangle_{eq} = \partial_t\langle\dot{A}(t)A(0)\rangle_{eq} = \partial_t\langle\dot{A}(0)A(-t)\rangle_{eq} = -\langle\dot{A}(0)\dot{A}(-t)\rangle_{eq} \tag{5.42}$$

Finally, using Eq. 5.27 and Wick's theorem to compute Eq. 5.40:

$$-\partial_t^2 g_n(t=0) = n_n(\omega_n^2 + \Gamma_n(t=0)) \tag{5.43}$$

where as we recall $g_n(t=0) = n_n$ (in this section). This discussion proves some interesting. Firstly, we are consistent in our calculation, as long as we use Mori formalism without any approximation, the zero-time derivatives are correct, at least up to the second one. Secondly, to have the correct second sum rule/time-derivative only $\Gamma(t=0)$ matters. This is extremely useful. It does mean that as long as we approximate $\Gamma(t)$ using a function that have the same initial value and it reproduces that long-time exponential behaviour, we have already an improved propagator.

5.5 Langevin approach

All these results could have been found using a Generalized Langevin equation. However, even if the derivation in the Mori Formalism is more straightforward, the Langevin equation gives a more intuitive physical description of the phenomena. Therefore a brief comparison between these two methods will be presented(for details see Ref. [10]).

A Generalized Langevin (GL) Equation for a variable X has the following expression :

$$\partial_t X(t) = -i\Omega X - \int_0^t dt' \; \Gamma(t-t')X(t') + R(t) \qquad\qquad t > 0, \tag{5.44}$$

where Ω is a frequency responsible for an harmonic oscillation, $\Gamma(t)$ is a memory/-damping function and there is also the stochastic force $R(t)$. Such a force has the following properties:

$$\langle R(t) \rangle = 0 \tag{5.45}$$

$$\langle R(t_1)X(t_2) \rangle = 0 \qquad if \quad t_1 \geq t_2 \tag{5.46}$$

With just these definition it is straightforward to see the well-known connection Mori-Langevin. If we right-multiply Eq. 5.44 by $X(0)$ and then perform an average, we obtain:

$$\partial_t \langle X(t)X(0) \rangle = \partial_t C_X(t) = -i\Omega C_X(t) - \int_0^t dt' \; \Gamma(t-t')C_X(t'), \tag{5.47}$$

where $\langle R(t)X(0) \rangle = 0$. This is a Mori equation. This roughly shows the connection between Mori formalism and Langevin Generalized equation: if physical observable obeys a GL equation, then its average autocorrelation must obey a Mori equation. Indeed, in its original article [13] Mori started by a GL kind equation.

What is the role of $R(t)$?. Those that are familiar with Langevin equation (general or not) know that an evolution with only damping does not conserve some quantities. For instance, a free particle with just damping does not conserve the energy, and with only a white-noise like stochastic force it does increase, on average, its kinetic (which for a free particle is all) energy. So, in order to maintain the stationarity of certain quantities like energy or the occupation of a mode $\langle \hat{a}_n^\dagger(t_0)\hat{a}_n(t_0) \rangle = n_n$ there must be an equilibrium between the stochastic force and the memory/damping function. This is a particular case of the **Fluctuation-Dissipation Theorem** [10](FDT). In this case the FDT claims that:

$$\Gamma(t) \propto \langle R(t+t_0)R(t_0) \rangle, \tag{5.48}$$

where the proportionality $\propto$ is due to the omission of a normalization constant, which is determined by the observable we are treating.

In our phonon problem, what has the role of the stochastic force. In Eq. 5.27 the equation of motion of the annihilation operator is determined by an harmonic part and an anharmonic one. Comparing that equation to Eq. 5.44 it seems reasonable to identify the stochastic force to the anharmonic part. The zealous reader is suggested to try to obtain the Mori's results in the Langevin's framework using the assumption that:

$$\langle \hat{R}_n^\dagger(t)\hat{R}_n(0)\rangle = \langle \hat{F}_{A,n}^\dagger(t)\hat{F}_{A,n}(0)\rangle - \langle \hat{F}_{A,n}^\dagger(t)\rangle\langle \hat{F}_{A,n}(0)\rangle \tag{5.49}$$

where $\hat{F}_{A,n}$ is the anharmonic part of Eq. 5.27:

$$\hat{F}_{A,n} = -\frac{i\hbar^{1/2}}{2}\sum_{jl}\frac{V_{njl}}{\sqrt{8\omega_n\omega_j\omega_l}}(\hat{a}_j^\dagger + \hat{a}_j)(\hat{a}_l^\dagger + \hat{a}_l).$$

The average value of this anharmonic force is the reason why the average position of the mode is not null at not-zero temperatures, but as a spring in constant force field, the average position is translated. This is an unavoidable effect of working with potentials which are not symmetric in respect of the equilibrium position, which is natural for potentials expanded up to third order.

5.6 From Markovian to Gaussian memory approximation

In the next chapter an approximation to the memory function and the relative results will be discussed. The memory function will be modeled with a Gaussian. Such a choice is quite common for this kind of problem concerning response function and propagators, and it presents various advantages. Not only a Gaussian memory simplify the calculations and it keeps almost everything analytic, but as we will see it ensures the existence of all the sum rules.

Before entering in the details, it is worth understanding the physical meaning of such a choice. The original exponential propagator can be obtained in Mori Formalism within the Markovian or instantaneous memory approximation. Indeed, if

$$\Gamma_n(t) = 2\gamma_n\delta(t),$$

then Eq. 5.1 becomes Eq. 5.30 and we go back to the original propagator. There is a 2 factor because one of the extremes ($t = 0$) of the integration is the condition for the δ function and this produce an extra 1/2 factor: $\int_a^b dx\ \delta(x-a)f(x) = \frac{1}{2}f(a)$.

Looking at Eq. 5.38, it can be noticed that the divergence of this $\Gamma(t)$ at $t = 0$ is the reason of the divergence of the zero-time second derivative. Since this second derivative is composed by ω_n^2 plus $\Gamma_n(t = 0)$, to have a finite derivative/sum rule a finite a regular $\Gamma(t)$ is needed.

Therefore, let us try a smoother version of the δ:

$$\Gamma_n(t) = 2\gamma_n \frac{1}{\sqrt{2\pi}\tau_n} e^{-t^2/2\tau_n^2} \tag{5.50}$$

With this ansatz we are saying that now the dynamics of $g_n(t)$ is not determined only by the same-time /instantaneous contribute, but also from what happens in a time-range of order τ_n (not to be confused with the matrix τ_{nm}). Needless to say, if $\tau_n \to 0$ $\Gamma_n(t)$ goes back to a δ function. Moreover, if $\tau_n > 0$,

$$\Gamma_n(t = 0) = \gamma_n \frac{1}{\sqrt{2\pi}\tau_n} \tag{5.51}$$

is finite. In the next chapter, it will be studied how this memory function changes the propagator and consequently the conductivity and how this parameter τ depends on the physics of the system.

Chapter 6

Quasi-Harmonic Green-Kubo with Gaussian Memory

In this chapter we will obtain and thoroughly study a more physical phonon propagator $g_n(t)$ using Mori formalism together with a Gaussian memory function. This is a way of going beyond the Instantaneous/Markovian memory approximation, which would lead to the Lorentzian spectrum, as explained in the previous chapter.

One of the advantage of working with a Gaussian is that most of the calculations concerning Fourier Transform can be done analytically. Indeed:

$$\begin{cases} \Gamma_n(t) = 2\gamma_n \frac{1}{\sqrt{2\pi}\tau_n} e^{-t^2/2\tau_n^2} \\ \tilde{\Gamma}^{LF}(\omega) = \gamma_n e^{-\tau_n^2\omega^2/2} \left[1 - iErfi[\frac{\tau_n\omega}{\sqrt{2}}]\right] = \gamma_n e^{-\omega^2/\sigma_n^2} \left[1 - iErfi[\frac{\omega}{\sqrt{2}\sigma_n}]\right], \end{cases} \tag{6.1}$$

where clearly $\sigma_n = \frac{1}{\tau_n}$ and where $Erfi$ is the imaginary error function as defined on Mathematica. Using Eq. 5.24 and the relations between LF and FT transforms, we obtain:

$$\tilde{g}_n(\omega) = \frac{2\,\mathrm{Re}\,\tilde{\Gamma}_n^{LF}(\omega)}{(\omega - \omega_n - \mathrm{Im}\,\tilde{\Gamma}_n^{LF}(\omega)) + (\mathrm{Re}\,\tilde{\Gamma}_n^{LF}(\omega))^2} = \tag{6.2}$$

$$\frac{2\gamma_n e^{-\omega^2/2\sigma_n^2}}{|\gamma e^{-\omega^2/2\sigma^2} + i(\omega - \omega_n - \gamma_n e^{-\omega^2/2\sigma_n^2} Erfi(\omega/\sigma_n\sqrt{2}))|^2}. \tag{6.3}$$

6.1 General observations and sum rules

Few general observations must be done about this spectrum:

- asymptotically goes to zero as a Gaussian, faster than any inverse polynomial⇒ all the momenta/sum rules are finite.

- for small ω and therefore long times it behaves like a Lorentzian
- if $\tau_n \to 0$ and $\sigma \to \infty$, then $\tilde{\Gamma}_n^{LF}(\omega) \approx \gamma_n$ and the spectrum goes back to a Lorentzian

The first observation can be proved using the asymptotic expansion of Erfi function (for details see the PDF in this link) :

$$Erfi(z) \propto \frac{z}{\sqrt{-z^2}} + \frac{1}{\sqrt{\pi} z} e^{z^2}(1 + O(\frac{1}{z^2})); \ |z|^2 \to \infty$$

since the $Erfi$ function in Eqs. 6.1-6.2 is multiplied by a Gaussian with an opposite exponent, the denominator of Eq. 6.2 is at most polynomials asymptotically. Therefore the decay for $\omega \to \infty$ is dominated by the Gaussian at the numerator.

The second point is proved reminding that $Erfi(0) = 0$ and obviously $e^0 = 1$, therefore:

$$\tilde{g}_n(\omega \approx 0) \approx \frac{2\gamma_n}{(\omega - \omega_n)^2 + \gamma_n^2}$$

which is exactly the Lorentzian spectrum. Since for a regular function the very long time-limit is determined by the low- frequency behaviour of the transform, this proves that the long time limit is indeed an exponential decay with the same γ_n exponent.

In Figs. 6.1-6.2 some properties of $g_n(t)$ can be observed for some parameters arbitrary chosen, together with a comparison with the "old" propagator $e^{(i\omega_n - \gamma_n)t}$. In Fig. 6.1 $\mathrm{Re}\, g_n(t)$ presents an oscillating behaviour together with an overall decay, as expected. In Fig. 6.2 the decay is studied. First the oscillation is eliminated multiplying $g_n(t)$ by $e^{-i\omega_n t}$, then the natural logarithm is applied. Comparing $ln(\mathrm{Re_n(t)e^{-i\omega_n(t)}})$ to $-\gamma_n t$, it can be observed a good agreement. However, in the latter figure not all the oscillating part is eliminated. Due to the memory function there is a frequency shift of the peak and therefore $g_n(t)$ is oscillating with frequency $\omega_n + \delta\omega_n$.

Indeed the shift of the resonance is a common phenomena and in quantum field theory it is associated with the self-energy of the phonons. As long as this shift is small compared to ω_n, $\mathrm{Im}\, \tilde{\Gamma}^{LF}(\omega)$ can be approximated by a costant near ω_n and $\delta\omega_n$ can be estimated by:

$$\delta\omega_n \approx \mathrm{Im}\, \tilde{\Gamma}^{LF}(\omega) = \gamma_n e^{-\omega_n^2/\sigma_n^2} Erfi[\frac{\omega_n}{\sqrt{2}\sigma_n}]$$

We have a $\delta\omega_n$ proportional to γ_n, so in the quasi-harmonic limit it should be negligible, however it is interesting to notice that is not constant for any mode, therefore it could change the "distance" between modes $\omega_n - \omega_m \to \omega_n - \omega_m + \delta\omega_n - \delta\omega_m$.

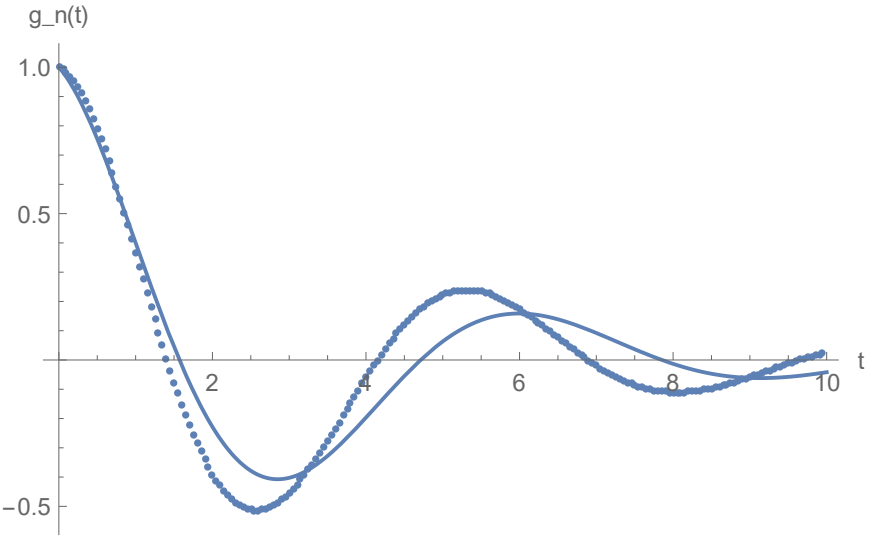

Figure 6.1: Dashed line: $\mathrm{Re}\, g_n(t)$ for $(\omega_n, \gamma_n, \sigma_n) = (1, 0.3, 3.3)$ obtained by Numerical Inverse fourier transform. Straight line: $g_n(t) = e^{(i\omega_n - \gamma_n)t}$. Calculations performed using Mathematica.

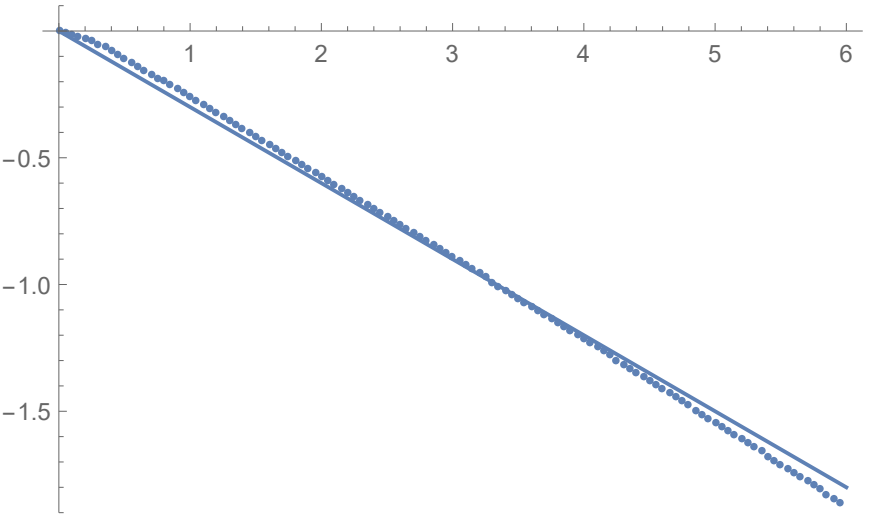

Figure 6.2: $\mathrm{Re}\ln(g_n(t)e^{-i\omega_n t})$ for $(\omega_n, \gamma_n, \sigma_n) = (1, 0.3, 4)$ obtained by Numerical Inverse fourier transform and $-\gamma_n t$. Calculation performed using Mathematica.

Now it is time to check the sum rules. Mori formalism with the correct $\Gamma_n(t=0)$ should automatically guarantee the zero, first and second sum rules, here reminded:

1. $g_n(t=0) = 0$
2. $\partial_t g_n(t)|_{t=0} = i\omega_n = \frac{i}{2\pi}\int_{-\infty}^{\infty} d\omega\ \omega\tilde{g}_n(\omega)$
3. $-\partial_t^2 g_n(t)|_{t=0} = \omega_n^2 + \frac{2\gamma_n}{\sqrt{2\pi\tau_n}}$

All the following plot has been done using the software Mathematica. In Figs. 6.3-6.4 it can be observed how the normalization is respected while varying τ_n and ω_n, respectively. Also the first sum rule is perfectly respected, as showed in Fig. 6.5. Finally, in Fig. 6.6 there are various plots of the second sum rule as function of τ_n, for different values of ω_n. Also in this figure, the analytical formula and the results obtained by a numerical calculation of the second momenta of the spectrum coincide. Moreover, this plot shows how the second momenta diverges when $\tau \to 0$, or in other words when we go back to the Markovian propagator/Lorentzian spectrum. Finally, from Eq. 6.1 it is clear that the second momenta converges to ω_n^2 when $\tau_n \to \infty$

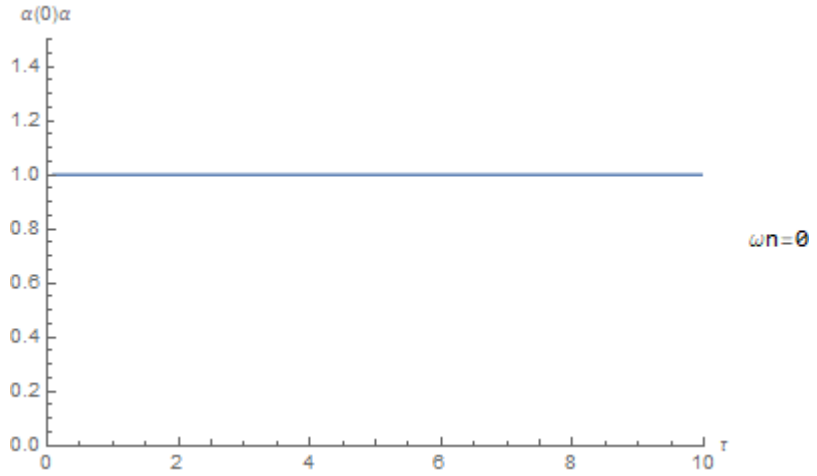

Figure 6.3: Normalization of the spectrum as a function of τ.

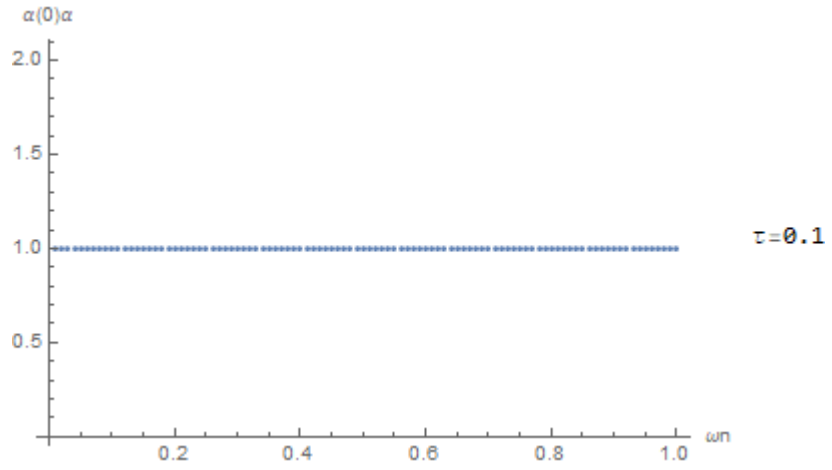

Figure 6.4: Normalization of the spectrum as a function of ω_n.

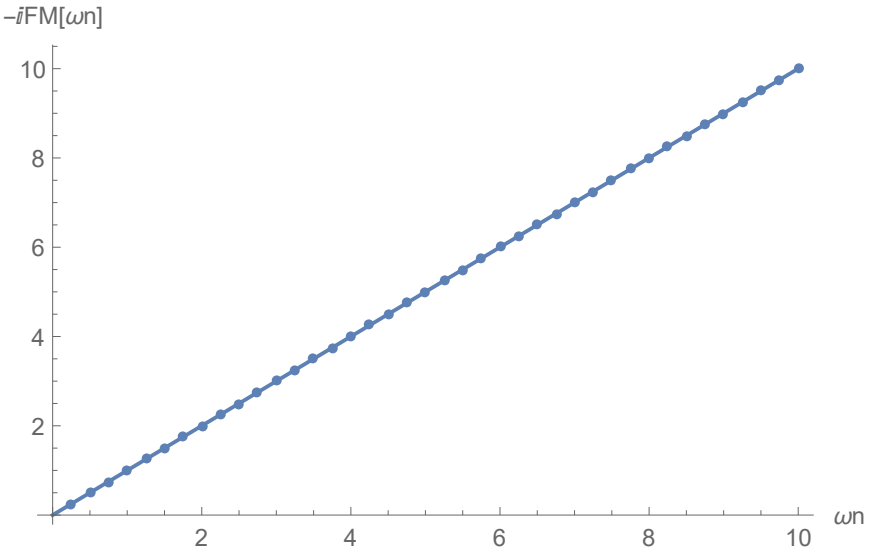

Figure 6.5: First moment (FM) of $\tilde{g}_n(\omega)$ for $\sigma_n = 1$ and $\gamma_n = 0.1$

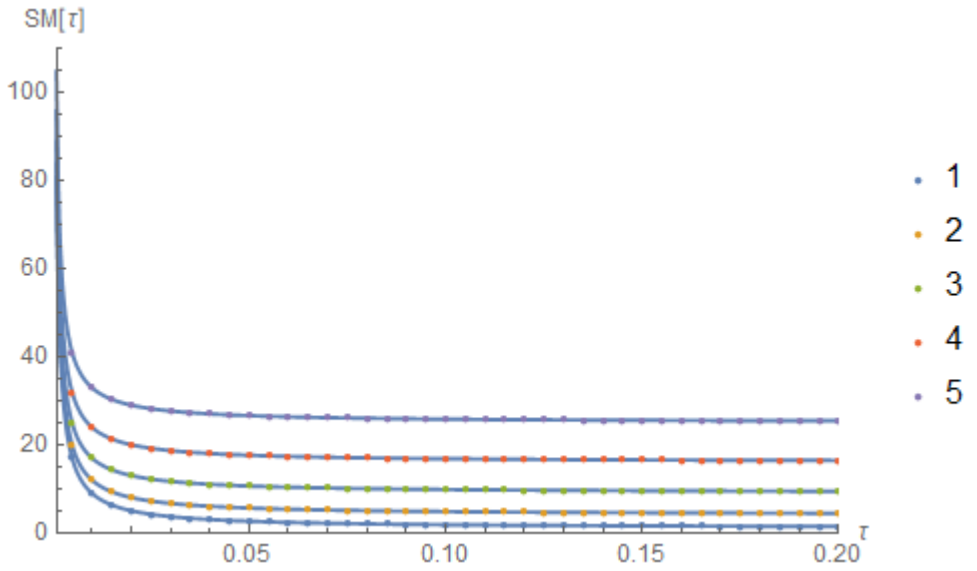

Figure 6.6: Second moment of the spectrum and $f(\tau_n) = \omega_n^2 + \frac{2\gamma_n}{\sqrt{2\pi\tau_n}}$ for $\omega_n = 1, \ldots, 5$. $\gamma_n = 0.1$

6.2 Spectrum

Now that we have verified the consistency of our calculation and implementation of this new propagator in the time domain, it is time to study its spectrum, which is more directly connected to τ_{nm}

The spectrum will be studied as a function of the parameters $(\gamma_n, \omega_n, \sigma_n)$. In order to keep this study useful for future purposes, we will work in a "reasonable" range of values. With reasonable I mean $\gamma/\omega \ll 1$ and $\omega \lesssim \sigma$, which is indeed the situation that we will find studying our a-Si. In Fig. 6.7 there is a comparison of a Lorentzian with parameters $(\omega_n, \gamma_n) = (1, 0.01)$ with various spectrums $\tilde{g}_n(\omega, \sigma_n)$. All these spectrum have the same normalization, the zero sum rule $\int d\omega \tilde{g}_n(\omega, \sigma_n) = g_n(t = 0)$, so what is happening in the figure is a "squeezing". For smaller σ_n the tails are lower and therefore the peak must be higher. It is interesting to notice that the increase of the peak is surely not linear, there is a dramatic difference between the plot for $\sigma_n = 2.5 - 5$ and $\sigma_n = 1$. Moreover, also a frequency shift is visible, as expected.

The $\delta\omega_n$ does not seem to depend on σ_n very strongly. However, it is proportional to γ_n and therefore even spectrum with almost the same shape can have a considerable $\delta\omega_n$ if γ_n is large enough, as in Fig. 6.8. What is the role of this shift in our theory? As seen in Eq. 4.6 $\tau_{nm} \propto \int d\omega \tilde{g}_n(\omega)\tilde{g}_m(\omega)$, a kind of overlap of the spectrums. If the spectrum have a near peak, τ_{nm} is large and viceversa. If only the "distance" of the modes $|\omega_n - \omega_m|$ were important, then a translation of all the modes would be irrilevant. However, since every mode has a different γ_n and as we will see a different σ_n the frequency shift is different and consequently τ_{nm} can change.

To summarize, τ_{nm} can change for two main reasons: firstly because the spectrum are "squeezed", higher peaks and lower tails, secondly because due to the frequency shift, two spectrums do not overlap anymore or the do overlap more. Obviously the diagonal, or near diagonal, terms τ_{nn} are immune from the second effect since they have the same frequency shift.

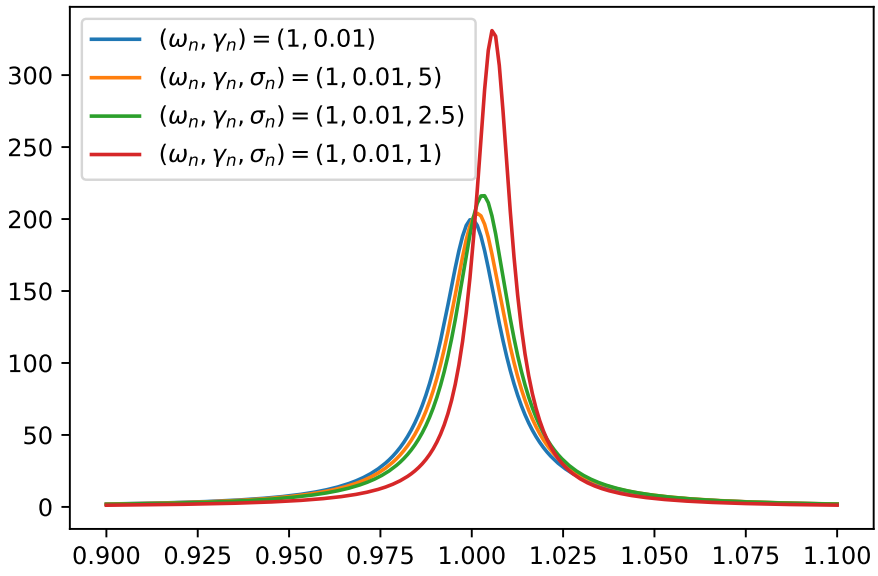

Figure 6.7: Examples of $\tilde{g}_n(\omega)$. Arbitrary units.

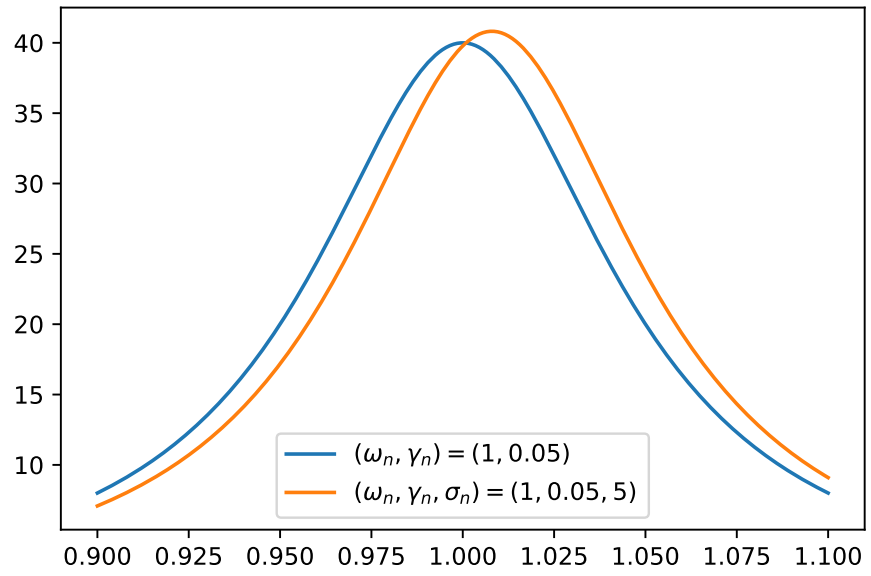

Figure 6.8: Examples of $\tilde{g}_n(\omega)$ as a function of γ_n. The resonance shift $\delta\omega_n \approx Im\tilde{\Gamma}_n(\omega_n) \propto \gamma_n$.

6.3 Determining the characteristic time of the memory function

All our new theory is controlled by one parameter (for each mode): σ_n. Such parameter, or better its inverse, gives an estimate of how long the memory lasts. But how do we compute it practically?

To determine σ_n it is needed to equal $\Gamma(t=0)$ of the Gaussian ansatz and the real one, obtained with Mori formalism. In other words:

$$\Gamma_n(t=0) = \frac{2\gamma_n\sigma_n}{\sqrt{2\pi}} = \frac{1}{2n_n}\sum_{nm}|V_{nml}|^2\ldots \tag{6.4}$$

where the last term is Eq. 5.28. Thus:

$$\sigma_n = \sqrt{\frac{\pi}{2}}\frac{\Gamma_n(t=0)}{\gamma_n} \tag{6.5}$$

This formula has already been implemented in a previous version of Kaldo and it is being implemented in the actual version (ask the author for the codes). Luckily, since the calculation of $\Gamma_n(t=0)$ is extremely similar to the calculation of γ_n, the calculations can be done almost at the same time using the same quantities. Roughly speaking, to calculate σ_n you have only to omit the $\delta_{\omega-\omega_m\pm\omega_l}$.

This formula to obtain σ_n has been firstly tested for a-Si 512, whose simulations require less time to be run. In Figs. 6.9-6.10-6.11 are represented for different temperatures $\sigma_n(\omega_n)$, $\sigma_n(\omega_n)/\omega_n$ and $\gamma_n(\omega_n)$ respectively.All this plot have the $\omega = 2\pi\nu$ instead of the frequencies. This choice has been done because in the calculation of τ_{nm} those that matter are the former ones. About the γ_n we have to remind that the 512 system has smaller linewidth than the 1728 one, which is more trustworthy and in better agreement with experiments.

In Fig. 6.9 it can be observed that also σ_n seems a function of the ω. Again this property is not automatic, since in a real harmonic system it is possible to have eigenmodes with the same ω but totally different direction and other properties. Moreover, while $\sigma_n(\omega_n)$ seems on average an increasing function of ω, there is a negative trend about the temperatures: the higher the temperature, the lower the $\sigma_n(\omega_n)$. This trend is totally opposite in the γ_n, which does increase with temperature.

To compare this data to the previous study, let us give some indicative value. To this purpose also $\sigma_n(\omega_n)/\omega_n$ has been plotted. Roughly speaking $\sigma_n/\omega_n \sim 3.5-10$, where the minimum is for higher temperatures and $\gamma_n/\omega_n \sim 0.01 - 0.001$. In this analysis as always the very low frequency range must be omitted, since it does require far larger systems to be described properly.

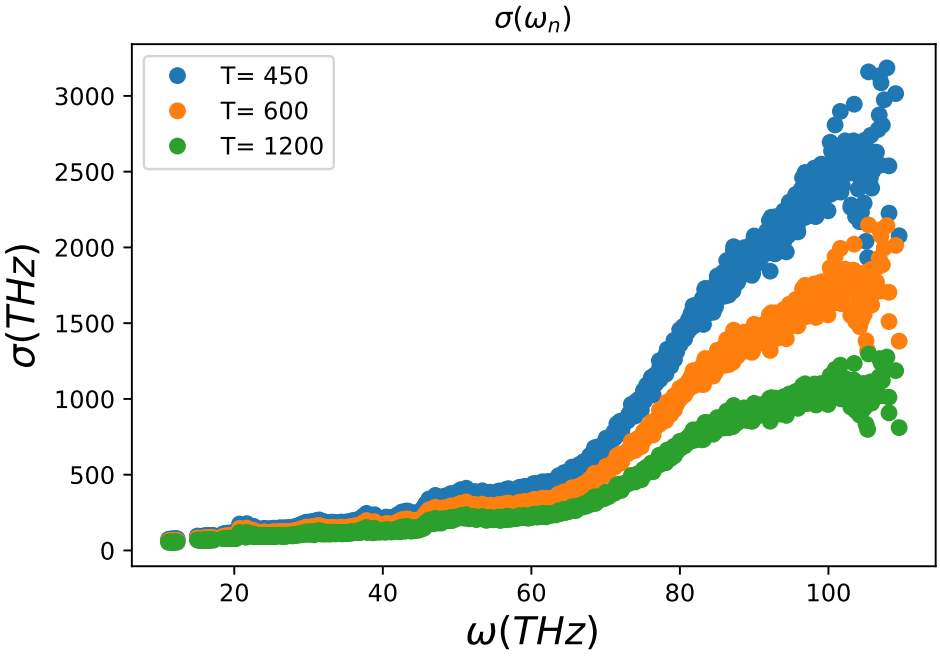

Figure 6.9: $\sigma_n(\omega_n)$ for a-Si 512 for various temperatures.

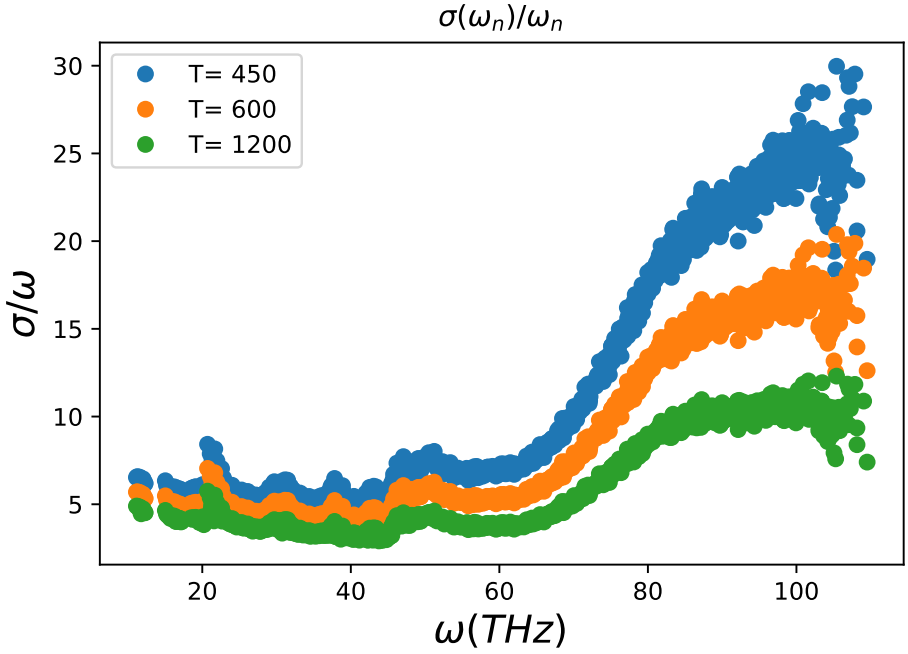

Figure 6.10: $\sigma_n(\omega_n)/\omega_n$ for a-Si 512 for various temperatures.

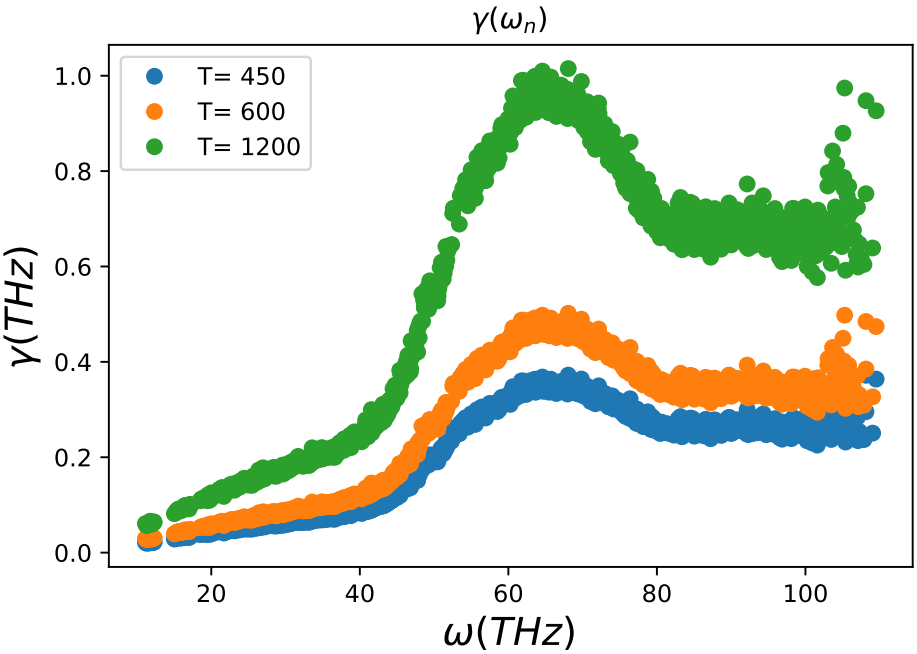

Figure 6.11: $\gamma_n(\omega_n)$ for a-Si 512 for various temperatures.

6.4 Implementation details of the new propagator: QHGK-Memory

Let us make the point of the situation. Now we have for any modes ω_n, γ_n, and σ_n and consequently $\tilde{g}_n(\omega)$, whose analytical expression is given by Eq. 6.2. The last remaining thing to do is calculate:

$$\tau_{nm} = \frac{1}{4\pi} \int_{-\infty}^{\infty} d\omega' \ \tilde{g}_n(\omega')\tilde{g}_m(\omega')$$

which is Eq. 4.6 omitting the Re(), since the spectrum is already real (and it also symmetric). However, this integral is not analytical, or at least software of symbolic calculus like Mathematica are not able to do it analitically. Therefore, it must be evaluated numerically. The straightforward answer is to compute a numerical integration. However, it has been found that this integral can be approximated by the following formula (for both codes see App. 8.2):

$$\begin{cases} \tau_{nm} = \frac{1}{4\pi} \int_{-\infty}^{\infty} d\omega' \ \tilde{g}_n(\omega')\tilde{g}_m(\omega') = \frac{\gamma'_n+\gamma'_m}{(\omega'_n-\omega'_m)^2+(\gamma'_n+\gamma'_m)^2} \\ \gamma'_n = \gamma_n e^{-\omega_n^2/2\sigma_n^2} \\ \omega'_n = \omega_n + \delta\omega_n = \omega_n + \gamma'_n Erfi[\frac{\omega_n}{\sqrt{2}\sigma_n}] \end{cases} \tag{6.6}$$

What's the reasoning behind this going back to a Lorentzian? Simply a difference in scale between $\gamma_{n,m}$ and $\sigma_{n,m}$. An overlap integral is significantly different from zero only if the two peak overlap, which means that they must be nearer than few γs: $|\omega_n - \omega_m| \sim \gamma_n + \gamma_m$. But $\gamma_n \ll \omega_n \lesssim \sigma_n$ and thus the Gaussian Erfi function multiplied by the Gaussian are pretty much constant in the significant interval. An example of such difference in scale is visible in Fig. 6.12, there is no apparent variation of the Gaussian in that range.

In addition to this qualitative discussion, in Fig. 6.13 there is the relative difference between the τ_{nm} calculated with the numerical integration and the Lorentzian one τ^0_{nm}, while in Fig. 6.14 there is the relative difference between τ_{nm} and τ^{app}_{nm}, which is the Mori result approximated. Both the figure are done for a-Si 512 at $T = 600K$ and for sake of simplicity just for the first 50 frequencies. In the former figure it can be noticed that τ_{nm} is $\sim 2\%$ larger than τ^0_{nm} near the diagonal and smaller elsewhere, a similar behaviour of τ^g_{nm} (Fig. 4.2). In the latter one, there is a relative comparison between τ_{nm} and τ^{app}_{nm}. On average these relative differences are 10 times smaller than the former ones, moreover near the diagonal this numerical approximation works almost perfectly. This is very convenient and important, since our experiments with the threshold prove that somehow the near-diagonal part of these matrices is the most important one. For all these reasons, and to avoid to slow down the program τ^{app}_{nm} has been used in the following calculations.

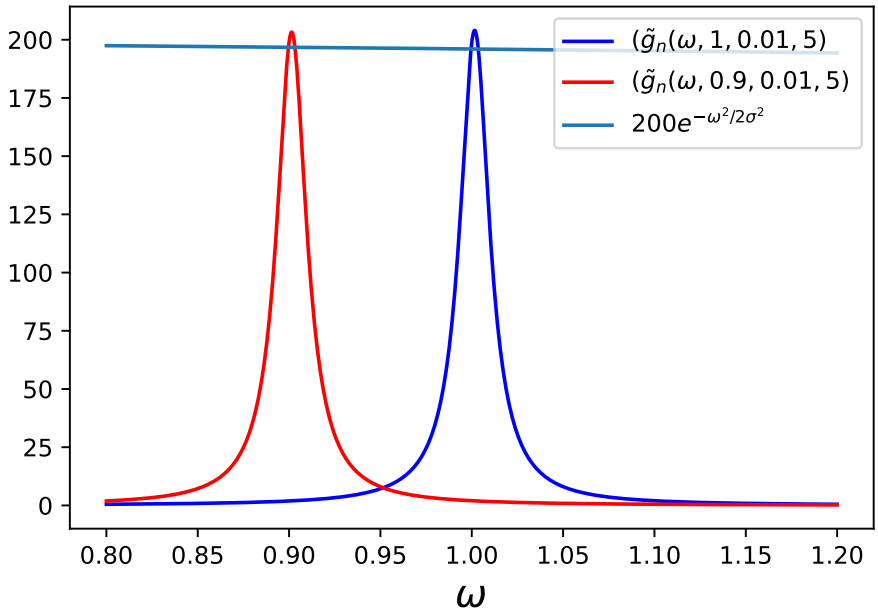

Figure 6.12: Two spectrum with reasonable parameters and a properly scaled Gaussian.

Obviously, if it were necessary for other materials with far smaller σ (or far larger γ) it is easy to implement an "if else" condition, in order to switch from the "Mori-Lorentzian" approximation to the numerical integration when necessary.

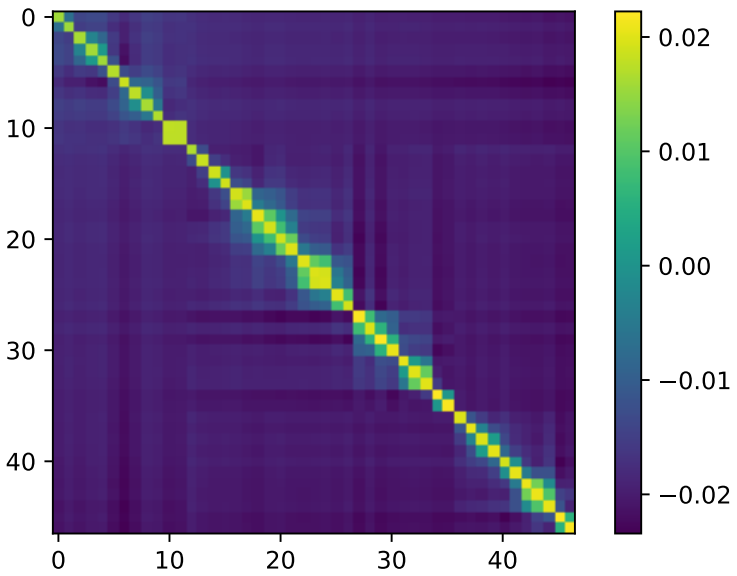

Figure 6.13: Example of $\frac{\tau_{nm}-\tau^0_{nm}}{\tau^0_{nm}}$. $T = 600K$ for a-Si 1728.

Going back to Lorentzian can seems disappointing, however this only a way to calculate the overlap integral. Mori formalism allowed us to find a squeezed and shifted not-Lorentzian spectrum, but for the overlap only a small zone around the peak is important and therefore just in the last calculation the real spectrum is approximated with a Lorentzian with some modified parameters.

6.4.1 New heat conductivity

Finally we can use these τ_{nm} to evaluate the heat conductivity. In Figs. 6.15-6.16 there is the relative variation of the conductivity using the Mori formalism or the Fermi approximation, respectively for the a-Si 1728 and 512. We already know that the 512 system is not large enough to give correct conductivities, but it is interesting to see how the the new phonon propagator/τ_{nm} affects the conductivities for different sizes. In these figures the correction is very small and can change sign. To be more accurate, it is negative for smaller temperatures and positive for higher ones. This resembles the previous experiment with the Gaussian τ^g_{nm},

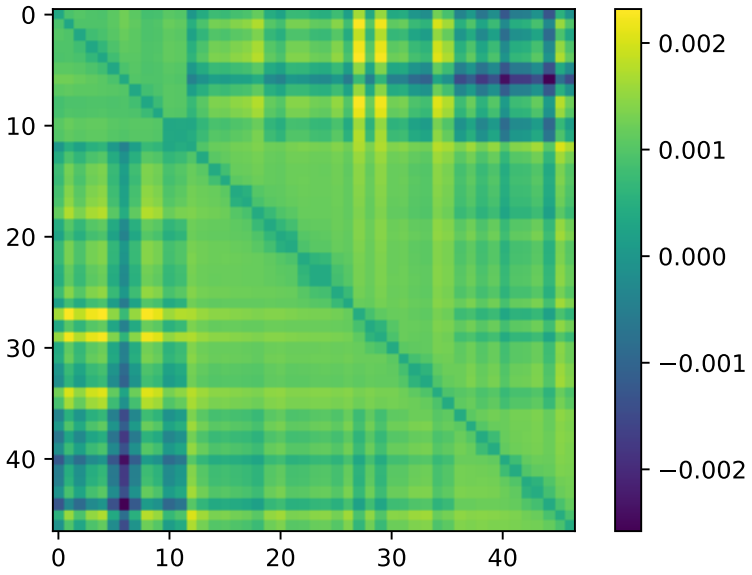

Figure 6.14: Example of $\frac{\tau_{nm}-\tau_{nm}^{app}}{\tau_{nm}}$

see Fig. 4.3. However, the transition temperature between positive and negative correction, is far lower for the larger sample. Approximately $800K$ and 1350. This is most likely due to the fact that a-Si 1728 has larger γs, Fig. 4.7, and therefore there is a broader range in which the new τ_{nm} is larger than the old one.

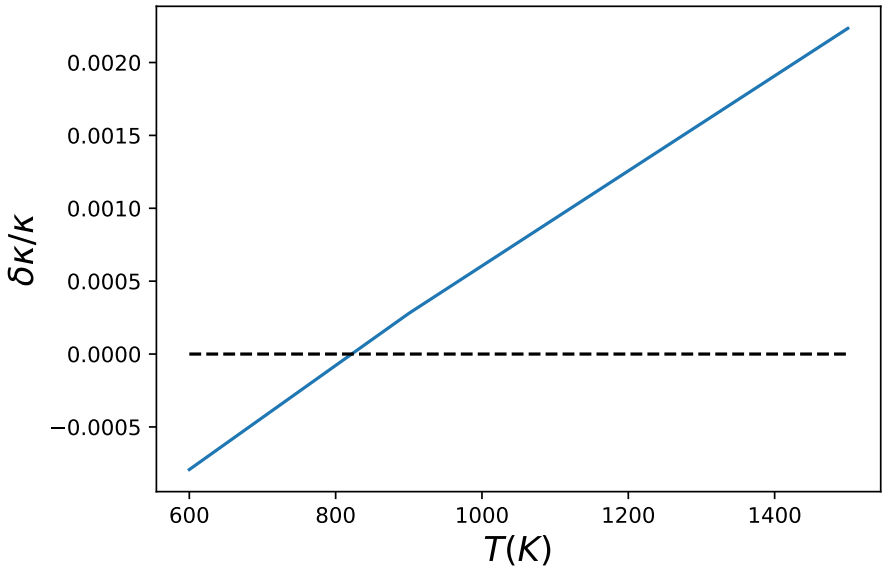

Figure 6.15: $\frac{\kappa-\kappa_0}{\kappa_0}$ as a function of T for a-Si 1728. κ_0 is original one, κ is the one calculated with Mori formalism.

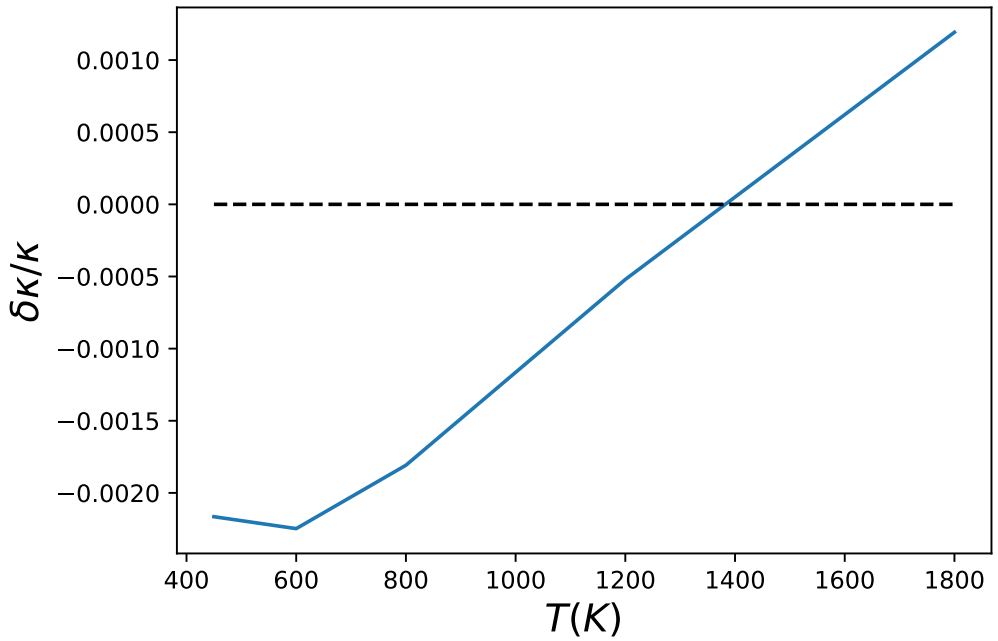

Figure 6.16: $\frac{\kappa-\kappa_0}{\kappa_0}$ as a function of T for a-Si 512.

6.5 When is Mori theory relevant?

Up to this point, it seems that this improved phonon propagator while being physically more reliable (it does not have any diverging sum rules) it is absolutely equivalent from the previous one (the $e^{i\omega_n t-\gamma_n t}$) from a pratical point of view. This could be a boring but important news, it would justify all the previous works where such approximation has been done. However, this is not necessary true.

There are two main questions to answer:

- Is this "Gaussian-Mori" model theoretically capable of describing something far different from the "Lorentzian" one?
- In which physical condition/kind of material does it happen?

The answer to the first question is absolutely yes. As it can be observed in Fig. 6.7 when $\sigma_n \approx \omega_n$ there is an undeniable difference. In particular the height of the peak does seems increasing faster than any polynomials, like a Gaussian with positive exponent. This can be observed in the approximation of τ_{nm} where indeed in case of resonance $\tau_{nn}^{app} = \frac{1}{2\gamma_n'} = \frac{1}{2\gamma_n} e^{\omega_n^2/2\sigma_n^2}$. Such behaviour of the peak can be also numerically verified, as it is shown in Fig. 6.17. In this figure it is clear that when $\sigma_n \leq \omega_n$ the height of the peak of the spectrum increases considerable. Indeed, the peak follows almost perfectly the function $e^{1/(2\sigma^2)}$. For the a-Si we explored the zone 3.5 or higher, where the peak and the spectrum is almost Lorentzian, but with just a slightly better "memory" the effect would be far more significant. In addition, it can be noticed that this effect depends mainly on σ/ω, it is almost independent by γ/ω. Changing ω_n and σ_n while keeping the same ω_n/σ has been tested, and there are no visible effects.

Now, the second question, which properties should have a material (that amorphous silicon does not have) to have a significant memory effect? To answer that, we must go back to the original definition of $\Gamma_n(t)$ of Eq. 5.28, which was a sum of $g_m(t)g_l^*(t)$. Then, we fitted this memory with a Gaussian $\sim e^{-t^2/2\tau_n^2}$. If the modes have far different frequencies, those product of propagator oscillates. On the other hand, in case of resonance that contribute remains for a long time of order $\sim 1/\gamma_m$. Let us better define the question:

$$\begin{cases} \Gamma_n(t) = \frac{2\gamma_n\sigma_n}{\sqrt{2\pi}} e^{-\sigma_n^2 t^2/2} \\ \tilde{\Gamma}_n(\omega) = 2\gamma_n e^{-\omega^2/2\sigma_n^2} \\ \sigma_n = \frac{1}{\sqrt{2\pi}} \frac{\Gamma_n(t=0)}{\tilde{\Gamma_n}(\omega=0)} \end{cases} \tag{6.7}$$

where we just used the definition of the Gaussian memory and its Fourier transform. But

$$\tilde{\Gamma_n}(\omega = 0) = \int_{-\infty}^{\infty} dt\ \Gamma_n(t) \tag{6.8}$$

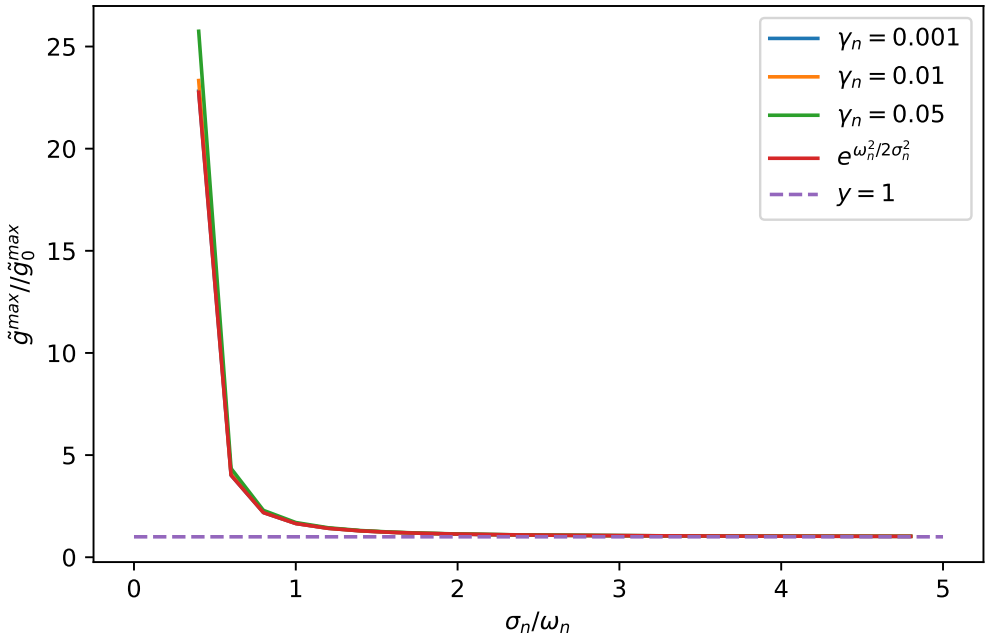

Figure 6.17: Maximum of $\tilde{g}_n(\omega)$ as a function of σ_n and $\gamma_n = 0.01$ while $\omega_n = 1$. The "double" in the legend refers to a calculation where both $(\omega_n, \sigma_n) \to 2(\omega_n, \sigma_n)$. The numerical results are compared to the function $e^{1/(2\sigma^2)}$.

Let us consider the extreme condition, where the DOS is very peaked and then almost every frequency is in resonance and consequently $g_m(t)g_l^*(t) \approx e^{-2\gamma_m|t|}$. Substituting this in Eq. 5.28 and integrating we obtain

$$\tilde{\Gamma}_n(\omega = 0) \sim \frac{1}{\gamma_n}\Gamma_n(t = 0) \Rightarrow$$
$$\sigma_n \sim \gamma_n$$

The minimum σ_n in case of a very peaked DOS is of order $\sigma_n \gtrsim \gamma_n$! So, it is theoretically possible to obtain a σ_n far smaller than the ones obtained for a-Si, which indeed it has a broad DOS with two peaks Fig. 3.6. Obviously such a peaked DOS seems unrealistic, but to have relevant effect we just need σ few times smaller.

Another important feature of this Mori propagator is that the effect of memory can be notable even if the quasi-harmonic limit is well respect. Indeed, in Fig. 6.17 it is shown how the "squeezing" of the spectrum, the ratio between the Mori spectrum's maximum and the lorertzian one, can be far bigger than one even if $\gamma_n/\omega_n \sim 0.01 - 0.001$. Such kind of "indipendence" of the the memory effect can

be seen also in the formula for σ_n, which has roughly the following form:

$$\sigma_n \sim \frac{\Gamma_n(t=0)}{\gamma_n} \sim \frac{\sum_{ml} |V_{nml}|^2 \dots}{\sum_{ml} |V_{nml}|^2 \delta(\omega_n - \omega_l - \omega_n) \dots} \tag{6.9}$$

The only relevant difference between numerator and denominator is the presence of the δ-function, while, for instance, multiplying by a factor all the anharmonic potential would not have any effect . The δ-function counts how many modes satisfy the resonance condition. The densier the DOS the higher should be this number. Indeed in the continuous limit where

$$\sum_{ml} \delta(\omega_n - \omega_l - \omega_n) \to \int\int d\omega_j d\omega_m \ \rho(\omega_j)\rho(\omega_m)\delta(\omega_n - \omega_l - \omega_n) =$$

$$= \int d\omega_m \ \rho(\omega_m)\rho(\omega_n - \omega_m)$$

the connection between the DOS and the δ-function is clear. Let us do a mental experiment to understand how should be a material to have a significant memory effect. Let us transform $\omega_n \to \omega_n/2$. In this way, the DOS is squeezed by a factor 2, see Fig. 6.18,and let us assume that $V_{nml} \approx$ *constant* and let us ignore the occupation function, which are both at the numerator and at the denominator. Then, the numerator would not change, because the number of modes it is the same, while the denominator would double. As a consequence $\sigma_n \to \sigma_n/2$ and the memory effect would be stronger. Therefore, if there are glassy materials with a DOS few times more squeezed than a-Si 1728, than they should have a significant memory effect on the conductivity.

6.6 QHGK-Memory on crystals: some considerations

The QHGK method has the remarkable property of unifying the description of heat transport in amorphous and crystalline solid insulators, as explained in Ch. 2. The discussion about the short time of the phonon propagator is general: as long as the phonon spectrum is a Lorentzian, it does not respect the sum rules. In this thesis the correction of the propagator and the consequent implementation of the QHGK-Memory method presented has been done only for amorphous systems, but obviously the crystalline case is the very next step. Indeed, there are already papers about the effect of memory on the spectrum and other properties spectrum of crystals, *Gotze et al.* [8], but a study of transport properties in the quasi-harmonic limit is still missing. However, even if there is still some work to do before

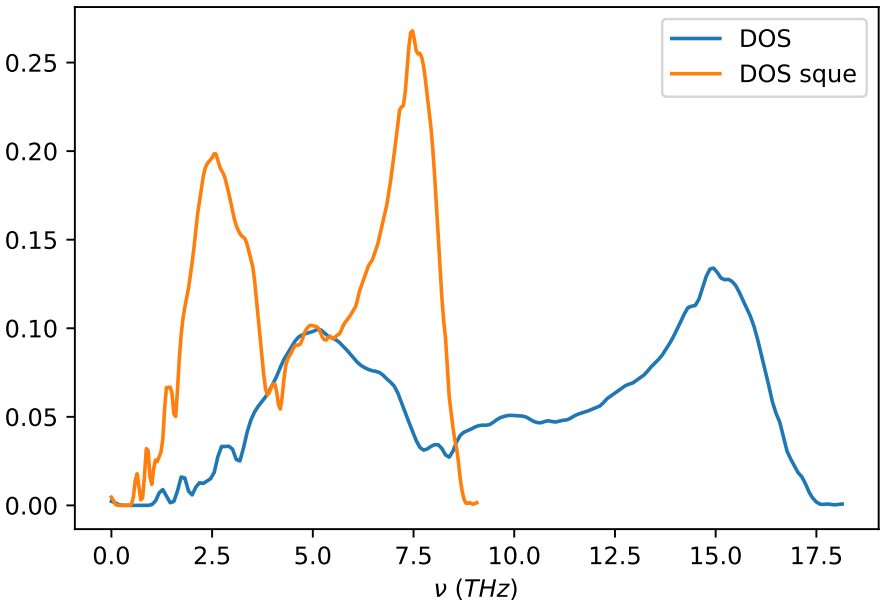

Figure 6.18: DOS a-Si 1728 and its squeezed version by the transformation $\omega_n \to \omega_n/2$.

applying the QHGK-Memory method on crystals, let us do some consideration to what expect.

In the Bloch basis, as explained in Ch. 2 , the velocity matrix becomes diagonal in the wave-vector $\mathbf{q}$. As a consequence, if the phonons band are not (quasi-)degenerate, only the diagonal terms of τ_{nm} ($\tau_{\nu_\mathbf{q},\nu_\mathbf{q}}$) matter, as shown in Eq. 3.24. This is very interesting, because the diagonal terms of τ_{nm} are the ones that most increase, as shown in Fig. 6.13. Moreover, it can be observed from Figs. 6.13-6.15 that since the diagonal, or almost diagonal, terms of τ_{nm} are higher than the Lorentzian ones but the off-diagonal ones are lower, they kind of compensate each other a bit. Indeed, while the diagonal terms of τ_{nm} increase of $2-6\%$ for $600-900K$, the variation of κ is ten times smaller. As shown in Figs. 6.16-6.15, for both the systems, a-Si 1728 and 512, there is even a temperature for which the variation of κ is zero because the positive and negative variations of τ_{nm} somehow compensate each other. Such compensation would not possible for crystals!

This leads to an interesting supposition, if a crystal had the same memory properties, same σ_n/ω_n, then the difference between QHGK-Memory and QHGK heat conductivity would be many times greater, let us say 10 times if we stick to our example of a-Si, and it would be always positive.

Chapter 7

Conclusions

In this thesis the QHGK [9] method has been completely revised. A vast study of the effect of the lineshape of the phonon propagator's spectrum on the heat conductivity has been done. Firstly, using some *ad hoc* lineshape functions it has been studied the contribute of the degenerate and not-degenerate couples of modes and how a more squeezed lineshape could affect the transport coefficient. After this general discussion, we actually proposed and studied a novel propagator with an improved short-time behaviour, which was obtained using Mori memory function formalism. A secondary result worth of mention it is the treatment of the finite-size dependence. This problem was greatly affecting the results at low temperatures for amorphous systems and it has been partially resolved with a novel numerical technique.

In regard of the size, in Ch. 4 it has been shown that a glassy system would require very large systems to have a reliable DOS in the low frequency regime. Such lack of low frequencies has a very small effect for temperatures of order of few hundreds K, but it has been proved fundamental at low temperature $T \lesssim 50K$, where the low frequency modes are by far the most occupied and therefore they dominate the heat conduction. In Ch. 4 the following technique has been proposed: obtaining a better DOS replicating few times the amorphous supercell and then evaluate the conductivity using a model for the phonon lifetimes, fitted from the amorphous system. Comparing the results between a-Si 1728 and a-Si 13824 together with the ones between a-Si 1728 and its replicated $(3, 3, 3)$ system there are many similarities. This suggests that this fit-and-replica technique could be fundamental to find reliable heat conductivity, also at low temperatures, while avoiding the enormous cost of simulating very large materials. The only point that is maybe missing from this technique is the fit $\gamma_n(\omega)$ for very low frequencies. Since as we said our small sample 1728 has a good DOS for higher frequencies but not for low ones, one could argue that its $\gamma_n - \omega_n$ data, and consequently the fit, is not too reliable for small frequencies. There are two possible solution for this

problem, a theoretical and a numerical one. The numerical one would consist of simulating a larger system but calculating only the first γ_ns. In such a case the cost would not be N^3 but only $c*N^2$, where c is the small number of low-frequency γ_n that I'm interested in. The theoretical solution instead would be to find the $\gamma_n(\omega \to 0)$ using the theory for crystal and then combine the numerical fit with this result. According to [6]-[8] the low frequency limit should be $\gamma_n \sim q^2 \sim \omega^2$, where obviously q indicates a wave-vector.

The greatest achievement of this thesis is finding a reliable ansatz for the phonon propagator and implementing it in the calculation of the conductivity, developing the novel QHGK-Memory method. While the idea of using propagator with Gaussian memory already existed, see for instance [6], its real implementation and use for the conductivity is novel. In particular the formula to determine the parameter σ_n is original, Eq. 6.5. From a theoretical point of view, such propagator has wonderful properties, it has the right long-time decay while satisfying the $0, 1, 2$-sum rules. Moreover the successive sum rules are still finite instead of being divergent. How much this new propagator differs from the previous one depends on τ_n, or better its inverse σ_n, which is the characteristic time of the memory. It has been proved in Ch. 5-6 that the Lorentzian spectrum is a consequence of assuming an instantaneous memory. Therefore, when $\tau_n \to 0$, $\sigma_n \to \infty$, the old and new propagator coincide. Obviously, when we talk about a large or small memory time, we must compare it with something else. Indeed, such time must be compared with the typical oscillation time of the mode: the fundamental parameter is σ_n/ω_n. Indeed, in Fig. 6.17 it has been shown that as long $\gamma_n \ll \sigma_n, \omega_n$, the "squeezing" of the spectrum, the ratio between the old maximum and the new one, only depends on the ratio σ_n/ω_n. This is an outstanding feature. It means that this memory effect is not something you could include with just perturbation theory: as shown in Fig. 6.17 it is possible to have very weak perturbation, but still a strong memory effect. The "squeezing" function it is a very sharp one $:e^{1/x^2}$, where $x = \sigma_n/\omega_n$. Due to the nature of this function, it is very easy to move from a parameter zone where the squeezing factor is practically one, which means no effect, to a zone where it is far greater than one.

Finally, the new Mori-propagator has been applied for the computation of heat conduction in the glassy system, a-Si 1728. The changes were minimal, even if a slight positive trend of the effect was observed, at any reasonable temperature below the melting point (the glass usually melts at $\sim 1600 - 1900K$) the effects were less than 1%, see Fig. 6.15. However, this is not evidence that for every material the memory effect can be neglected. Indeed, a material with a σ/ω just few times smaller would have a very significant effect. What does it mean to have a material with stronger memory effects? Coherence is the key here. Having many phonons which oscillate at near frequency means that they stay correlated in time,

and so it do also their anharmonic force. For instance, if we could split in haf the frequency range of the a-Si 1728 DOS, and consequently doubles the value of the DOS, the σ_n/ω_n would be reduced already by a factor 2. It is evident that further experiments on different materials must be done. Luckily, the implementation of this Mori-QHGK did not slow down considerable the computation. The calculation of the σ would require pretty much the same time of the calculation of the γ, but since they have similar formulas, computing both of them at the same time requires far less than two times the time needed for just one. Finally, in Ch. 6 we briefly outlined the possibility that memory could have a greater effect on the conductivity in crystal solid insulators than in amorphous ones.

In conclusion, in this thesis we studied the possible effects of memory in the heat transport of glassy materials, while outlining the consequences of a finite size. We implemented a Mori-QHGK, a QHGK [9] method with an improved propagator obtained by Mori memory function formalism. As a future project we intend to test our QHGK-Memory method with different and larger solid insulator samples and extend the method also to crystals.

Chapter 8

Appendix

8.1 Appendix I: Fourier and Fourier Laplace Transforms

The Fourier Transform for a generic function $f(t)$ is :

$$\tilde{f}(\omega) = \int_{-\infty}^{\infty} dt' \ f(t')e^{-i\omega t'}$$

while its Inverse Fourier Transform is:

$$f(t) = FT^{-1}[\tilde{f}(\omega), t] = \frac{1}{2\pi}\int_{-\infty}^{\infty} d\omega' \ \tilde{f}(\omega')e^{i\omega' t}$$

A Fourier-Laplace Transform is defined as:

$$LF[f(t)](\omega) = \int_{0}^{\infty} dt' \ f(t')e^{-i\omega t'}$$

Using the Heaviside function $\Theta(t)$ we can rewrite the LF transform as

$$LF[f(t)](\omega) = \int_{-\infty}^{\infty} dt' \ \Theta(t')f^c(t')e^{-i\omega t'} = FT[\Theta(t)f^c(t)](\omega)$$

where $f^c(t)$ is a symmetric/conjugated version of $f(t)$ such that $(f^c(-t))^* = f^c(t) = f(t)$. Using the Fourier Transform of the Heaviside function and the convolution properties we obtain:

$$LF[f(t)](\omega) = FT[\Theta(t)f^c(t)](\omega) = \frac{1}{2}\tilde{f}^c(\omega) + \frac{1}{2\pi i}\int_{-\infty}^{\infty} d\omega' \frac{1}{\omega'}\tilde{f}^c(\omega - \omega')$$

Since the FT of a conjugated function is real, this gives us an easy connection between the two transforms. The real part of the Laplace ones is half of the Fourier one, while the imaginary part is that integral.

8.2 Appendix: codes

Fitting γ_n

The sampling to make the $\gamma_n - \omega_n$ plot smoother has been done with the following function:

```
def resample(frequency, gamma, n_samples=30, alpha=1):
    rescaled_freq = np.linspace(0, 1, n_samples)
    rescaled_freq = (frequency.max() - frequency.min()) * rescaled_freq
 + frequency.min()
    resampled_freq = np.zeros(rescaled_freq.shape[0] - 1)
    resampled_gamma = np.zeros(rescaled_freq.shape[0] - 1)
    prev_freq = rescaled_freq[0]
    for j in range(0, rescaled_freq.shape[0] - 1):
        next_freq = rescaled_freq[j + 1]
        resampled_freq[j] = (next_freq + prev_freq) / 2
        mean = np.mean(gamma[(frequency > prev_freq) & (frequency < next
        resampled_gamma[j] = mean
        prev_freq = next_freq
    new_freq = np.append(0, resampled_freq)
    new_gamma = np.append(0, resampled_gamma)
    return new_freq.reshape(-1, 1), new_gamma.reshape(-1, 1)
```

τ_{nm} with Mori formalism

```
import numpy as np
import scipy.integrate as integrate
from scipy import special
import cmath
import matplotlib.pyplot as plt

def lor(w1,g1,w2,g2):
    w=w1-w2
    g=g1+g2
    return  ( g/(g*g+w*w) )

#parte mori
def fun(x,w,g,s):
    s=s*np.sqrt(2)
    z=complex(0,0)
```

```
    z=g*np.exp(-x*x/(s*s))*(1-special.erfi(x/s)*1j)+1j*(x-w)
    z=2/z
    return z.real
def tau(w1,g1,s1,w2,g2,s2):
    g_max=max(g1,g2)
    s_min=min(s1,s2)
    w_med=(w1+w2)/2
    result=integrate.quad(lambda x: fun(x,w1,g1,s1)*\
                                    fun(x,w2,g2,s2)/\
                                    (4*np.pi), -5*s_min+w_med,5*s_min+w_med)
    return result[0]
```

Then τ_{nm} can be approximated with:

```
def tau_appr(w1,g1,s1,w2,g2,s2):
    s1=s1*np.sqrt(2)
    s2=s2*np.sqrt(2)
    w1=w1+special.erfi(w1/s1)*g1*np.exp(-w1*w1/(s1*s1))
    w2=w2+special.erfi(w2/s2)*g2*np.exp(-w2*w2/(s2*s2))
    g=g1*np.exp(-w1*w1/(s1*s1))+g2*np.exp(-w2*w2/(s2*s2))
    w=w1-w2
    return ( g/(g*g+w*w) )
```

Bibliography

[1] Philip B. Allen and Joseph L. Feldman. "Thermal Conductivity of Glasses: Theory and Application to Amorphous Si". In: *Phys. Rev. Lett.* 62 (6 1989), pp. 645–648. DOI: 10.1103/PhysRevLett.62.645. URL: https://link.aps.org/doi/10.1103/PhysRevLett.62.645.

[2] Stefano Baroni et al. "Heat Transport in Insulators from Ab Initio Green-Kubo Theory". In: *Handbook of Materials Modeling: Applications: Current and Emerging Materials*. Ed. by Wanda Andreoni and Sidney Yip. Cham: Springer International Publishing, 2018, pp. 1–36. DOI: 10.1007/978-3-319-50257-1_12-1. URL: https://doi.org/10.1007/978-3-319-50257-1_12-1.

[3] O. N. Bedoya-Martínez, Jean-Louis Barrat, and David Rodney. "Computation of the thermal conductivity using methods based on classical and quantum molecular dynamics". In: *Phys. Rev. B* 89 (1 2014), p. 014303. DOI: 10.1103/PhysRevB.89.014303. URL: https://link.aps.org/doi/10.1103/PhysRevB.89.014303.

[4] David G. Cahill, M. Katiyar, and J. R. Abelson. "Thermal conductivity ofa-Si:H thin films". In: *Physical Review B* 50.9 (1994), pp. 6077–6081. DOI: 10.1103/physrevb.50.6077. URL: https://doi.org/10.1103%2Fphysrevb.50.6077.

[5] Joseph L. Feldman et al. "Thermal conductivity and localization in glasses: Numerical study of a model of amorphous silicon". In: *Phys. Rev. B* 48 (17 1993), pp. 12589–12602. DOI: 10.1103/PhysRevB.48.12589. URL: https://link.aps.org/doi/10.1103/PhysRevB.48.12589.

[6] Dieter Forster. *Hydrodynamic Fluctuations, Broken Symmetry, and Correlation Functions*. CRC Press, Mar. 2018. DOI: 10.1201/9780429493683. URL: https://doi.org/10.1201/9780429493683.

[7] Giorgia Fugallo and Luciano Colombo. "Calculating lattice thermal conductivity: a synopsis". In: *Physica Scripta* 93.4 (2018), p. 043002. DOI: 10.1088/1402-4896/aaa6f3. URL: https://doi.org/10.1088%2F1402-4896%2Faaa6f3.

[8] W. Götze and M. R. Mayr. "Evolution of vibrational excitations in glassy systems". In: *Physical Review E* 61.1 (Jan. 2000), pp. 587–606. DOI: 10.1103/physreve.61.587. URL: https://doi.org/10.1103/physreve.61.587.

[9] Leyla Isaeva et al. "Modeling heat transport in crystals and glasses from a unified lattice-dynamical approach". In: *Nature Communications* 10.1 (2019), p. 3853. ISSN: 2041-1723. DOI: 10.1038/s41467-019-11572-4. URL: https://doi.org/10.1038/s41467-019-11572-4.

[10] R Kubo. "The fluctuation-dissipation theorem". In: *Reports on Progress in Physics* 29.1 (1966), pp. 255–284. DOI: 10.1088/0034-4885/29/1/306. URL: https://doi.org/10.1088%2F0034-4885%2F29%2F1%2F306.

[11] Ryogo Kubo. "Statistical-Mechanical Theory of Irreversible Processes. I. General Theory and Simple Applications to Magnetic and Conduction Problems". In: *Journal of the Physical Society of Japan* 12.6 (1957), pp. 570–586. DOI: 10.1143/JPSJ.12.570. eprint: https://doi.org/10.1143/JPSJ.12.570. URL: https://doi.org/10.1143/JPSJ.12.570.

[12] Aris Marcolongo, Paolo Umari, and Stefano Baroni. "Microscopic theory and quantum simulation of atomic heat transport". In: *Nature Physics* 12.1 (Oct. 2015), pp. 80–84. DOI: 10.1038/nphys3509. URL: https://doi.org/10.1038/nphys3509.

[13] Hazime Mori. "Transport, Collective Motion, and Brownian Motion*)". In: *Progress of Theoretical Physics* 33.3 (Mar. 1965), pp. 423–455. ISSN: 0033-068X. DOI: 10.1143/PTP.33.423. eprint: https://academic.oup.com/ptp/article-pdf/33/3/423/5428510/33-3-423.pdf. URL: https://doi.org/10.1143/PTP.33.423.

[14] G.P. Srivastava. *The Physics of Phonons*.

[15] J. M. Ziman. "FORMAL TRANSPORT THEORY". In: *Electrons and Phonons*. Oxford University Press, Feb. 2001, pp. 257–287. DOI: 10.1093/acprof:oso/9780198507796.003.0007. URL: https://doi.org/10.1093/acprof:oso/9780198507796.003.0007.

[16] B. L. Zink, R. Pietri, and F. Hellman. "Thermal Conductivity and Specific Heat of Thin-Film Amorphous Silicon". In: *Phys. Rev. Lett.* 96 (5 2006), p. 055902. DOI: 10.1103/PhysRevLett.96.055902. URL: https://link.aps.org/doi/10.1103/PhysRevLett.96.055902.

Chapter 9

Ringraziamenti

Dietro ogni grande capolavoro c'è il contributo, piccolo o grande, di una moltitudine di persone senza la quale ciò non sarebbe stato possibile. Probabilmente questo non è un grande capolavoro, ma comunque ci sono molte persone che devo ringraziare.

Innanzitutto Stefano, il mio relatore, che da un anno mi ha rapito e portato nel mondo del trasporto e della fisica fuori equilibrio. Negli ultimi sei mesi in cui abbiamo lavorato alla tesi ho potuto apprezzare il puro entusiasmo con cui ricerca in fisica ed esserne contagiato. Parlando di aiuto per la tesi non ci si può dimenticare del distaccamento californiano: Davide, Giuseppe e altri ragazzi che sono intervenuti occasionalmente. Una speciale menzione va a Giuseppe, grande dj con l'hobby del dottorato in fisica, che è probabilmente la persona con cui ho più parlato (e rotto le scatole) in lockdown.

Come sempre ringrazio la mia famiglia, e specialmente mia madre, per il supporto immancabile.

In questi due anni mi sono innamorato di Trieste. Arrivato smarrito, ho avuto la fortuna di avere come guida iniziale due vecchi amici, Ciccia e quel disgraziato di Gallo, e i gentilissimi e simpaticissimi Giacomo ed Enrico. Poi ho conosciuto il resto della squad SISSA: Pietro, Cez e Michè, con cui ho condiviso lezioni, palle e scherzi di/a Giacomo e partite a ping pong. Oltre alla sissa c'è anche l'università dove ho potuto conoscere Vito col suo modo unico di fare e Valerio B., strano personaggio che mi capisce come un libro aperto.

Fuori dall'ambiente accademico, non ho comunque avuto tempo di annoiarmi, in compagnia dei miei fantastici compatrioti (acquisiti o originali): Matteo, Gabri, Emmanuele, Mavi, Fabiola , Angelica, e Roberta. Quest'ultime grandi compagne di corsa e chiacchere.

Infine, un po' in ordine sparso devo ringraziare i ragazzi ESN, incrociati per puro caso, come le migliori cose della vita: Ilaria, Giovanni, Mattia, PG e Luca. Infine ringrazio Albita, Vale T., Solex ed Elisa per i bei momenti passati insieme

e magari anche per quelli futuri.